1   (The Far Infrared Earth_November 23_2007)

2

3

4   **The Far Infrared Earth**

5

6

7   J. Harries[1], B. Carli[2], R. Rizzi[3], C. Serio[4], M. Mlynczak[5], L. Palchetti[2], T. Maestri[3], H.

8   Brindley[1], and G. Masiello[4].

9

10

11

12

13

[1] Blackett Laboratory, Imperial College, London, SW7 2AZ, UK
[2] Istituto di Fisica Applicata "Nello Carrara", CNR, 50019 Sesto Fiorentino, Firenze, Italy
[3] Atmospheric Dynamics Group, Dipartimento di Fisica, Universita di Bologna, 40127, Bologna, Italy
[4] Dipartimento di Ingegneria e Fisica dell' Ambiente, Universita di Basilicata, Potenza, Italy
[5] NASA Langley Research Center, Hampton, Virginia, USA

1   **Abstract.**

2

3   The paper presents a review of the far infrared (FIR) properties of the Earth's atmosphere, and

4   the role of these properties in climate. These properties have been relatively poorly

5   understood, and it is one of the purposes of this review to demonstrate that, in recent years,

6   we have made great strides in improving this understanding. Seen from space, the Earth is a

7   cool object, with an effective emitting temperature of about 255 K. This contrasts with a

8   global mean surface temperature of ~ 288 K, and is due primarily to strong absorption of

9   outgoing longwave energy by water vapour, carbon dioxide and clouds (especially ice). A

10   large fraction of this absorption occurs in the FIR, and so the Earth is effectively a FIR planet.

11   The FIR is important in a number of key climate processes, for example the water vapour and

12   cloud feedbacks (especially ice clouds). The FIR is also a spectral region which can be used to

13   remotely sense and retrieve atmospheric composition in the presence of ice clouds. Recent

14   developments in instrumentation have allowed progress in each of these areas, which are

15   described, and proposals for a spaceborne FIR instrument are being formulated. It is timely to

16   review the FIR properties of the clear and cloudy atmosphere, the role of FIR processes in

17   climate, and its use in observing our planet from space.

18

19   [225 words]

20

21

1. Introduction

This paper reviews our understanding of the long wave portion of the spectrum of the Earth's infrared emission to space. In all, this emission extends approximately from wavelengths of about 1 mm to about 4 μm (or those wavenumbers between about 10 and 2500 cm^{-1}) and includes the relatively unexplored part of the spectrum known as the far infrared (hereafter abbreviated to "FIR") and the better known mid infrared, the "MIR". The key feature of the FIR is that it is the spectral range characterised by transitions between pure rotational, or very low vibrational energy states, and therefore it is a cool, low energy part of the spectrum. What is our definition of the "FIR"? There is actually no precise definition of where the boundary of the FIR occurs, nor do we need, or encourage one. In this review, we will accept whatever definition the author has used in any particular piece of work that we are discussing, but for the sake of orientation we might take a wavelength of about 15 μm, or a wavenumber of about 670 cm^{-1}, as a rough boundary. The FIR, broadly, lies at longer wavelengths, or lower wavenumbers than this boundary.

We argue that the FIR is actually highly characteristic of the Earth as a system seen from space, and that it is of fundamental significance for planetary energy balance considerations and therefore for understanding climate; it may also be of great practical value in application to remote sounding of the composition of the atmosphere from space, and the characterisation of clouds (cirrus in particular). Our review will, therefore, be focused on the peculiarities of the FIR in the broader context of the Earth's emission spectrum.

The Earth is a cool object in space: this is the prime reason why the FIR is so important to an understanding of the climate system. If we measure the brightness temperature of the Earth (that is the temperature of an equivalent black body), with an instrument in space, we would measure something like 255 K [Harries, 1995; Andrews, 2000]. Differentiation of the Planck

1 radiation law to produce the Wien Displacement law [Goody, 1964] tells us that the peak

2 energy from a black body at 255 K occurs at about 500 cm^{-1}. Bearing in mind that the

3 temperature of the Earth's upper troposphere falls as low as 230 K or so, when we do the

4 calculations, we find that (depending on the latitude) up to 35% of the energy escaping to

5 space, so cooling the Earth, is at wavenumbers below 500 cm^{-1} [Sinha and Harries, 1995]. If

6 the "boundary" of the FIR is taken to be 667 cm^{-1} then this maximum fraction increases to

7 nearer 45%. So, it is very important that climate models include accurate details of the FIR

8 properties of the atmosphere if they are to produce accurate predictions of climate change.

9

10 Another area in which it is important to understand the FIR spectrum is in remote sounding of

11 the Earth and its atmosphere from space. Remote sounding at mid IR (MIR) wavelengths,

12 shorter than 15 μm, has been extensively used for measurements of temperature and

13 composition from space, as also has the microwave region at wavelengths longer than about 1

14 mm. The region in between has not been exploited, because it seemed to be at a disadvantage

15 in terms of low photon energy with respect to the mid IR, while not benefiting, for technical

16 reasons, from the multiplexing or heterodyne techniques usable in the mm region because of

17 the availability of suitable mixers and monochromatic sources. However, as we shall see, the

18 FIR, observed using modern techniques, offers the possibility of accurate remote sounding of

19 water vapour and other constituents, in both clear skies, and also (because of the relatively

20 high transparency of clouds in the FIR) in the vicinity of optically thin clouds.

21

22 It is timely to present a review of the scientific background to, and current understanding of,

23 the FIR spectrum of the Earth for two primary reasons: first, because the need to make ever

24 more accurate predictions of climate change demands a more profound understanding of

25 important FIR processes; and, second, because future satellite instrumentation may include

26 spectrometers and other devices that operate in this less familiar range of the electromagnetic

spectrum, between the mid infrared and the microwave region.   This paper presents a review

of the FIR properties of the Earth's atmosphere, and of those FIR processes which are

significant to the planetary energy balance, and also describes the application of the FIR to

remote sounding in the presence of clouds. It describes a range of current research in the

field, in which basic science, instrument development, and measurements from aircraft and

balloons are all being carried out.

[Insert Box 1 near here]

==

Box 1: Tutorial on infrared spectroscopy and radiative transfer in the atmosphere

Spectroscopy

Two classic text books which provide comprehensive introductions to the spectroscopy of the

atmosphere are Penner [1959] and Goody [1964]. We provide a brief introduction to the

subject here. In the absence of an atmosphere, radiative transfer for the Earth would be

simple. Incoming solar radiation would be partly reflected and partly absorbed by the surface,

depending on the 'albedo', or reflectance of the local surface. The absorbed energy would

warm the surface, and emission of thermal radiation, according to the Planck radiation law

[Goody, 1964], would take place, transferring energy back to space.   In balance, the two

fluxes of energy would be equal, on a globally averaged basis.

The effect of the atmosphere is to moderate these fluxes. Ignoring clouds to begin with, the

atmosphere contains molecules such as H_2O, CO_2, CH_4, O_3, and many others that are excited

by the available energy to move (translational energy), to rotate, to vibrate, and to excite their

constituent electrons to higher energy states. Since we are concerned here with the FIR, we

1   can restrict our view to the thermal or infrared region, for which electronic transitions are not

2   relevant, being of too high an energy. The vibrational and rotational energy levels of the

3   molecules are quantised [Rae, 2002], which means that energy levels can take up only certain

4   discrete values, and energy exchange can only occur at discrete energies. Since energy, E, is

5   proportional to frequency ($E = hf$, where h is Planck's constant, and f is frequency), we can,

6   therefore, say that the atmosphere will absorb or emit infrared radiation only at discrete

7   frequencies. It is common to use alternative but entirely equivalent parameters to describe the

8   energy scale, including frequency, f (in Hertz), wavelength λ, (usually in μm), or

9   wavenumber, ν (in cm^{-1}). The three are related via the speed of light, c, by

10

11                    $c = f\lambda;$

12                    $\nu = 1/\lambda = f/c .$ {B1}

13

14   In fact, energy transitions are not precisely monochromatic, but are broadened by inter-

15   molecular and other effects, such as collisions, and the Doppler effect, so that if we magnify a

16   single absorption or emission line, we find that it has the shape of a single resonance

17   maximum, and a definite half width at half peak height, both of which depend on parameters

18   like pressure and temperature [Goody, 1964].

19

20   Because the frequencies at which each molecule absorbs and emits IR radiation are different,

21   depending on molecular structure as well as molecular density, and atmospheric temperature

22   and pressure, the real atmospheric spectrum is a highly complex merger of individual lines,

23   and groups (bands) of lines from all of the absorbing molecules. In some regions of the

24   spectrum, the atmosphere may be highly transparent; in others, it is strongly absorbing, and

25   photons have a small mean free path before being absorbed.

26

1   [Figures B1 and B2 next to each other here in Box 1]

2

3   Figure B1 shows the total atmospheric optical depth at the centre of all the water vapour and

4   carbon dioxide absorption lines throughout the whole of the IR; similar information is

5   provided in Figure B2 for the remaining key absorbing species. Each absorption line is

6   represented by one point, the optical depth (see below for definition) of the atmosphere at the

7   central wavenumber. Note that the y-axis scale is logarithmic, so that each division represents

8   a factor of 10. This method of display allows a comparison of absorption strengths across the

9   whole IR spectral region with each band colour coded. The dominant effect of water vapour

10   in the mid and far IR may be seen, as can the important bands of CO_2 at 15 μm (667 cm^{-1}) and

11   4.3 μm (2325 cm^{-1}). The lower optical depths between 750 and 1250 cm^{-1}, and between 2400

12   and 3000 cm^{-1} represent regions of lower absorption, or higher transparency, commonly

13   referred to as "atmospheric windows".

14

15   The strength of absorption can be measured by a parameter known as the mass absorption

16   coefficient, α_v , which is related to the fractional transmittance, τ_v, of a path of length l

17   (maximum path L) and absorber density, ρ , by $\tau_v = \exp\left[-\int_0^L \alpha_v(l)\rho(l)dl \right]$. The term

18   $\chi_v = \left[\int_0^L \alpha_v(l)\rho(l)dl \right]$ is known as the optical depth.

19

20   In the FIR, the mechanism by which a molecule may absorb or emit radiative energy is either

21   through rotations or vibrations of the molecule in question, because the energies of such

22   processes correspond to the FIR. Each type of motion is quantised in terms of the allowed

23   energy states and transitions between them. Rotational spectral lines are lower in energy (i.e.

24   lower in characteristic frequency: see eq. B1 above) than vibrational energy transitions. The

1 frequencies of energy state transitions in the latter case depend on changes to the shape of the

2 molecule, and the atomic weights of the constituents, as well as on 'selection rules' that

3 determine whether transitions between particular energy states are allowed by quantum

4 mechanics or not.   The vibrations of a molecule are classified broadly by whether the

5 vibration represents a stretching of a particular inter-atomic bond, or a bending of the

6 molecule.   In this paper we refer to different vibration classes as v_1, v_2 or v_3: these refer, in

7 the case of tri-atomic molecules like CO_2 and H_2O, to symmetric stretching of the two C-O or

8 O-H bonds (v_1), bending of the molecule about the 'pivot' of the central atom (C or O) of the

9 three (v_2), and asymmetric stretching of the two C-O or O-H bonds (v_3).   Goody [1964]

10 provides a clear explanation of these definitions.

11

12 *Radiative transfer*

13

14 The transfer of radiative energy within and through the Earth's atmosphere is treated in a

15 number of classic text books, including Chandrasekhar [1960], and Goody [1964]. The

16 radiative transfer of the atmosphere is controlled by the spectra of atmospheric molecules,

17 described above. In the infrared, the transmittance of any given 1metre of path length

18 depends on the molecular density, the temperature and the atmospheric pressure along that

19 path, but is principally determined by whether the chosen spectral wavelength (wavenumber)

20 coincides with an absorption line, or a collection or band of lines.

21

22 At some wavelengths, away from such absorptions, thermal radiation emitted upwards by the

23 surface has a high probability of escaping to space: at more highly absorbing wavelengths, a

24 photon has a very low probability of escaping to space, instead being absorbed by a higher

25 (and usually colder) layer of the atmosphere: subsequently, some of the absorbed energy may

26 be re-emitted, this time at the lower local temperature, and so on, until eventually a photon is

1 able to escape to space. This process is the physical basis of the greenhouse effect. In local

2 thermodynamic equilibrium (effectively the case for the Earth's atmosphere below ~ 60 km),

3 the emission at a given local temperature, T, is governed by the Planck law. The Planck law

4 may be written as:

5

6
$$B_f(T) = \frac{2hf^3}{c^2\{\exp[hf/k_BT]-1\}} \qquad \{B2\}$$

7

8 where $B_f(T)$, the spectral radiance of a black body (unit emissivity), is the power per unit area,

9 per unit solid angle, per unit frequency interval at frequency, f, in a particular direction; in

10 addition to previously defined quantities, k_B is Boltzmann's constant, and h is Planck's

11 constant.

12

13 Radiative transfer within an atmosphere is described in terms of the Schwarzchild equation of

14 radiative transfer. This treatment is a little beyond the scope of this 'primer', but the

15 interested reader is referred to the texts by Chandrasekhar [1960], Goody, [1964], and Goody

16 and Yung [1989] for more information. This equation describes how radiation propagates

17 along a path through an atmosphere, where scattering, absorption and thermal emission may

18 all occur due to interactions with the molecules and cloud particles along the path. While

19 absorption (emission) will reduce (enhance) the intensity of the radiation as it propagates,

20 scattering processes can have either effect according to whether radiation is being scattered

21 into, or out of, the beam.

22

23 [Figure B3 near here in Box 1]

24

1   Figure B3 shows some calculations using a radiative transfer code[6] which illustrate some of

2   these points. Shown in Figure B3 are the upwelling, top of the atmosphere (commonly

3   abbreviated to TOA) spectra calculated for a warm, moist model atmosphere, and a cold, dry

4   model atmosphere (so-called "standard atmospheres", [Anderson et al, 1986]), both cloud-

5   free. The y-axis is in units of spectral radiance (power per unit area, per unit solid angle, per

6   unit wavenumber interval, in a particular direction). The black curve is the calculated

7   spectrum for each case. The red lines describe the shape of the Planck function for the

8   temperatures indicated. The line structure below about 500 cm^{-1} is mainly due to water

9   vapour; the band centred at 667 cm^{-1} is due to CO_2; the band centred at 1060 cm^{-1} is due to

10   O_3; and the extended band above about 1250 cm^{-1} is due primarily to H_2O and other gases,

11   including CH_4. In the window region, between about 800 and 1250 cm^{-1} the brightness

12   temperature seen at the TOA is close to the assumed surface temperature. In the centre of the

13   intensely absorbing CO_2 band, the brightness temperature is that of the tropopause/lower

14   stratosphere, because below these heights the atmosphere is opaque. In the pure rotational

15   band of water vapour, below about 500 cm^{-1}, the brightness temperature represents the

16   temperature at the level from which most of the radiation reaching the TOA is originating.

17

18   *Heating rates*

19

---

[6] [There are a number of powerful radiative transfer codes available, which allow the calculation of the transfer

of electro-magnetic radiation through an atmosphere made up of gases, aerosols and clouds. A detailed

treatment is beyond the scope of this work, but an excellent source in which to find references to and details of a

wide range of codes is given in the Wikipedia website at:

http://en.wikipedia.org/wiki/List_of_atmospheric_radiative_transfer_codes.

Specific publications include Cahalan et al. (2005), Edwards (1992), Rothman et al., (2005) and Stamnes K
(1988)].

1   The concept of a heating rate follows on from the basic concepts of radiative transfer given

2   above. The heating (or cooling) rate of a volume of the atmosphere, $\dfrac{dQ}{dt} = \dot{Q}$, where Q is heat

3   energy, is a measure of the rate of gain (or loss) of energy by that volume to space. The

4   heating rate is defined as the energy gained per unit volume, per unit time, into a 2π steradian

5   hemisphere centred on the vertical direction, and may be evaluated as a function of spectral

6   wavenumber, v, or as a spectrally integrated total rate. Unless otherwise indicated, we shall

7   consider the heating rate to be a function of wavenumber. Thus, the heating rate per

8   wavenumber, as a function of altitude, may be written as $\dot{Q}_v(z)$, which, in units of $Jm^{-3}s^{-1}(cm^{-1})^{-1}$,

9    $(cm^{-1})^{-1}$, is equal to the vertical gradient of the net radiative flux[7], $F_N(z)$ [Andrews, 2000].

10   For an atmosphere in hydrostatic equilibrium, with c_p being the specific heat at constant

11   pressure, and with the sign convention of net flux noted in the footnote:

12   $$\dot{Q}_v(z) = \rho(z)c_p \frac{dT_v}{dt} = \frac{dF_{v,N}(z)}{dz} \quad , \qquad \{B3\}$$

13

14   though by common practice, at least in meteorology, an alternative heating rate is more

15   usually expressed as a rate of change of temperature for the volume of air concerned (units

16   $Ks^{-1}(cm^{-1})^{-1}$):

17   $$h_v(z) = \frac{dT_v}{dt} = \frac{\dot{Q}_v}{\rho(z)c_p} = \frac{1}{\rho(z)c_p}\frac{dF_{v,N}(z)}{dz} \quad . \qquad \{B4\}$$

18

19   The total heating rate may be obtained by integrating over v and/or z, as appropriate.

20   **[End of Box 1]**

21   ==

---

[7] Net radiative flux = downwelling flux – upwelling flux, or $F_N = F^{\downarrow} - F^{\uparrow}$

1

2. Background: Spectral properties and energy balance of the Earth in the FIR

3

2.1. Clear sky spectral properties in the FIR

5

Box 1 gives a "tutorial" on the basic principles and concepts of spectroscopy and radiative

transfer which underlie a study of the IR properties of the Earth's atmosphere, and which

appear later in the paper. We now turn to a more specific examination of the FIR in

particular.

10

The spectral properties - that is the variation of the absorption coefficient with wavenumber -

of the cloud-free atmosphere at wavelengths longer than 15 μm are dominated by water

vapour, and only at the high frequency end of this range does CO_2 absorb significantly. The

absorption by these molecules in the FIR is so strong that from space the surface is entirely

obscured, except in the coldest and driest conditions near the poles. Thus, the study of the

FIR Earth from space is essentially a study of the atmosphere alone.

17

In the neutral atmosphere, in comparison to water vapour and CO_2, other absorbing molecules

or atoms absorb an insignificant amount of energy. In the FIR the pure rotational band of

water vapour extends from the microwave region (weak transitions at wavenumbers as low as

6 cm^{-1}), to the CO_2 ν_2 vibration-rotational band centred at 667 cm^{-1}. The centre of the pure

rotational band of water vapour is a broad feature around 100-150 cm^{-1}, comprising many

hundreds of strongly absorbing individual pure rotational lines [Goody, 1964]. At higher

wavenumbers, the intensities of transitions fall to lower values in the 400-600 cm^{-1} region,

where a partially transparent "window" occurs, and where the lower frequency edge of the

very strong CO_2 band begins, at about 500 cm^{-1}. At wavenumbers below the peak of the

1   water vapour band, the intensity of transitions also decreases. Other molecular species (and

2   atomic oxygen), including O_3, N_2O, HDO, HNO_3, and many others [Harries, 1977; Carli,

3   1984], have pure rotational or low energy vibrational transitions in the FIR, but these are

4   insignificant in terms of radiative energy transfer compared with water vapour. However, the

5   existence of spectral features due to these species does, of course, provide the possibility of

6   using the FIR for retrieval of atmospheric composition.

7

8   Following on from Figure B3, Figure 1 presents calculations of the transmittance of the

9   atmosphere in the FIR (Brindley, unpublished: see also Brindley and Harries [1998]) for the

10   expanded region 0-1000 cm^{-1}, which illustrate the dominant influence of water vapour on the

11   FIR spectrum. These calculations use a so-called line-by-line, or high resolution radiative

12   transfer code that calculates the atmospheric transmittance at very high spectral resolution so

13   that each individual spectral line shape is included. Spectrum (a) shows the fractional

14   transmittance from 12 km to the top of the atmosphere (TOA) for a moist, warm tropical

15   standard atmosphere [Anderson et al., 1986], and (b) shows the transmittance from the surface

16   to the TOA for the same model atmosphere. Figure 1(c) shows the transmittance from 8 km

17   to the TOA for a colder and drier polar standard atmosphere, while (d) shows, for this same

18   atmosphere, the transmittance from the ground to the TOA. This figure illustrates several

19   points:

20

21   •   The principal absorption features are the pure rotational band of water vapour between

22   about 20 and 400 cm^{-1}, and the CO_2 v_2 vibration band between about 600 and 720 cm^{-1}.

23   •   For much of the FIR, the atmosphere becomes partially transparent only in the upper

24   troposphere and stratosphere, due to the intense absorption strength of the pure rotational

25   water vapour band. Over much of the FIR, the lower troposphere is totally opaque.

1 • This means that the FIR is particularly useful for remote sensing of composition in the

2 stratosphere, where the water vapour absorption is weaker, and so does not block absorption

3 lines due to other absorbers [Carli, 1984].

4 • It also means that much of the energy that is emitted and which cools the Earth to

5 space comes, not from the surface, but from the upper troposphere, because the lower

6 troposphere over most of the planet in the FIR is totally opaque, the surface is obscured, and

7 no energy can escape to space.

8

9 [Figure 1 near here]

10

11 We can see from this evidence that in the FIR, the energy that the Earth emits to space as part

12 of the cooling processes which, in thermal steady-state, balance the heating due to the Sun, is

13 strongly modulated at different wavenumbers and different heights by water vapour. Bearing

14 in mind that the Earth is a FIR object in space, emitting at an effective temperature of about

15 255 K (we recall that at this temperature a Planck curve peaks at about 500 cm^{-1}), we can see

16 that water vapour acts in the FIR as an important greenhouse gas: it can absorb energy from

17 the warm surface below, and re-emit it to space at a lower temperature in, say, the upper

18 troposphere. Therefore, water vapour exhibits a strong feedback, in which any greenhouse

19 warming due to increasing levels of CO_2 is amplified if more water vapour enters the

20 atmosphere as a result. As CO_2 concentrations rise in the atmosphere, so the atmospheric and

21 surface temperatures rise: this rise in temperature in turn causes increased evaporation from

22 the oceans, and so more water vapour may be expected to enter the atmosphere. This

23 additional water vapour enhances the original greenhouse warming, and is a major

24 contribution to global climate change [IPCC, 2001 and 2007]. A corollary of these properties

25 is that from space in the FIR the surface is usually not visible, because of the very high

26 opacity of the atmosphere.

1

2 **2.2   Continuum absorption by water vapour**

3

4 The water vapour spectrum includes one aspect which is far from well understood

5 theoretically. Whereas the absorption around the centre of a spectral line of water vapour is

6 very closely described by the Voigt line shape [Andrews, 2000] because both collisional

7 broadening and Doppler broadening of the spectral lines are important in the FIR [Goody,

8 1964], the precise shape and properties of the absorption lines farther from line centre are not

9 well understood, despite having been the subject of considerable research over many years. It

10 is found that the absorption in these "far wings" of the lines is stronger than is predicted by

11 any of the current theories of collisional (pressure) or Doppler line broadening.

12

13 The ideas put forward to explain this feature fall into three classes: those which treat the

14 discrepancy as purely a matter of the wrong line shape in the far wings for molecule-molecule

15 interactions (so-called "continuum absorption": Ma and Tipping, [2002]; Ptashnik et al.,

16 [2004]); those that invoke the creation of a new molecule as a result of collisions (a dimer, or

17 double molecule of water vapour, and even higher polymers) that is responsible for the

18 "missing" absorption [Vaida et al., 2001]; and those which adopt a more pragmatic approach,

19 [Clough et al., 1989] using an empirical model to describe the measured excess absorption: in

20 this approach, two terms have been invoked, one a self-broadening effect due to water-water

21 molecule collisions, and the other due to water-foreign gas (eg N_2 or O_2) broadening.

22

23 In this last approach, the water vapour continuum was defined as all absorption due to water

24 vapour not attributable to a Lorentz (collisional broadening) line [Goody, 1964], within 25

25 cm^{-1} of each line centre [Clough et al. 1989]. The success of this approach, which employed a

26 common line shape for all spectral lines, led the authors to suggest that water vapour

1   continuum absorption was due to the intermediate and far wings of allowed water vapour

2   monomer transitions. Clough and colleagues claimed that their model effectively ended

3   speculation about the existence of discrete dimers or multimers. In [Mlawer et al 1999],

4   Clough and co-workers introduced a new formulation of the CKD approach to the water

5   vapour continuum, designated MT_CKD. The new model describes the contribution from

6   each spectral line as the sum of two terms: a sub-Lorentzian line shape, and a small, broad

7   additional line shape that provides the needed super-Lorentzian absorption in the intermediate

8   line wings. The MT_CKD version has been tuned to observations in the far infrared recorded

9   with an upward-looking ground-based Fourier transform spectrometer (Atmospheric Emitted

10   Radiance Interferometer) used in campaigns, for example, in cold dry Arctic conditions

11   [Tobin *et al.* 1999].

12

13   Estimates (Rizzi, unpublished) using the US standard atmosphere and the MT_CKD model,

14   show that the continuum absorption due to water vapour reduces the outgoing thermal

15   radiation at the TOA in clear sky conditions by about 2.2%, equivalent to a change in radiance

16   of about 2 $Wm^{-2}sr^{-1}$. The downwelling longwave radiation at the surface was found to

17   increase by almost 6 $Wm^{-2}sr^{-1}$, that is by about 5.8%. Recent work [Green, 2003; Green et al.,

18   2007] has shown that continuum absorption, particularly water-foreign gas continuum

19   absorption is significant, even in the centre of the strong pure rotational band of monomer

20   water vapour, and so cannot be ignored in a complete treatment of the FIR.

21

22   **2.3   Heating rates**

23

24   The primer in Box 1 gives a definition of the parameter known as the heating (or cooling)

25   rate. This is a measure of the rate of energy gain (or loss). It is interesting to calculate the

26   heating rate as a function of altitude and of spectral wavenumber, as was done by Kiehl

1   [1983] and Charlock [1984], and later by Clough et al [1992], and this has been repeated for

2   the US Standard Atmosphere [Anderson et al., 1986] tropical and sub-arctic models, in Figure

3   2 [Brindley and Harries, 1998].

4

5   [Figure 2 near here]

6

7   Figure 2 makes clear the dominant effect that the pure rotational band of water vapour has on

8   the Earth's atmospheric radiative energy balance. Because the opacity of the pure rotational

9   band varies with wavenumber, and peaks in the region of 100-200 cm^{-1}, we find that the

10   height at which maximum cooling (energy loss) to space occurs for a given wavenumber,

11   peaks in the mid- to upper troposphere, at altitudes that depend on the opacity and therefore

12   on the wavenumber. At any given wavenumber the cooling rate profile can be calculated

13   from the vertical gradient in net flux (equation B4). This quantity is itself determined by the

14   vertical gradient in the atmospheric transmission to space, which, for clear conditions in the

15   FIR, is effectively controlled by the vertical distribution of water vapour in the atmosphere.

16   The level of peak cooling occurs where the transmission gradient is a maximum. Below this

17   maximum the transmission to space tends to zero because the path to space at these lower

18   levels is blocked by the strongly absorbing layers above. Above the maximum the decay in

19   the amount of water vapour with height is sufficient to allow the transmission to tend to a

20   value of unity; when this occurs all of the radiation emitted from levels below this height

21   escapes directly to space.

22

23   Other notable features that can be seen in Figure 2 include:

24

25   •   Strong absorption (local heating) in the lower stratosphere by the ν_3 fundamental band

26   of ozone, O_3 centred at 1045 cm^{-1}, which switches to strong cooling above.

17

1

2 • Very intense absorption by the ν_2 fundamental band of CO_2 centred at 667 cm^{-1}, so

3 intense that no radiation can escape to space except from stratospheric heights, where a strong

4 cooling to space occurs at the band centre;

5

6 • Cooling to space in the atmospheric "window" region between about 800 and 1200

7 cm^{-1}, due to weaker water vapour lines, and to continuum emission and absorption.

8

9 **2.4 Sensitivity of the emitted spectrum to changes in water vapour content and**

10 **temperature**

11

12 As suggested by section 2.3 the FIR spectrum at the top of the atmosphere is highly sensitive

13 to changes in atmospheric water vapour [Rizzi et al., 2002].

14

15 [Figure 3 near here]

16

17 Figure 3 shows the difference in outgoing longwave radiance between three simulations:

18 • Case A (Tropical standard atmosphere with water vapour concentration scaled by 0.9

19 and skin temperature decreased by 1K);

20 • Case B (Tropical standard atmosphere with only water vapour concentration scaled by

21 0.9, and no other change);

22 • Case C: control (Tropical standard atmosphere, with no scaling).

23

24 Figure 3 shows the differences Case A-C, and Case B-C. Several features are apparent. First,

25 in the centre of the CO_2 band the radiance differences are zero in both cases, because the

26 atmosphere is so optically thick at these wavelengths that none of the changes to the

1 atmosphere are detected in the outgoing radiance: at these wavelengths the radiance

2 originates in the stratosphere (which remained unchanged in the simulation). The Case B-C

3 difference shows essentially the spectral profile of water vapour and continuum absorption.

4 The Case A-C difference shows the same difference as Case A-B in the pure rotational band

5 below 600 cm^{-1}, where the surface (reduced skin temperature) is not detected at the top of the

6 atmosphere because of the intense absorption by water vapour. However, in the more

7 transparent window region, the effect of the -1K skin temperature change in Case A is

8 apparent between about 750 and 1300 cm^{-1}. These differences indicate that spectral

9 differences are evident outside the optically thick spectral regions and therefore the spectral

10 signal provides information on the two separate physical processes.

11

12 Similarly, calculations for higher, including polar, latitudes (not shown, but see also Figure 2)

13 also show that the pure rotational band remains a strong absorber, even at the lower water

14 vapour concentrations. In fact, a very interesting partially transparent window in the 500-600

15 cm^{-1} region opens up, raising the intriguing question of enhanced surface to space radiative

16 cooling, as reported by Shaw et al, [1999] on the basis of low water content measurements

17 from a high mountain.

18

19 Rizzi et al., [2002] also demonstrated that the FIR was particularly sensitive to water vapour

20 changes in the upper troposphere, and suggested that spectrally resolved measurements were

21 more sensitive to humidity changes at all levels in the atmosphere than broad-band (spectrally

22 integrated) measurements.

23

24 **2.5   Cloudy sky properties in the FIR**

25

1   So far, we have reviewed the evidence for the FIR properties of a clear- i.e. cloud-free –

2   atmosphere. However, atmospheric condensed phases of water vapour, especially the ice

3   phase, play an important role on the infrared atmospheric outgoing radiation and the energy

4   balance of atmospheric layers. The fundamental importance of the ice phase is simply that to

5   replace a warm Earth surface with a very cold ice cloud surface has a larger energy balance

6   impact at the TOA than replacement by a low, warm liquid-phase cloud. Ice clouds in

7   particular are believed to be extremely important for climate in the tropics [Liou, 1986],

8   because of their prevalence and persistence, and it has been suggested that they represent a

9   significant feedback to climate forcing [Randall et al., 1989]. Bulk radiative studies of cirrus

10 clouds show that they may radiatively cool or heat the upper atmosphere in the thermal

11 infrared wavelengths depending upon height, geometrical and microphysical features [Slingo

12 and Slingo, 1988; Stephens et al., 1990; Stackhouse and Stephens, 1991].

13

14 Recent studies include the publication of the scattering and absorption properties of ice clouds

15 for the MIR and FIR [Yang et al (2005), and Baum et al, (2007)], and a demonstration of the

16 measurement of cloud phase using MIR and FIR observations [Turner et al (2003)]. Also,

17 Rizzi and Mannozzi [2000] quantified the importance of the FIR contribution to the spectrum

18 in outgoing top of the atmosphere fluxes, as a function of increasing cloudiness. They

19 showed that under clear conditions the ratio of energy emitted between 10 and 600 cm^{-1} to

20 total emission (computed from 10 to 2750 cm^{-1}) lies between 0.38 for the tropical and 0.48 for

21 the sub-Arctic winter standard atmospheres. The effect of cloud is to make the range below

22 600 cm^{-1} energetically more important than in the clear-sky case, with the same ratio

23 increasing up to about 0.56.   This is because, at typical cloud-top temperatures, the cold

24 cloud emission is strongly dominated by emission at FIR wavelengths.

25

1   Further studies have clarified the importance of the FIR when addressing the problem of

2   radiative cooling in the presence of clouds. Initial studies [Maestri and Rizzi, 2003] have

3   shown that flux divergence, integrated over the whole cloud depth for a tropical cirrus cloud,

4   reveals two well defined spectral regions: the FIR where net emission of radiation occurs, and

5   the atmospheric window regions and near infrared where net absorption dominates. Therefore

6   the integrated heat balance and the net diabatic effect on the cloud layer requires

7   consideration of two large contributions of opposite sign.

8

9   [Figure 4 near here]

10

11   In the lower panels of Figure 4, examples of vertically propagating net fluxes in the FIR and

12   in the 8-14 μm window region, for three different tropical atmospheric conditions (clear sky,

13   semi-transparent cirrus and opaque cirrus) are reported. The cirrus cloud base is at 10.5 km,

14   and has a thickness of 1.8 km. The ice water paths are zero, 26.7 g m^{-2} and 890 g m^{-2},

15   respectively. In the upper panel the layer spectral energy balance is shown: across the layer

16   there is a FIR net emission (cooling) even for clear skies, because of the strong absorption by

17   the pure rotational band of water vapour. With ice cloud, this cooling is enhanced. In the

18   window region, the only significant changes of energy balance occur when cirrus is

19   introduced.

20

21   Cloud ice water content (IWC) strongly affects the proportion of energy absorbed and emitted

22   by the layer, but once a cloud level and atmospheric profile are predefined, the crossover

23   wavenumber between cloud net absorption and net emission is well defined, quite

24   independently from cloud transmittance. The atmospheric temperature profile is recognized as

25   the main factor in establishing the crossover wavenumber.

26

1 Maestri and Rizzi [2003] also point out that the presence of a cloud layer changes the diabatic

2 heating of all layers below the cloud and observe that the atmospheric concentration of water

3 vapour has an important impact on the cloud's energy balance, since the more the atmosphere

4 below the cirrus is transparent, the more energy is absorbed by the cloud. The role of mid and

5 lower troposphere water vapour in absorbing FIR and window downward radiation emitted by

6 high level cirrus clouds is also highlighted, thus stressing another interaction between water

7 vapour and clouds.

8

9 The calculation and the observation of cloud radiative interactions in the FIR, as at all

10 wavelengths, is difficult. The dynamical and transient nature of cloud formation and

11 destruction, the importance of knowledge of the cloud microphysical properties (especially

12 for ice clouds, where ice particle shape is important), and the problem of sampling the

13 changing, complex cloud field and associated radiation field, all conspire to make the problem

14 extremely difficult. Nevertheless, as has been demonstrated, the impact of clouds on the FIR

15 is very significant, and the work to date has impressed upon us the urgency of addressing the

16 cloud-radiation problem at these long wavelengths. Given all the uncertainties mentioned, it

17 is most unlikely that climate models include accurate descriptions of these processes, or of

18 how they affect the climate under changing conditions.   Solving this problem is of the utmost

19 urgency.

20

21 **3.   The FIR and climate: water vapour and cloud feedback**

22

23 As we have seen, both water vapour and clouds have strong FIR effects on the energy balance

24 of the Earth's climate system. Here we review work which has attempted to improve our

25 quantitative understanding of how the water vapour and the cloud radiative feedback

26 processes affect climate.

1

2 **3.1 Water vapour feedback and the FIR**

3

4 An excellent review of the physics of the water vapour feedback may be found in Held and

5 Soden [2000], in which they discuss the feedback in physical terms, and its dependence on

6 humidity and temperature. Also, they discuss the impact of dynamics on the feedback

7 process, and a controversy over the sign of the feedback (see later). Many of their ideas may

8 be extended to other processes than water vapour absorption.

9

10 Adapting the analysis provided by Held and Soden, we may consider a balance between the

11 globally averaged absorbed solar energy, or power into the system P_{in}, and the globally

12 averaged output emitted longwave radiation, P_{out}, as in

13

14
$$P_{in} = P_{out} + \Delta P \qquad , \qquad \{1\}$$

15 Where,

16
$$\left.\begin{array}{l} P_{in} = \dfrac{S}{4}(1 - A) \\ and \\ P_{out} = \sigma(1 - g)T_s^4 \end{array}\right\} \qquad \{2\}$$

17

18 Here, $S =$ solar constant, $\sigma =$ Stefan-Boltzmann's constant, A is the global albedo, T_s is the

19 surface temperature, ΔP is discussed below, and g is the normalised greenhouse parameter:

20

21
$$g = \frac{G}{\sigma T_s^4} = \frac{\sigma T_s^4 - \sigma T_e^4}{\sigma T_s^4} \quad . \qquad \{3\}$$

22 Here

23

1

$$G = \sigma(T_s^4 - T_e^4) \qquad \{4\}$$

2

3   is the absolute greenhouse parameter.

4

5   We may introduce the spectral variation of both g and G by inserting the Planck radiation law

6   (equation {B2}) in place of the Stefan-Boltzmann law in equations {3} and {4}. If we do

7   this, and calculate spectrally resolved values of G_ν (solid lines), and also the surface emission,

8   E_ν (broken lines: assumed to be a black body at the surface temperature, and to be described

9   by the Planck radiation law), we obtain the results shown in Figure 5 [Brindley and Harries,

10   1998]. Results are given for two model atmospheres, tropical and polar, in units of W m^{-2}

11   (cm^{-1})$^{-1}$.

12

13   [Figure 5 near here]

14

15   Figure 5 clearly shows the dominating effect of the FIR on the water vapour greenhouse

16   effect.

17

18   In equation {1} above, the term ΔP was introduced, and in passing we might comment on its

19   significance in climate research. If ΔP is positive, it represents the energy stored in the

20   system, due to any processes, (an extreme example being deep ocean circulation), that causes

21   a delay in the temperature response to solar energy absorption. If ΔP is negative, this

22   represents energy lost to the system, for example, by scattering of sunlight back to space by

23   volcanic aerosol. The stored energy term depends principally on ocean parameters such as

24   deep ocean circulation rates and thermal mass, as well as transient parameters such as

25   atmospheric aerosol loading, and it has been suggested recently that ΔP may be measured

1   from broad band TOA net fluxes (from polar orbiting satellites, see: Wielicki et al., [2002];

2   Wong et al., [2006]; and from geostationary satellite, see Harries et al. [2005]. It is possible

3   that such detections of stored energy may be better attempted using spectrally resolved

4   measurements (e.g: see Brindley and Harries [1998] and Harries et al. [2001]): this will be

5   discussed in a future paper.

6

7   The question of the magnitude of the contribution of the FIR to the total infrared greenhouse

8   effect in the climate system is important: if, as Figure 5 suggests, it is a significant

9   component, then it must be treated in detail and with accuracy in climate models. In a series

10   of studies, Sinha and Harries [1995; 1997] used tropical and sub-arctic standard atmospheres

11   and a band model to simulate the OLR spectrum at the TOA, and integrated the spectrum to

12   estimate the FIR[8] and total fluxes leaving the TOA. The principal findings are shown in

13   Table 1, and refer back to Figure 5.

14

15   [Table 1 here]

16

17   The parameters shown in the Table for the two standard atmospheres represent the spectrally

18   resolved total greenhouse parameter, G_v and the normalised greenhouse parameter, g_v, as

19   defined above. The Table also shows the change in the total outgoing longwave radiation

20   (OLR) due to a doubling of CO_2 in the band model; and the change in water vapour amount

21   required to give the same OLR change as the doubling of CO_2. As we can see, the FIR

22   contribution to the total water vapour radiative forcing at wavenumbers less than 500 cm^{-1}

23   amounts to between $^1/_5$ and $^1/_2$: expressed as a fraction of the total greenhouse effect (for all

24   absorbers) of the atmosphere, the fraction below 500 cm^{-1} lies between ¼ and $^1/_3$ Of course,

25   taking a different boundary for the FIR, for example 15 μm, would increase these fractions.

1

2　This discussion of the contribution of the FIR to the total integrated OLR raises the issue of

3　whether, in reverse, measurements of broadband fluxes by ERB radiometers in space could be

4　analysed so as to throw light on the FIR radiative energy budget. At first it would seem a

5　difficult prospect, since so many variables (surface temperature and emissivity, cloud type,

6　height and extent, and atmospheric temperature and composition) all affect the balance

7　between the MIR and FIR.   Nevertheless, such a study would be worthwhile, since the

8　increase in our understanding of the role of the FIR could be significantly enhanced.

9

10　Earlier in this section we mentioned a controversy over the sign of the water vapour feedback:

11　is it positive or negative? The most obvious analysis would indicate a positive feedback:

12　higher temperature means more evaporation and more water vapour, which means further

13　warming. However, Lindzen [1990], controversially suggested that the feedback could be

14　negative, depending on the drying of the upper troposphere by descending, desiccated air.   A

15　number of rebuttals of this view have since been published, which we will not review at

16　length here, because it is some way from our main theme of the FIR. So, we refer to the

17　valuable review of the water vapour feedback by Held and Soden [2000], where much more

18　detail can be obtained. We also note in passing that the use of the Mt Pinatubo volcanic

19　eruption as a means of demonstrating the positive feedback of water vapour, by Soden et al

20　[2002] was a sophisticated riposte to the Lindzen view.

21

22　**3.2　Cloud feedback and the FIR**

23

24　The greenhouse effect of both water and ice clouds have been recognized to be of particular

25　importance in the mid-infrared window and in the FIR regions [Maestri, 2000; Rizzi and

---

[8] Note that in the studies reported, Sinha and Harries chose the range 0-500 cm^{-1} to represent the FIR.

1   Maestri, 2001]. Simulations of the impact of ice clouds on the spectral greenhouse

2   parameters, g_ν and G_ν, are reported in Figure 6. In the plot a tropical standard atmosphere is

3   considered. Calculations of the greenhouse parameters are repeated for various values of the

4   cloud optical depth (and hence transmittance), values of which are provided in the upper

5   panel. The upper panel shows the absolute effect: as the transmittance through the ice cloud

6   gets smaller, so the radiance escaping to space decreases, and G_ν gets larger (equation {4}).

7   A strong effect is obviously revealed in the 800-1200 cm^{-1} window region, but a similar

8   amount of energy is also trapped in the atmosphere in the FIR region by the cirrus cloud.

9   The lower panel shows, for the same three cases, the normalised greenhouse parameter, g_ν.

10   This indicates that, relative to the emission from the surface, the greenhouse trapping

11   increases with wavenumber: however, in absolute terms (upper panel), the FIR is clearly very

12   important in the effect of ice clouds on the planetary radiation balance.

13

14   The upper panel of Figure 6 also shows that the spectral region near 400 cm^{-1} is as sensitive as

15   the 750-1000 cm^{-1} window to the presence of ice clouds in the high atmosphere. This occurs

16   because at the heights typical of cirrus clouds [Poore et al., 1995], even the strong FIR water

17   vapour absorption is not strong enough to obscure the clouds when seen from space. This

18   would not be the case for lower, liquid water clouds: at the lower altitudes typical of liquid

19   water clouds, the FIR transmittance to space is very small, and they have little impact in the

20   FIR on the greenhouse effect. Further investigation [Rizzi and Maestri, 2001] of the results

21   shown in Figure 6 were able to demonstrate that the radiance to space depends in a complex

22   way on both the physical (height and thickness) and optical (effective radius, ice water mass)

23   ice cloud parameters.

24

25   [Figure 6 near here]

26

1   Rizzi and Maestri [2003] also studied the FIR contribution of clouds to the radiative balance

2   through the use of the parameter known as the cloud radiative forcing (CRF) [Ramanathan,

3   1987; Hartmann et al., 1986; Cess and Potter, 1988; Cess et al, 1990, 1996]. The CRF can also

4   be computed by differencing the clear-sky and total-sky radiative fluxes, and by using satellite

5   radiation budget data it is possible to estimate the effects of actual cloudiness on the TOA heat

6   balance and the dependence of these effects on location and season [Hartmann et al., 1986].

7   CRF is especially useful in quantifying the interactions between clouds, radiation and climate at

8   the TOA [Stuhlmann, 1995] since it provides an immediate picture of how much emitted

9   radiation is trapped and of how much solar radiation is reflected by clouds with respect to clear

10   sky conditions. Although cloud radiative effects do respond to greenhouse forcing as a

11   feedback, nevertheless, this view of a stand-alone forcing has its merits. A positive CRF

12   indicates that the clouds cause a warming of the overall Earth-atmosphere system, and *vice*

13   *versa* [Doelling et al., 2001]. The major limitation of this parameter is that the vertical

14   distribution of the cooling and warming is not dealt with. Nevertheless CRF is a fundamental

15   quantity needed to constrain the effects of clouds within short or long-term climate models and

16   should be determined as accurately as possible [Doelling et al., 2001].

17

18   Despite its theoretical simplicity, the calculation of the CRF from broadband Earth Radiation

19   Budget measurements is a very demanding task [Hartmann et al., 1986; Stuhlmann, 1995;

20   Tian and Ramanathan, 2002; Futyan et al, 2005]. For example, in many tropical convective

21   regions the large long-wave and short-wave cloud forcing more or less compensate each

22   other, so that it is extremely important to be able to measure very accurately the two

23   contrasting terms constituting the total CRF. Rizzi and Maestri [2003] were interested in the

24   FIR contribution to long-wave CRF (LCRF) in the presence of realistic clouds, focusing their

25   attention on the tropical and the sub Artic winter standard atmospheres. They studied the error

26   that can be introduced in the estimate of LCRF when radiation is measured by broadband

1 radiometers with an incomplete long-wave spectral coverage, since this is a common

2 instrumental problem.

3

4 Following these authors, the LCRF expressed in terms of radiance, R_t [W/m^{2}sr], is given by

5 F_t:

6

7 $$F_t = R_t - R_t^*$$ {5}

8

9 where the asterisk indicates a cloudy scene, and the subscript, t, denotes a perfect

10 measurement (ie the actual LCRF), extending over the whole long-wave emission spectrum.

11 By analogy with equation {5}, a similar expression ($F_m = R_m - R^*_m$) can be written for the

12 LCRF derived from a broadband radiometer which is insensitive to part of the FIR emission

13 spectrum, for example by the use of a spectral filter. Here the subscript m stands for

14 measured. The error in LCRF due to incomplete spectral coverage is given by F_t - F_m and the

15 quantity $D = 100*(F_t - F_m) /F_t$ defines the percentage fraction of energy that cannot be

16 measured for technical limitations, weighted against the real LCRF.

17

18 Rizzi and Maestri [2003] showed that D is always positive (except possibly in some SAW

19 conditions when stratus clouds are embedded into a temperature inversion), so that

20 uncorrected measurements from sensors with incomplete spectral coverage produce a

21 systematic underestimation of the real LCRF. The value of D becomes particularly important

22 in presence of cirrus clouds (1 to 5% for the case considered by the authors), especially for the

23 highest cirrus cloud (15.4 km in the cited paper), not an uncommon situation in the tropics.

24

25 D is plotted in Figure 7 as a function of cloud transmittance at 900 cm^{-1} for three cases of

26 tropical cirrus and one of sub-arctic cirrus. It was assumed that an instrument having a filter to

1   block all radiation below 350 cm^{-1} was used. The Figure shows that for a given cloud type D

2   can be considered nearly constant with transmittance (that is for various values of ice water

3   content, IWC), and this same result (albeit with different numerical values) is obtained with

4   other types of filters and different cut-off values. The nearly constant behaviour is obtained

5   since the difference between the unmeasured part of the spectrum in clear and cloudy

6   condition, due to a particular type of cloud, increases almost linearly with decreasing

7   transmittance, and the rate of increase is almost the same as the rate of increase of the real

8   LCRF with transmittance.

9

10 **4.   Retrieval of atmospheric composition and clouds in the FIR**

11

12 **4.1   Retrieval of water vapour profiles using the FIR**

13

14 Water vapour vertical profiling from space using the inversion of emission features in the

15 outgoing longwave spectrum has been limited for the past 30 years mainly to measurements

16 in the ν_2 water vapour vibrational-rotational band, centred at 1595 cm^{-1}, for both operational

17 and research sensors. One early project which attempted to measure the water vapour profile

18 from space using the pure rotational band was the SIRS-B radiometer [Nithianandam et al.,

19 1993], and recent work described below has pointed to advantages that may exist using FIR

20 techniques.

21

22 Recently, Rizzi et al. [2002] analysed the potential water vapour retrieval performance

23 attainable from spectral measurements with a resolution of 0.5 cm^{-1} in the FIR, from 200 to

24 1000 cm^{-1}. A technique known as the σ-IASI methodology [Amato et al., 2002] was applied,

25 and it was found that the sensitivity of the rotational band to water vapour perturbations, as

26 measured by the matrix of the derivative of spectral radiance with respect to water vapour

1 amount (the Jacobian), may reach values 6 to 7 times greater than that exhibited using the ν_2

2 band: this implies greater sensitivity of the radiance to changes in water vapour amount in the

3 FIR than in the mid-IR.

4

5 As an example, for the case of a tropical atmosphere standard model, Figure 8 shows a mesh

6 surface of the Jacobian derivative matrix, defined by

7

8
$$K(\nu,z) = \frac{\partial R(\nu)}{\partial q(z)} \qquad \{6\}$$

9

10 where K is the Jacobian, ν and z are wave number and altitude, respectively, R denotes the

11 spectral radiance and $q(z)$ is the water vapour mixing ratio profile. In practice the kernel, K, is

12 computed for a discrete set of $\nu \equiv \nu_1, \quad ,\nu_M$ and $z \equiv z_1, \quad ,z_N$, so that the size of the resulting

13 matrix, K is $M \times N$. Figure 8 illustrates the magnitude of $K(\nu, h)$ for the pure rotational band

14 (top) and the ν_2 vibrational-rotational band (bottom), illustrating the much greater magnitude

15 of the Jacobean in the FIR. Of course, the Jacobian does not take account of the fact that

16 photon energies, and therefore radiances, R, are intrinsically larger at higher wavenumbers, an

17 effect which must also be taken into account. Nevertheless, to demonstrate a greater intrinsic

18 sensitivity is of interest.

19

20 [Figure 8 near here]

21

22 Since it is not immediately possible to capture all information present in a Jacobian

23 computation because of its 2-dimensional complexity, the problem of water vapour retrieval

24 capability using information content analysis has been addressed by a number of authors

25 [Tarantola, 1987, Rodgers, 1976, Serio et al 2007]. This method also properly addresses the

1 problem of the accuracy of the observations, which, in turn depends on the detector

2 technology.

3

4 In order to simulate a FIR sensor retrieval performance, we need to define the following:

5

6 1. A suitable set of atmospheric states to be used as reference in all the calculations.

7   This basic set is used to compute an a-priori covariance matrix [Rodgers, 1976].

8 2. A minimum set of parameters which define a given technology, i.e. in this case an

9   IR/FIR spectrometer, used to record the spectral observations. The set used includes:

10   - the radiometric noise (used to build up the observational covariance matrix);

11   - the Instrumental Response Function, $S(\nu)$, of the measuring instrument

12   (convolved with the infinite resolution spectrum to simulate the finite

13   resolution of the real spectrometer), assumed to be a Fourier transform

14   spectrometer.

15 3. A reference inverse methodology [Rodgers, 1976].

16

17 *Item 1: Atmospheric states.*

18

19 • A set of *state vectors*, which are representative of the widest atmospheric conditions,

20 has been used. This set has been developed at ECMWF by Chevalier [2001].

21

22 *Item 2: Instrument parameters*

23

24 We assume the use of a Fourier Transform Spectrometer (FTS), which is defined by the

25 spectral range or bandwidth, $S(\nu)$, and the radiometric noise budget. The spectral coverage is

1　assumed to be 200 to 1000 cm^{-1}; $S(v)$ has been assumed to be a pure sinc function [Bell,

2　1972]:

3

$$S(v) = 2L \frac{\sin(2\pi vL)}{2\pi vL} \qquad \{7\}$$

5

6　where the maximum path difference of the FTS spectrometer L is chosen in such a way to be

7　consistent with a spectral resolution of $\Delta v = 0.5$ cm^{-1}, that is $L = \dfrac{1}{2\Delta v} = 1$ cm.

8

9　The radiometric noise budget applies at the level of a single detector, whose footprint at nadir

10　is assumed to be 10 km [Palchetti et al., 2006].

11

12　*Item 3: Reference inverse methodology*

13

14　To provide an extensive description of the inversion theory used would be beyond the scope

15　of this paper, and since references already exist, it is not necessary to go into details.

16　Basically, we move in the context of Statistical Regularization [Rodgers 1976] and derive the

17　information content tool by transforming the inverse solution to Principal Components space

18　via Singular Value Decomposition [Amato et al, 1995, Carissimo et al 2005, Serio et al 2007]

19

20　To make a comparison to the retrieval performance achieved with a realistic sounder in the

21　mid infrared (IR), we have used the results from a recent analysis in which the performance of

22　the mid infrared radiometer sounder (IR sounder) for the Meteosat Third Generation (MTG),

23　observing the v_2 vibrational band of water vapour between 1210 and 2000 cm^{-1}, was assessed

24　[Grieco et al., 2004].

The comparison shows that the H_2O retrieval capability in the far infrared is comparable to and sometimes slightly better than that obtained for the MTG IR sounder. This is illustrated in Figure 9, which shows the simulated H_2O retrieval accuracies for the case of the FIR rotational band, and for the MIR vibrational band. Apart from the tropopause level, the expected H_2O retrieval performance is better than 10% in the troposphere for both instruments. The FIR retrieval shows a slightly better performance than the MIR sounder in the tropopause/lower stratosphere region. This is to be expected because of the stronger intensity of the rotational band lines by comparison with the v_2 band. The water vapour accuracy can be improved, of course, by considering FIR sounders with a larger FOV (reduced horizontal spatial resolution), so that more photons reach the detector and the signal-to-noise is improved. A study by Serio et al [2007] provides quantitative information on the relation between horizontal and vertical spatial resolution and the number of independent pieces of information that are available in the retrieval.

4.2   Water vapour retrieval in the presence of clouds (and vice-versa).

Infrared data are frequently affected by clouds. Thus, observations must be processed for operational data assimilation and inversion for geophysical parameters (temperature and water vapour), either by screening to remove cloud-contaminated soundings or by a so-called process of cloud clearing. It should be stressed that, for meteorological applications, operational numerical weather prediction centres currently use cloud-screened or cloud cleared data. This is mostly because of time processing constraints. Forward calculations in the presence of clouds remain time-consuming, making real time applications difficult. Cloud

1   screening or cloud detection is the first step in the assimilation chain of infrared radiances and

2   it has been proved that high spectral resolution infrared observations in the atmospheric

3   window (800 to 900 cm^{-1}) can be effectively used for this task [Serio et al., 2000, Masiello et

4   al., 2002].

5

6   The cloud clearing process can increase the uncertainty in the observed spectral radiances.

7   However, the spectral radiance uncertainty is typically confined below 1 K (in terms of

8   brightness temperature) for most of the cases [Rizzi, 1994, Rizzi et al., 1994, Li et al., 2005],

9   and the retrieval accuracy is only slightly degraded with respect to that shown in Figure 9 for

10   clear sky.

11

12   Another approach which is now becoming popular is to retrieve water vapour only above the

13   cloud [Li et al, 2007], which again takes us back to the clear sky case discussed in the

14   previous section. Crucial to this method is the correct determination of the cloud top height

15   and temperature. The most powerful method to perform this task is the so-called CO_2 slicing

16   method, which exploits the altitude sensitivity of narrow-band CO_2 channels located in the

17   CO_2 absorption band at 15 μm [Chahine, 1974].

18

19   For water vapour retrieval in the upper part of the atmosphere, the limb sounding

20   measurement mode is commonly used. In this mode, we observe the atmosphere with a long

21   horizontal optical path, and with this geometry of observation even optically thin (in the

22   vertical) clouds can significantly attenuate the atmospheric signal, and jeopardise the

23   sounding of the atmospheric composition. However, this effect is not the same at all

24   wavelengths. Figure 10 illustrates this by showing the variation of ice particle extinction

25   coefficient (the sum of both absorption coefficient and scattering coefficient) as a function of

26   ice particle size and wavenumber. The variations shown in Figure 10 suggest the possibility

1   that the FIR might in some cases be used to penetrate deeper into a cloud that at MIR

2   wavelengths. Indeed, it is possible that more detailed studies may reveal that the FIR and the

3   MIR have sufficiently complementary properties of absorption and scattering that they may

4   advantageously be used in combination to detect the presence of clouds [Raspollini et al.,

5   2006; Reburn et al., 1998]. Further work is required.

6

7   [Figure 10 near here]

8

9   Turning to much longer wavelengths, in the millimetre wavelength region, a very useful

10   region of high transparency is observed even for the most dense ice cirrus clouds. In a case

11   study performed for the MARSCHALS instrument [Oldfield et al., 2001], which observes the

12   atmospheric emission in the millimetre wave region with a spectral resolution of 200 MHz ,

13   Del Bianco et al. [2007] have quantified the loss of information caused by ice clouds when

14   making atmospheric composition measurements with this instrument. They showed that the

15   effect of most clouds is adequately described with a model of atmospheric continuum

16   absorption. In the case of optically thick clouds, retrieval errors can occur because of

17   scattering effects and the problem of detecting sharp discontinuities in a cloud, when

18   observing with limited vertical resolution. When cloud altitude and scattering are correctly

19   modelled, a limited loss of information is caused by the presence of cloud. In the worst case it

20   has been shown that there is a loss of about 7% in terms of information content, relative to

21   cloud free conditions [Carli et al, 2007].

22

23   [Figure 11 near here]

24

25   Obviously, whatever the observation geometry, there is a complementary issue, which is the

26   characterisation of cirrus clouds from observations of the real atmosphere in the presence of

1   the interfering effects due to water vapour, carbon dioxide and other absorbers. Del Bianco

2   [private communication, 2007] has carried out calculations of how the FIR and MIR spectra

3   are affected by ice crystals. Figure 11 shows some examples of such calculations for a variety

4   of parameters including cloud altitude, ice water path, crystal habit and phase. Frame (a)

5   shows clear sky, water cloud and ice cloud spectra. Frames (b) to (f) show a series of

6   difference spectra, identifying how the difference signals between clear sky and cloudy skies

7   depend on water phase, altitude, ice content, particle radius and shape.   Clearly, there is a

8   large amount of information contained in these difference spectra, which can be used to

9   characterise clouds from spectral measurements. Yang et al (2003) were able to show that

10   FIR spectral signatures of ice are useful in the retrieval of ice cloud properties: for example,

11   they show that the brightness temperature near 400 cm^{-1} is sensitive to ice crystal size, and

12   that the brightness temperature difference between 250 and 560 cm^{-1} is sensitive to optical

13   thickness. However, these signals are not unambiguous, and more detailed studies are needed

14   to determine precisely how much information on an unknown cloud can be extracted from

15   FIR spectral measurements.

16

17   **5.**   **Observational studies of the FIR spectrum of the atmosphere and Earth system**

18

19   In this section we review experimental work on the properties of the FIR spectrum of the

20   Earth's atmosphere. Following a short historical perspective, we describe work using

21   commercial interferometers to understand the continuum absorption of water vapour, and new

22   instrument developments to measure the FIR spectrum from aircraft and balloons (TAFTS,

23   REFIR and FIRST), and refer to efforts to develop a design for a future satellite FIR

24   spectrometer (REFIR).

25

26   **5.1**   **Early submillimetre and FIR investigations**

1

2 With the development of the energy-efficient technique of Fourier transform spectroscopy

3 [Bell, 1972] in Europe (pioneered by workers such as Jacquinot and Fellgett), the weak

4 photon energies typical of the FIR became accessible when ambient temperature detectors,

5 such as the Golay cell, and the pyroelectric detector were used. Groups in the UK (National

6 Physical Laboratory; Queen Mary College), France (Observatoire de Meudon; Office

7 National d'Etudes et Recherches Aeronautique), Canada (U. Calgary), Italy (U. of Florence;

8 the National Research Council, CNR), and the USA (Smithsonian Astrophysical Institute;

9 National Center for Atmospheric Research) began to develop Fourier spectrometers,

10 detectors, and Fourier transform analytical techniques, to study the lower atmosphere (a

11 hindrance to astronomy at these wavelengths), and the stratosphere (which, because of the

12 very high line strengths in the FIR, and very low water vapour mixing ratios, proved to be an

13 ideal part of the atmosphere to be probed in the FIR).

14

15 The earliest work established the existence of transparent windows in the stratospheric

16 spectrum at submillimetre wavelengths, and a partly transparent troposphere from the surface

17 to space at millimetre wavelengths. Using the FIR to measure the humidity of the

18 stratosphere (still a controversial question at the time: was the stratosphere wet or dry?)

19 proved very successful [Gebbie et al., 1968, Burroughs and Harries, 1970, Harries, 1973,

20 1976]. With the advent of helium-cooled solid state detectors, the capability of FIR systems

21 increased dramatically, and measurements at higher resolutions (down to a few hundredths of

22 1 cm^{-1}) on aircraft and balloons became possible, introducing the possibility of measuring not

23 just the principal spectral features, due to H_2O, and O_2 and O_3, but many other minor

24 constituents, through their pure rotational spectra. Numerous experiments to study this

25 spectral region from aircraft [Harries et al., 1972; Bussoletti and Baluteau, 1974; Marten and

26 Chauvel, 1975; Mankin, 1975; Carli et al., 1977] were used to study the FIR spectrum and the

1   composition of the upper troposphere and lower stratosphere. Other systems were developed

2   for the more exposed environment of high altitude (40 km) balloon flights, when mid-

3   stratosphere water vapour and other constituents were measured [Harries , 1977; Clark and

4   Kendall, 1976; Carli et al, 1980].

5

6   The science of FIR spectroscopy in the laboratory also developed fast, with measurements of

7   the quantitative positions, strengths and half-widths of spectral lines becoming available,

8   essential, of course, for making quantitative determinations of atmospheric concentrations.

9   Work on many species took place, including polar molecules like H_2O, O_3 and more exotic

10   species such as nitric acid HNO_3 [Harries et al., 1971], as well as the collision-induced dipole

11   absorption in symmetric molecules such as CO_2 and N_2 at high pressures [Harries, 1970].

12

13   These measurements confirmed the spectroscopic properties of the atmosphere in the FIR.

14   For example, the long wavelength region from 4 to 200 cm^{-1} was studied by Baldecchi et al,

15   [1984, 1988]: this region was where most of the rotational spectra of those atmospheric

16   constituents with a permanent or transient dipole moment can be observed. Figure 12 shows

17   an example of the high resolution atmospheric emission spectrum measured with the IBEX

18   balloon experiment [Carli et al., 1984] from an altitude of 38 km at the limb with a zenith

19   angle of 91.6°. A portion of the spectrum between 45 and 65 cm^{-1} is displayed. The upper

20   panel shows a synoptic view of this 20 cm^{-1} spectral interval where it is possible to note some

21   general characteristics. Water vapour is present with some prominent spectral features that are

22   irregularly distributed (since the water molecule is a so-called asymmetric rotor [Herzberg,

23   1959]). A regular pattern of triplet lines is caused by molecular oxygen. Ozone is present with

24   some Q-branches that appear with a constant period and with many other ubiquitous lines.

25   When the fine structure of the spectrum is analysed (see lower panel for the expanded 61-69

26   cm^{-1} region), the contribution of several minor constituents can be observed. In this spectral

1 interval emission lines due to HCl (with its two isotopes), CO and OH can be observed. Other

2 interesting contributions are those of some isotopes of water vapour (HDO and H_2O^{17}) and of

3 ozone (^{18}OOO and $O^{18}OO$) as well as some rotational transitions of vibrationally excited

4 ozone, identified with their vibrational quantum numbers.

5

6 [Figure 12 near here]

7

8 Several other features have been observed in the spectral region between 4 and 200 cm^{-1}, in

9 addition to those already mentioned: these include HNO_3 , N_2O, NO_2, HCN, ClO, HF, HBr,

10 HOCl, H_2O_2, HO_2 and atomic oxygen, O. Notably missing in the FIR are the features of CO_2

11 and N_2 which do not have a permanent dipole moment, and therefore no rotational spectrum:

12 these gases absorb in the FIR only under high pressures, when transient dipole moments are

13 induced in the symmetric molecules by forceful inter-molecular collisions [Harries, 1970].

14 Annex 1 provides a list of atmospheric constituent species which have been detected by FIR

15 spectroscopy in the Earth's atmosphere.   Since all molecules possessing a dipole moment

16 have rotational transitions in the FIR, this list is by now extensive.

17

18 Measurements in the FIR region have the disadvantage that the signal is intrinsically weak,

19 because the Planck function falls to low values at long wavelengths. However, there are also

20 advantages in the FIR. The atmospheric emission is observed in the Rayleigh-Jeans region of

21 the black-body distribution where the dependence on temperature, *T*, is only linear[9], so that

22 any errors in our knowledge of the atmospheric temperature cause less error in composition

23 retrieval than in other regions of the black body distribution, where the dependence of

24 radiance on temperature goes as a much higher power of *T*. Also, the line strength of the

25 rotational features can be accurately determined from dipole moment measurements, so that

1 measurements made with rotational spectra are intrinsically of high accuracy, and can be used

2 as a validation tool for the more difficult measurements made in other spectral regions

3 [Mencaraglia et al., 2006].

4

5 The typically weak signal in the FIR may be efficiently detected either using cryogenic

6 detectors or (where suitable local oscillators exist) heterodyne techniques. The latter

7 technique is currently exploited for spaceborne observation of minor atmospheric constituent

8 in the millimetre and submillimetre spectral region (e.g. the Microwave Limb Sounder

9 experiments: see Waters et al. [2006]).

10

11 **5.2   Ground based FIR observations and studies of continuum emission.**

12

13 **5.2.1   Background**

14

15 The continuum absorption due to water vapour was described in section 2.2, and continues to

16 be an un-resolved problem, meriting further work. With the advent and success of the

17 empirical CKD model [Clough et al 1989] for the water vapour continuum, a number of

18 experimental determinations of this absorption in the laboratory and the atmosphere have

19 taken place. This has led to a series of revisions to the empirical CKD model. A number of

20 the field campaigns have been based on an instrument whose basic design is due to ABB

21 Bomem Inc (ABB Bomem MR-100 series interferometer). [Knuteson et al, 2004a, 2004b].

22 The instrument is now deployed in many of the American ARM (Atmospheric Radiation

23 Measurement program) sites, where it is known as AERI (Atmospheric Emitted Radiance

24 Interferometer) [Ackerman and Stokes, 2003]. Most notable among these observations are

25 those taken with the version extended in the far infrared from SHEBA (Surface Heat Budget

---

[9] In equation B2, if $hf << k_BT$, then the exponential function can be simplified to $1 + hf/k_BT$

1   of the Artic Ocean) and the North Slope of Alaska ARM Atmospheric Radiation

2   Measurement) site [Tobin et al. 1999].

3

4   **5.2.2. Instrument Design**

5

6   In its basic version, the ABB-Bomem MR100 (hereafter MR100) is an FTS with a liquid

7   nitrogen cooled sandwich MCT/InSb detector to cover the 500 to 5000 cm^{-1} spectral region.

8   More precisely the detector provides sensitivity for 5 - 20 μm (MCT) and 2 - 5.5 μm (InSb) in

9   two separate channels. The spectral sampling is 0.4822 cm^{-1} for double-sided interferograms.

10   The absolute infrared spectral radiance of the sky is measured and calibrated using two

11   accurately (±0.01 K) stabilized infrared black body sources. A typical measurement cycle

12   consists of a sky dwell period followed by two dwell periods, one for each of the blackbodies.

13   The instrument field of view is about 40 mrad. The mirror movement is effected by means of

14   a flexi-pivot, which minimises wavefront tilt and shear.

15

16   **5.2.3. Campaign measurements**

17

18   The MR-100 instrument has been used during the Italian phase of the European AQUA

19   Thermodynamic Experiment (EAQUATE) [Taylor et al 2007] to acquire nearly continuous

20   observations of atmospheric emitted spectral radiance in the range 500 to 2000 cm^{-1} [Esposito

21   et al, 2007a]. During the campaign, atmospheric temperature and water vapour were profiled

22   by radiosondes, with a time sampling rate of approximately 2 hours. In addition, a microwave

23   radiometer was operated continuously with a time sampling rate of 5 minutes and a

24   ceilometer was used to detect the presence of clouds, with a time sampling rate of 20 seconds.

25   These additional data were used to provide the atmospheric state input to the forward model

26   to yield synthetic spectral radiance for comparison with the observations.

1

2 The comparison was aimed at testing the reliability of state-of-art line and continuum water

3 vapour absorption parameters in the far infrared. An example of this comparison is provided

4 in Figure 13, where various editions of the HITRAN database [Rothman et al., 1998, 2003,

5 2005], and two version of the newest MT_CKD Clough continuum model are compared

6 against the observations. While allowing us to check the quality of state-of-art line and

7 continuum absorption parameters, Figure 13 also highlights that there are still appreciable

8 differences among the various data base versions, which, in turn, lead us to conclude that

9 there is still need of research efforts towards the understanding of a portion of the spectrum

10 which plays a fundamental role in the Earth's radiation budget.

11

12   [Figure 13 near here]

13

14 A MR-100 spectrometer has recently been extended by the DIFA group and colleagues at

15 IMAAA[10] in Basilicata, Italy, to operate at longer wavelengths by the replacement of the

16 usual zinc selenide beamsplitter by a silicon one, and by adding a deuterated tri-glycine

17 sulphate (DTGS) detector. Further studies of the continuum using this extended instrument

18 are planned.

19

20 **5.3   Measurement of FIR heating rates with TAFTS – The Tropospheric Airborne**

21 **Fourier Transform Spectrometer**

22

23 **5.3.1   Instrument concept**

---

[10] IMAAA: Istituto di Metodologia per l'Analisi Ambientale

1   A novel radiometer, the Tropospheric Airborne Fourier Transform Spectrometer (TAFTS)[11],

2   has been developed at Imperial College to operate specifically in the FIR on aircraft

3   platforms, with the capability to observe nadir and zenith radiances, and to derive heating

4   rates. The aim is to study the in-situ radiative properties of the upper troposphere. A general

5   description of the TAFTS instrument and performance may be found in Murray et al [2007].

6   An example of early data may be found in Cox et al, [2007].

7

8   **5.3.2 Instrument design**

9

10   TAFTS is a differential, dual-input, polarising Fourier Transform Spectrometer (FTS), of the

11   Martin-Puplett kind [Martin and Puplett 1969]. This type of interferometer makes

12   simultaneous differential measurements of spectrally resolved radiance from two input ports.

13   TAFTS employs a sampling system that is particularly simple, and which also yields

14   diagnostic information on the vibration environment of the instrument as it affects the optical

15   path (vibration is often a problem on aircraft deployments of a FTS, and can give rise to

16   'ghosts' of real spectral features appearing in shifted spectral positions in the measured

17   spectra). TAFTS covers a wide spectral range at high spectral resolution: currently it operates

18   across two spectral bands covering 80 to 320 cm^{-1} and 320 to 600 cm^{-1}, but could operate up

19   to 1000 cm^{-1} with other detectors and optical filters. The instrument has a un-apodised

20   resolution of 0.1 cm^{-1} (see Bell [1972] for an explanation of 'apodisation', a process for

21   removing unwanted oscillations in the spectra measured by a FTS). The optical and detector

22   system employed in TAFTS provides two differential signals within each spectral band. The

23   cryogenic optical design makes use of high-efficiency non-imaging components such as light

24   pipes and concentrators. TAFTS is controlled by an on-board computer that employs a real-

---

[11] For extensive information about TAFTS, see: http://www.sp.ph.ic.ac.uk/tafts/

1   time Linux operating system. The instrument is designed to be fully autonomous or capable of

2   remote control via the internet. Table 2 details the instrument specifications.

3

4   [Figure 14 and Table 2 near here]

5

6   TAFTS comprises four units. These are: the pointing optics (scene selection including

7   calibration targets); the interferometer (dual input combiner and beamsplitter, sampling laser,

8   moving mirror and associated drive); the cryostat (cooled detector housing); and the

9   electronics control box. Figure 14 shows a simple schematic diagram of the optical layout of

10   TAFTS, showing the first three of these units. Each of the two inputs can be steered to view

11   either a hot or ambient temperature blackbody or a sky view. The radiation from these views

12   are steered into the interferometer housing and combined at the polariser beam-combiner P1.

13   P2 is a second polariser at 45° to the first, which acts as the beamsplitter. L1, L2 and L3 are a

14   combination of off-axis parabola and spherical mirrors which define the field of view and a

15   virtual aperture cold stop. LN2 and He represent low-pass filters at 79 K and 4.2 K

16   respectively, mounted on the radiation shields of the cryostat. P3 is a third polariser, which

17   acts as an analyser to separate the two complementary outputs of the interferometer [Martin

18   and Puplett, 1969]. Dichroic filters are used to transmit/reflect the radiation to the separate

19   long-wave and short-wave detectors. These detector blocks consist of an off-axis mirror and

20   hyperbolic concentrator, designed to reject off-axis radiation, and an integrating cavity which

21   houses the photoconductor. Further details of each of the four units are given in Murray et al.

22   [2007], and may be found via the web site quoted in the footnote.

23

24   **5.3.3   Laboratory performance**

25

In order to measure the instrument spectral sensitivity and ground-based performance, TAFTS

was placed within a N_2-purged polystyrene box with free-standing liquid nitrogen sources and

water vapour traps. The up-welling blackbody temperature was maintained at 337 K, and the

down-welling blackbody at 304 K. Interferograms were recorded, and the corresponding

spectra computed by complex Fourier transformation. The input blackbody temperature

difference was used to convert the raw spectral signal (a voltage) to a brightness temperature

scale, which was used to derive noise equivalent brightness temperature as a function of

frequency from the voltage noise fluctuations: this is shown in Figure 15. Both the longwave

and shortwave spectra are the sums of 30 2-second interferometer scans, equivalent in total to

a 60-second integration. The apodized spectral resolution is approximately 0.12 cm^{-1}. The

broad absorption features apparent in the short-wave channel (panel b) are caused by the

window and polariser substrate absorption (polypropylene and mylar). The increase in noise

equivalent brightness temperature towards the edges of the bands is due to falling instrument

throughput at the edges of filters and other components.

[Figure 15 near here]

5.3.4   Flight performance

TAFTS has now been flown on a number of aircraft missions. As an example, in November

and December 2002 TAFTS participated in the EMERALD II (Egrett Microphysics

Experiment with Radiation Lidar and Dynamics in the Tropics) campaign based in Darwin,

Australia. Atmospheric spectra were observed during an aircraft ascent from 4.6 km to 13.3

km, and measurements of the on-board TAFTS black body calibration targets were also taken.

The observed spectra were calibrated using laboratory calibration data, corrected for local

water vapour absorption in the instrument, and for any drift in detector sensitivity (as its

temperature changes during the flight), and finally averaged for a series of roughly equally

1   spaced flight levels. In order to derive the heating rate (see Box 1), the net flux in the vertical

2   is obtained by differencing the up- and down-welling spectra, and the vertical gradient of this

3   net flux then calculated, using the observations at the different flight levels. This vertical flux

4   divergence is then used to derive the heating rate in the local atmosphere, using equations

5   {B3} and {B4}.

6

7   Some of the calibrated net radiance spectra measured during this campaign are reproduced in

8   Figure 16, which shows the net radiance measured at a number of flight levels between 7.5

9   and 13.55 km on the 19th November 2002: the heights are shown on the Figure. The

10   background slopes of these radiance spectra, of course, follow the shape of the Planck

11   function at the local air temperature. The increasing transparency of the many windows

12   between the strong water vapour lines as the aircraft flies at higher levels is clear. Bearing in

13   mind that the recording time for the spectra shown varies between 2 and 10 s, the signal to

14   noise ratio is excellent. The heating rates have been derived from these spectra in the manner

15   described in Box 1 and section 2.3, and an example of early data is shown in Figure 17

16   [Straine, 2005]. Initial comparisons with simulated heating rates show these measurements to

17   be similar, except that the effect of variations with height in the vertical distribution of water

18   vapour causes very significant variability in the heating rates. For this reason, direct

19   observations are essential to establish that we understand this sensitivity. Further work on

20   heating rate determination from TAFTS is being prepared for publication.

21

22   [Figure 16 near here]

23

24   [Figure 17 near here]

25

26   **5.4   REFIR - Radiation explorer in the far infrared**

5.4.1   Instrument concept

A European consortium has proposed the flight of a FIR spectrometer plus ancillary instrumentation in low Earth orbit. The concept of the REFIR space mission was developed to address several important issues relating the climate and the hydrological cycle, exploiting the FIR [Rizzi et al., 2000; Rizzi et al., 2001].

In the initial REFIR design, the FTS was a polarizing interferometer with a novel optical scheme with double-port configuration (Figure 18) that is capable of resolving the upwelling radiation from the Earth, seen from the low Earth orbit, with sufficient spectral resolution (0.5 cm^{-1}) and signal-to-noise ratio (SNR>100) in broadband operations (100-1100 cm^{-1}), to allow scientific investigations of the atmosphere and climate.

[Figure 18 near here]

Figure 18 shows the optical configuration, described in more detail in Carli et al., [1999], which optimises the reliability of the spectrometer in particular for long lifetime space applications, and its performance for ambient temperature operations. Two prototypes of the REFIR FTS have been developed for laboratory testing and use in field operations [Serio et al.,, 2002]: REFIR-BB (Breadboard) for ground-based campaigns [Palchetti et al., 2005] and REFIR-PAD (Prototype for Applications and Development) for air-borne campaigns [Bianchini, 2006 a and b].

5.4.2 Prototype characteristics and performance

1   The two prototypes have been used to study different solutions. The main design requirement

2   of wideband coverage with uncooled operation can be met by using efficient wideband beam

3   splitters (BS) and high-performance room-temperature detectors. The detectors chosen were

4   doped tri-glycine sulphate (DLATGS) pyroelectric effect detectors, with low noise equivalent

5   spectral radiance (NESR). Polariser BS were developed and tested, but efficiency was found

6   to be poor, especially above 700 cm^{-1}. Best performances were obtained with amplitude BS

7   (using a thin germanium (Ge) film deposited on Polyethylene Terephthalate (PET)

8   membrane) in combination with the pyroelectric detectors. In this case, the input/output

9   polariser (the one at 45° in Figure 18) is removed and the interferometer configuration

10   becomes the Mach-Zehnder scheme [Jenkins and White, 1981]. The other optical

11   characteristics, such as the double-port configuration, and the full tilt compensation of the

12   moving mirror are maintained.

13

14   Table 3 provides a summary of the main parameters that characterise the prototype design.

15

16   [Table 3 near here]

17

18   Both prototypes were characterised under vacuum and in laboratory conditions. The noise was

19   dominated by the detector component and was found to be constant under different working

20   conditions. Figure 19 shows, for instance, the NESR measured under vacuum with REFIR-

21   PAD (operated with Ge-coated PET BS and 30 s acquisition time) and REFIR-BB (operated

22   with polarising BS and 120 s acquisition time). This performance was also obtained during

23   the field operations described in the following section.

24

25   [Figure 19 near here]

26

1 **5.4.3   Ground based and stratospheric balloon observations**

2

3 The REFIR-BB instrument was tested in June 2004 in a ground-based field campaign held at

4 Toppo di Castegrande at 1285 m altitude in South Italy [Esposito, 2007a and b]. The

5 downward atmospheric emission spectrum was measured and compared with that measured

6 by a commercial FTS (BOMEM MR100) measuring above 500cm^{-1}, and is shown in Figure

7 20.   This shows the atmosphere to be opaque below about 450 cm^{-1}, so that radiance curve

8 follows the Planck radiation law for some local temperature. Between 450 and 620 cm^{-1} the

9 partially transparent window between the water vapour pure rotational band and the CO_2 ν_2

10 band shows some transparency, before the intense centre of the ν_2 band again causes the

11 atmosphere to be opaque. On the high frequency side of the ν_2 band the downwelling

12 radiation rapidly falls to much lower intensity in the atmospheric window. The lower panel of

13 Figure 20 shows that the two measured spectra agree to within about ± 5% error.

14

15   [Figure 20 near here]

16

17 The measurement was simulated for clear sky using the Line-by-Line Radiative Transfer

18 Model (LBLRTM: See Clough et al, [1992]; Clough and Iacono, [1995]), which was used to

19 compute spectra based on water vapour and temperature vertical profiles measured by

20 radiosonde observations during the mountain observations.

21

22   [Figure 21 near here]

23

24 Figure 21 shows the result expressed in terms of brightness temperature (BT), for the

25 expanded spectral band 500-650 cm^{-1}. This result demonstrates that REFIR-BB is able to

26 accurately measure the spectral structure in the water vapour rotational band from ground-

1 based observations. Thus, this first attempt seems to demonstrate that the REFIR concept,

2 using un-cooled components is feasible. This is a realisation of great importance to the

3 feasibility of a future FIR satellite experiment.

4

5 REFIR-PAD was integrated in 2004 on board a gondola belonging to the Laboratoire de

6 Physique Moleculaire pour l'Atmosphere et l'Astrophysique (LPMAA-CNRS, France), which

7 also carried the balloon-borne simulator of the Infrared Atmospheric Sounding Interferometer

8 (IASI) instrument. The instruments were flown for the first time on the 30th of June, 2005

9 from the Timon airfield, near Teresina, located in the North-East Brazil (5°5'S, 42°52' W).

10 The flight reached the mean floating altitude of 34 km for about 8 h, and a total of 1080

11 spectra of the upwelling atmospheric emission spectrum were measured.

12

13 Figure 22 shows a typical result and the comparison with the measurement of the IASI-

14 balloon prototype sharing the same platform and covering the spectral range above 650 cm^{-1}.

15 The results [Palchetti et al., 2006; Bianchini et al., 2006a and b] indicate agreement within a

16 few percent between the observation and the simulation, and therefore confirm that the

17 different components of the Earth's OLR, including the FIR, can be detected with a single

18 uncooled instrument using uncooled detectors, with a NESR of about 2 mW (m^2 sr cm^{-1})$^{-1}$

19 (see Figure 19), and an absolute calibration error which is less than 0.5 K at 280 K.

20

21   [Figure 22 near here]

22

23 These developments and results for REFIR clearly indicate that the feasibility is very high of

24 developing a FIR spectrometer with moderately high spectral resolution (0.25 cm^{-1}: see Table

25 3) for accurate measurements of the FIR spectrum of the Earth from space.

26

1   **5.5   The Far-Infrared Spectroscopy of the Tropsophere (FIRST) Instrument**

2

3   **5.5.1   Instrument Concept**

4

5   The FIRST instrument was developed by the NASA Langley Research Center, USA, in

6   partnership with the Space Dynamics Laboratory (Utah State University) and the Harvard

7   Smithsonian Center for Astrophysics, both also from the USA: the project was funded by

8   NASA.   FIRST is a Michelson Fourier Transform Spectrometer (FTS), designed to

9   demonstrate the ability to measure the spectrum between 1000 and 100 cm^{-1} (10 to 100 μm)

10   globally on a daily basis at high spatial resolution (10 km from low earth orbit), high spectral

11   resolution (0.625 cm^{-1}), and high temporal resolution (one spectrum every 1.4 sec), on a

12   single focal plane. A critical aspect of the FIRST design is the ability to measure the spectrum

13   between 10 and 15 μm in addition to the far-IR spectrum from 15 to 100 μm. The former

14   interval allows for direct comparison with conventional mid-infrared spectral sensors for the

15   purpose of calibration and validation, which is essential for confidence in the calibration of

16   the far-IR part of the spectrum for which accurate radiometric standards are not as well-

17   developed.

18

19   **5.5.2   Instrument Design**

20

21   The FIRST instrument consists of a scene select mirror, the FTS, aft optics, a detector

22   assembly, and associated electronics [Mlynczak et al., 2005]. The FTS and aft optics are

23   cooled to ~180 K by liquid nitrogen, to reduce background and simulate spacecraft

24   conditions. The detectors are cooled to 4.2 K, and the rest of the instrument is at ambient

25   temperature. Thin polypropylene windows isolate the cold FTS optics from the scene select

26   mirror and from the detector cryostat. During balloon flights the scene select mirror alternates

between a nadir view of the Earth, a high elevation angle space view that is used to estimate

instrument background, and an ambient-temperature blackbody calibration source. The FTS is

a compact plane mirror Michelson interferometer that achieves very high throughput (0.47

cm^2 sr) with a modest 7 cm diameter beam. Broadband response (50-2000 cm^{-1}) is made

possible by a bilayer thin-film beamsplitter. FTS scanning and detector sampling are

controlled by a separate metrology laser interferometer that monitors the position of the scan

mirror. Interferometer alignment (for both the infrared and laser interferometers) can be

adjusted if necessary during the balloon flight by remotely controlling the tip and tilt of the

non-scanning interferometer mirrors.

The FTS scans over optical path differences of $\pm$ 0.8 cm to achieve the nominal unapodized

resolution of 0.625 cm^{-1}; the scan time varies from 1.4 to 8.5 s, depending on the detector

sample interval. Trimming and centering the interferograms reduces the realized unapodized

resolution to 0.643 cm^{-1}, which is the resolution of all the FIRST data presented in this paper.

The aft optics focus the collimated FTS output onto an array of Winston cone concentrators,

coupled to discrete silicon bolometers in individual integrating cavities. The focal plane is

37.5 x 37.5 mm, large enough for a 10x10 array of cones and detectors, although for the

demonstration flight the focal plane was populated with a total of 10 cones (2 in each corner

and 2 in the center.) The focal plane is sized to demonstrate the technology required to obtain

daily global coverage from a cross-track scanning instrument on an orbiting satellite. The 100

detector focal plane, with each detector recording a spectrum every 1.4 seconds, and scanned

$\pm$ 48 deg from nadir, would achieve daily global coverage, approximately 5 million spectra

per day, from a low-earth orbiting satellite.

To simulate the space observation configuration, FIRST was designed to operate from a

gondola on a high altitude balloon. The instrument first flew on June 7, 2005, and achieved an

1   altitude of 28 km, lifted by an 11 million cubic foot helium-filled balloon. The results from

2   this flight are reported by Mlynczak et al. [2006]. A second flight occurred on September 18,

3   2006, and achieved an altitude of 33 km. Both flights were successful in recording

4   approximately 6 hours of data at the balloon float altitude, simulating operation in and

5   observations from a space-like environment. The flights occurred from the NASA Columbia

6   Scientific Balloon Facility located in Ft. Sumner, New Mexico. In addition, both flights

7   occurred with a simultaneous overpass of the NASA Aqua satellite at approximately 2:00

8   p.m. local time, offering the opportunity to compare directly spectra measured by the AIRS

9   instrument in the mid-infrared part of the spectrum common to both sensors, and to compare

10   the measured far-IR spectrum with those computed from AIRS temperature and moisture

11   profiles. With the exception of the latter part of the 2006 flight, both flights observed clear-

12   sky conditions.

13

14   [Figure 23 near here]

15

16   Figure 23 shows a radiance spectrum recorded by FIRST from the June, 2005 flight. The

17   spectrum clearly shows the complex spectral structure of the far-IR (see earlier in this paper)

18   with alternating regions of strong and weak lines, evidenced by the variation in radiance (or

19   equivalently, in the brightness temperature) of the lines. The spectrum covers the spectral

20   region from approximately 2000 cm^{-1} (5 μm) to wavenumbers less than 100 cm^{-1}. There are

21   some gaps in the spectrum which correspond to regions in which the FIRST beamsplitter

22   exhibits significant absorption, and whose effects have not yet been corrected. Otherwise,

23   Figure 23 confirms not only the complexity of the far-IR structure, but also shows the ability

24   of the instrument to observe essentially the entirely energetically significant infrared spectrum

25   of the Earth and its atmosphere between 5 and 100 μm.

26

1   [Figure 24 near here]

2

3   Figure 24 presents a comparison of a FIRST brightness temperature spectrum and a spectrum

4   from the AIRS instrument recorded during the June 2005 flight. The agreement between the

5   two spectra, typically to within 1-2 K, demonstrates remarkable consistency between the two

6   sensors, especially considering that from balloon flight altitude the FIRST footprint is about

7   200 meters diameter while the AIRS sensor is 14 km diameter, nearly 5000 times larger than

8   FIRST. The comparison illustrated here validates the calibration of the FIRST sensor.

9

10   [Figure 25 near here]

11

12   In Figure 25 we show far-IR spectra recorded about 2 p.m. local time from the 2005 and 2006

13   flights. The radiances recorded in 2006 are clearly smaller than in 2005 from 400 to 600 cm^{-1},

14   by as much as 15% (see black difference spectrum). Based on the brightness temperatures in

15   Figure 23, the radiation in this interval comes from the lower troposphere between 600 and

16   850 hPa. The temperature and moisture profiles recorded by the AIRS instrument

17   simultaneously with the FIRST spectra indicate that the lower troposphere between 700 and

18   850 hPa is 5 to 25 K colder during 2006 than in 2005, while the mass mixing ratios of water

19   vapor are slightly larger. At 600 cm^{-1}, a decrease of 15 K (from 270 K) results in a decrease in

20   radiance of approximately 20%. We therefore attribute the smaller radiances observed in 2006

21   primarily to a cooler lower troposphere.

22

23   The spectra from both FIRST flights have been processed and approximately 16,000 nearly

24   contiguous, nadir view spectra of the Earth are now available (approximately 9000 spectra

25   from the 2005 flight and 7000 spectra from the 2006 flight). The spectra may be obtained

26   from one of the authors (MGM).

6.   The future

We have seen from this review that the Earth is, indeed, a far infrared planet. Because of the heavily absorbing atmosphere at FIR wavelengths, the energy that is emitted to space comes from layers well above the surface, which are colder than the surface. Because the planet presents a colder emission temperature to space, so the peak black body energy is emitted at longer wavelengths, further into the FIR, than the emission from the surface. Conversely, the opacity of the atmosphere in the FIR is a major contributory process in keeping our planet's surface far more comfortable for mankind than otherwise. While it is unnecessary to define a specific arbitrary border between the FIR and elsewhere in the IR, it is vital to recognise that to fully understand the energy budget of the Earth, and to fully exploit the spectrum for remote sounding, a better knowledge of the longwave part of the spectrum, the FIR, is mandatory.

Up to recent times, our knowledge of the FIR, and our ability to explore the region, in the laboratory, in the field and in space, has been limited. However, as this review has shown, the last decade or two has been a period of major progress, in spectroscopy, in radiometry, in technology, and in measurements on the real atmosphere. We are now achieving measurements in the FIR with differing configurations (balloon, aircraft and ground based) that have a spectral resolution suitable for the observation of the atmospheric features, over a wide spectral range, and that are suitable for the characterisation of the radiation budget in clear skies, and in the presence of clouds. Preliminary comparisons of the measurements with models show that we have a good understanding of the radiative transfer in this spectral region.

Now, as we have seen in this review, we have several new instruments (TAFTS, REFIR, FIRST) that are capable of observing the far-IR from suborbital (aircraft and balloon) platforms. These instruments have also operated from the ground, observing in the zenith view the downwelling radiation from the atmosphere. Further experiments are planned from aircraft, balloons, and the surface (especially at cold sites, near the poles, or on mountains). We are also using these instrumental developments to set the scene for future FIR spectrometers that can be flown as part of all-IR instruments, in space.   There are still experimental difficulties, of course. We need more efficient, un-cooled detectors for the FIR, to remove the inconvenience of using liquid cryogens; more use of advanced cooling engines, when cooling is unavoidable; beam-splitter technology has some way to go to maximise efficiency; and there is always the hope of new, more efficient spectrometer designs.

Of course, scientific problems also remain. One of the most obvious spectroscopic problems that needs much further work is that of the water vapour continuum: this effect is still the major source of uncertainty in gaseous radiative transfer in the FIR. Because models for continuum absorption are constrained by laboratory and atmospheric measurements, it is important to improve the quantity and quality of spectrally resolved observation in the H_2O rotational band. Along this line there are programmes in both Italy (the ECOWAR[12] project) and the UK (the CAVIAR[13] project) which seek to make a concerted effort though laboratory and field measurements, theory and modelling, to put our understanding of this phenomenon on a much firmer basis.

---

[12] ECOWAR: Earth Cooling by Water Vapour Radiation: see: www.difa.unibas.it

[13] CAVIAR: Continuum Absorption at Infrared wavelengths and its Atmospheric Relevance: see: http://www.met.rdg.ac.uk/~sws01ivp/

A further scientific and observational problem is that we need to disentangle the interference between gas and cloud properties through a chain of validation activities. With a well calibrated instrument it will be possible to complete the on-going assessment of the spectroscopy of the clear atmosphere (line strengths; pressure broadening coefficients; line mixing effects; water vapour continuum). While cloud properties have been mainly derived from the mid infrared, Evans et al. [1999] have demonstrated that complementary information on cloud properties can be obtained in the very FIR (sub-millimetre) region. Spectrally resolved observations of the cloud in a broad spectral band that includes the FIR could provide exhaustive information on cloud composition, phase, altitude, IWP and equivalent particle size. The problem of cirrus cloud studies is twofold: to characterise their climatology, and to verify the mechanisms that govern the radiative exchange of the different types of cirri. In both cases field measurements are needed and observations in the FIR can provide a new and powerful measurement capability which fills a long due observation requirement.

We have shown through this review that, as a result of the research described, we now know far more than even just a decade ago about how to make measurements on the real atmosphere, and how to start the job of disentangling the absorption and emission by molecules, and the corresponding processes in clouds. We know more about how the FIR contributes to the TOA energy balance of the Earth, and the role that water vapour and ice clouds play in that balance. Knowing about these processes means that we are closer to being able to understand more accurately how global warming might affect the Earth. Finally, we have a much better idea about how to build the sensitive instruments that we need, and can now start to look forward with more expertise than before to the prospect of making measurements of our planet in the FIR from space.

1   Turning to the future, we note that it has been approximately 30 years since the last spectra of

2   the Earth at wavelengths longer than 15 μm were recorded from an instrument on an orbiting

3   satellite [Spankuch and Dohler, 1985], and nearly four decades since the Nimbus IV satellite

4   produced such amazing Earth IR emission spectra [Hanel et al., 1970; 1971]. In that time the

5   importance of the far-IR has been fully realized, especially with respect to the role it plays in

6   climate, and also in offering the possibility for the remote sensing of cirrus optical properties

7   from space.

8

9   For space based observations it now seems obvious that we must monitor our planet's state in

10 the FIR: a far-IR instrument should be flown as soon as possible. The recent Decadal Survey

11 [National Research Council, 2007] conducted by the U. S. National Research Council

12 recommends as its highest priority a mission with an instrument capable of covering 200 to

13 2000 cm^{-1} (5 to 50 μm) with a 1 cm^{-1} spectral resolution. The instrument must be

14 exceptionally well-calibrated (and stable) to detect small changes with time in the spectral

15 distribution of outgoing longwave radiation. After many years of investment we are on the

16 doorstep of a far more penetrating understanding of the FIR properties of our Earth, and of

17 realizing a measurement from space that is destined to revolutionize our knowledge of the

18 Earth's climate system.

19

20

21

22

23

1　Mr Michael Watson, Dr Gail Bingham, and Mr Stanley J. Wellard.

2

9

10

References

Ackerman T. and G. Stokes, (2003). The atmospheric radiation measurement program, *Physics Today*, 38-44.

Amato U., Carfora F., Cuomo V. and C. Serio, (1995). Objective algorithms for the aerosol problem, *Appl. Opt., 34*, 5442-5452.

Amato U., Masiello M., Serio C. and M. Viggiano, (2002). The sigma-IASI code for the calcultaion of infrared atmospheric radiance and its derivatives. *Environ. Modelling and Software, 17*, 651-667.

Anderson G., Clough S., Kneizys F., Chetwynd J. and E. Shettle, (1986). *AFGL atmospheric constituent profiles (0–120 km).* Geophysics Laboratory, Hanscom Air Force Base (See also: U.S. Standard Atmosphere, 1976, U.S. Government Printing Office, Washington, D.C.: http://modelweb.gsfc.nasa.gov/atmos/us_standard.html)

Andrews D., (2000). *An Introduction to Atmospheric Physics*, Cambridge Univ. Press.

Baldecchi M., Carli B., Mencaraglia F., Bonetti A. and M. Carlotti, (1984). Atlas of stratospheric submillimetre lines. 1. The 7-20 cm^{-1} interval, *J. Geophys. Res. 89*, 1689-1704

Baldecchi M., Carli B., Mencaraglia F., Barbis A., Bonetti A. and M. Carlotti, (1988). Atlas of stratospheric submillimetre lines. 2. The 20-40 cm^{-1} interval, *J. Geophys. Res., 93*, 5303-5318

1   Baum B., Yang P., Heidinger A., Heymsfield A., Li J. and S. Nasiri, (2007). Bulk scattering

2   properties for ice clouds. Part 3. High resolution spectral models from 100 to 3250 cm-1. *J.*

3   *Appl. Meteor. Clim*., 46, 423-434.

4

5   Bell J., (1972). *Introductory Fourier Transform Spectroscopy*, Academic Press, New York

6

7   Bianchini G., Palchetti L. and B.Carli, (2006a). A wide-band nadir-sounding

8   spectroradiometer for the characterisation of the Earth's outgoing long-wave radiation,

9   *Proceedings of SPIE, 6361,* 63610A.

10

11   Bianchini G., Palchetti L., Belotti C., Del Bianco S. and U. Cortesi, (2006b). Wide-band

12   spectrally resolved measurement of the Earth's up-welling radiation with the REFIR-PAD

13   spectroradiometer, *Proc. SPIE Int. Soc. Opt. Eng.,, 6362,* 63622K.

14

15   Brindley H. and J. Harries, (1998). The impact of far ir absorption on clear sky greenhouse

16   forcing: Sensitivity studies at high spectral resolution, *J. Quant. Spec. Rad. Trans., 60*, 151-

17   180

18

19   Burroughs W. and J. Harries, (1970). Direct method of measuring stratospheric water vapour

20   mixing ratios, *Nature, 227*, 824-826

21

22   Bussoletti E. and J. Baluteau, (1974). Determination of H_2O-O_2 stratospheric mixing ratio

23   from high resolution spectra in far infrared, *Infrared Physics 14*, 293-302

24

1   Cahalan, R., Oreopoulos L., Marshak A., Evans K., Davis A., Pincus R., Yetzer K., Mayer B.,

2   Davies R., Ackerman T., Barker H., Clothiaux E., Ellingson R., Garay M., Kassianov E.,

3   Kinne S., Macke A., Ohirok W., Partain P., Prigarin S., Rublev A., Stephens G., Szczap F.,

4   Takara E., Varnai T., Wen G. and T. Zhuravleva, 2005. The International Intercomparison of

5   3D Radiation Codes (I3RC): Bringing together the most advanced radiative transfer tools for

6   cloudy atmospheres. *Bull. Amer. Meteor. Soc.*, 86, 1275-1293.

7

8   Carissimo A., De Feis I. and C. Serio, (2005). The physical retrieval methodology for IASI:

9   the *δ*-IASI code, *Environmental Modelling & Software, 20,* 1111-1126

10

11 Carli B., Martin D., Puplett E. and J. Harries, (1977). Very high resolution far infrared

12 measurements of atmospheric emission from aircraft, *J. Opt. Soc. Am. 67,* 917-921

13

14 Carli B., Mencaraglia F. and A. Bonetti, (1980). Fourier spectroscopy of the stratospheric

15 emission, *Int. J. Infrared and Millimeter Waves, 1,* 263-276

16

17 Carli B., 1984. The high resolution submillimeter spectrum of the stratosphere, *J. Quant.*

18 *Spec. Rad. Trans., 32,* 397-405.

19

20 Carli B., Mencaraglia F. and A. Bonetti, (1984). Submillimeter high resolution FT

21 spectrometer for atmospheric studies, *Appl. Opt., 23,* 2594- 2603,

22

Carli B., Barbis A., Harries J., and L.Palchetti, (1999). Design of an efficient broad band far

infrared FT spectrometer, *Appl.ied Opt.ics , 38,* 3945-3950.

23

1   Carli B, Bazzini G, Castelli E, Cecchi-Pestellini C, Del Bianco S, Dinelli BM, Gai M,

2   Magnani L , Ridolfi M, and Santurri L, (2007), .MARC:A code for the retrieval of

3   atmospheric parameters from millimeter-wave limb measurements, *J. Quant. Spec. Rad.*

4   *Trans., 105,* 476-491

5

6   Cess, R. D., and G. L. Potter, (1988): A methodology for understanding and intercomparing

7   atmospheric climate feedback processes in general circulation models. *J. Geophys. Res., 93***,**

8   8305–8314.

9

10   Cess, R. D., G. L. Potter, J. P. Blanchet, G. J. Boer, A. D. Del Genio, M. Déqué, V.

11   Dymnikov, V. Galin, W. L. Gates, S. J. Ghan, J. T. Kiehl, A. A. Lacis, H. Le Treut, B. J.

12   McAvaney, V. P. Meleshko, J. F. B. Mitchell, J.-J. Morcrette, D. A. Randall, L. Rikus, E.

13   Roeckner, J. F. Royer, U. Schlese, D. A. Sheinin, A. Slingo, A. P. Sokolov, K. E. Taylor, W.

14   M. Washington, R. T. Wetherald, and I. Yagai (1990), Intercomparison and interpretation of

15   climate feedback processes in 19 atmospheric general circulation models*, J. Geophys. Res.,*

16   *95,* 16601-16615.

17

18   Cess, R. D., M. H. Zhang, W. J. Ingram, G. L. Potter, V. Alekseev, H. W. Barker, E. Cohen-

19   Solal, R. A. Colman, D. A. Dazlich, A. D. Del Genio, M. R. Dix, M. Esch, L. D. Fowler, J. R.

20   Fraser, V. Galin, W. L. Gates, J. J. Hack, J. T. Kiehl, H. Le Treut, K. K.-W. Lo, B. J.

21   McAvaney, V. P. Meleshko, J.-J. Morcrette, D. A. Randall, E. Roeckner, J.-F. Royer, M. E.

22   Schlesinger, P. V. Sporyshev, B. Timbal, E. M. Volodin, K. E. Taylor, W. Wang, and R. T.

23   Wetherald (1996), Cloud feedback in atmospheric general circulation models: An update*, J.*

24   *Geophys. Res., 101*, 12791-12794.

25

1   Chahine MT, (1974), Remote sounding of cloudy atmospheres I: The single cloud layer, *J.*

2   *Atmos. Sci.*, *31*, 233-243.

3

4   Chandrasekhar, S.,(1960), *Radiative Transfer*, Dover Publications, Inc., New York, (ISBN 0-

5   486-60590-6).

6

7   Charlock T, (1984), CO_2 induced climatic change and spectral variations in the outgoing

8   terrestrial infrared radiation, *Tellus, B36*, 139-148

9

10   Chevalier, F., (2001), Sampled databases of 60-level atmospheric profiles from the ECMWF

11   analyses, Research Report No. 4, SAF programme, EUMETSAT/ECMWF, Reading, UK,

12

13   Clark T A and D.J.W. Kendall, (1976), Far infrared emission spectrum of stratosphere from

14   balloon altitudes, *Nature, 260*, 31-32.

15

16   Clough, S. A., F. X. Kneizys, and R. W. Davies, (1989): Line shape and the water

17   vapour continuum,. *Atmos. Res.*, *23,* 229-241.

18

19   Clough, S. A., Iacono, M. J. and Moncet, J.-L., (1992), Line-by-Line Calculations of

20   Atmospheric Fluxes and Cooling Rates: Application to Water Vapor, *J. Geophys. Res., 97,*

21   15761-15785

22

23   Clough, S. A. and Iacono, M. J.(1995), Line-by-line calculation of atmospheric fluxes and

24   cooling rates 2. Application to carbon dioxide, ozone, methane, nitrous oxide and the

25   halocarbons, *Journal of Geophysical Research, 100* , 16519-16536.

26

1   Cox CV., Murray JE, Taylor JP, Green PD, Pickering JC, Harries JE and

2   Last AE, (2007), Clear-Sky Far Infra-Red Measurements Observed with TAFTS during the

3   EAQUATE Campaign, September 2004, *Q J Roy Met Soc.*, In Press.

4

5   Del Bianco S, B. Carli, C. Cecchi-Pestellini, B.M. Dinelli, M. Gai, and L.Santurri, (2007)

6   Retrieval of minor constituents in a cloudy atmosphere with remote sensing millimeter wave

7   measurements, submitted to *Q. J. Roy. Met. Soc.Q. J. R. Meteorol. Soc.*

8

Doelling, D. R., P. Minnis, D. A. Spangenberg, V. Chakrapani, A. Mahesh, S. K. Pope, and F.

P. J. Valero, (2001) Cloud radiative forcing at the top of the atmosphere during FIRE ACE

derived from AVHRR data*, J. Geophys. Res., 106*, 15279-15296.

9   Edwards, D. P. (1992), GENLN2: A general line-by-line atmospheric transmittance and

10 radiance model, Version 3.0 description and users guide, *NCAR/TN-367-STR*, National Center

11 for Atmospheric Research, Boulder, Co.

Esposito F., G.Grieco, L.Leone, R.Restieri, C.Serio, Palchetti L., G.Bianchini, Pellegrini

M,V.Cuomo, G.Masiello, and G.Pavese, (2007a.), REFIR/BB initial observations in the water

vapour rotational band: results from a field campaign, *J. Quant. Spectrosc. Radiat. Trans.fer,*

103, 524-535,

12

13 Esposito F, G. Grieco, G. Masiello, G. Pavese, R. Restieri, C. Serio, and V. Cuomo, (2007b),

14 Intercomparison among line-parameters spectroscopic databases using downwelling spectral

15 radiance, *Q. J. R. Meteorol. Soc.,* in press.

1   Evans, K.F., A.H. Evans, I.G. Nolt, and B.T. Marshall, (1999), The Prospect for Remote

2   Sensing of Cirrus Clouds with a Submillimeter-Wave Spectrometer, *J. Appl. Meteor. 38*, 514

3   - 525

Futyan JM, Russell JE, and Harries JE, (2005), Determining cloud forcing by cloud type from

geostationary satellite data, *Geophys. Res. Letts., 32*, Art. No. L08807 APR 21 2005

4   Gebbie H A, W.J. Burroughs, J.E. Harries and R.H. Cameron, (1968), Submillimetre wave

5   spectroscopy of the Eath's atmosphere above 39,000 feet", *Astrophys. J.. , 154*, 405-407

6

7   Goody RM, (1964), *Atmospheric Radiation*, Oxford Univ. Press.

8

9   Goody RM and Yung Y L, (1989), *Atmospheric Radiation, 2nd Ed.*, Oxford Univ. Press

10

11 Green P.D., (2003), The Development of a Fourier Transform Spectrometer to Measure Far

12 IR Fluxes in the Upper Troposphere , *PhD Thesis*, University of London, UK

13

14 Green PD, Murray JE, Canas A, Taylor JP and Harries JE, (2007), Atmospheric Foreign-

15 Broadened Water Vapour Continuum Measurements in the Far-IR: $80 - 250$ cm^{-1}, In

16 preparation.

17

18 Grieco G., Masiello G., and Serio C., (2004), MTG IR Sounder water vapour retrieval:

19 Assessment of the performance using sounder bands IRS-5 and IRS-6, versus IRS-5 or IRS-6.

20 Final Report to EUMETSAT, (contract EUM/CO/04/1285/RST, updated version, 22

21 September 2004).

22

Hanel, R. A., B. Schlachman, F. D. Clark, C. H. Prokesh, J. B. Taylor, W. M. Wilson, and L. Chaney, (1970), The Nimbus III Michelson interferometer, *Appl. Opt., 9*, 1767-1774,

Hanel, R. A., B. Schlachman, D. Rogers, and D. Vanous, (1971), Nimbus 4 Michelson interferometer, *Appl. Opt., 10*, 1376-1382,

Harries JE, (1970), Quadrupole moment of CO_2, measured from far infrared spectrum, *J. Phys B., 3*, L150-152.

Harries JE, Burroughs WJ, and Duxbury G, (1971), Pure rotation spectrum of HNO_3 vapour, *Nature-Physical Science, 232*, 171-173

Harries JE, N.R. Swann, J.E. Beckman and P.A.R. Ade, (1972), High resolution observations of submillimetre stratospheric emission spectrum, *Nature 236*, 159-160

Harries JE, (1973), Measurements of stratospheric water vapour using far IR techniques, *J. Atm. Sci., 30*, 1691-1698

Harries JE, (1976), Distribution of water vapour in stratosphere, *Rev. of Geophysics, 14*, 565-575

Harries JE, (1977), Submillimetre wave spectroscopy of the atmosphere, *J. Opt. Soc. Am., 67*, 880-894

Harries JE, (1996), The greenhouse earth: A view from space, Q J Roy Met Soc., 122, 799-818

Harries JE, Brindley HE, Sagoo PJ, and Bantges R J, (2001), Increases in greenhouse forcing inferred from the outgoing longwave radiation spectra of the Earth in 1970 and 1997 *Nature*, 410, 355-357

Harries JE, Russell JE, Hanafin JA, et al., (2005), The Geostationary Earth Radiation Budget Project , *Bull. Am. Met. Soc*., 86, 945+

Hartmann DL, Ramanathan V, Berroir A and Hunt GE, (1986), Earth radiation budget data and climate research, *Rev. Geophys., 24*, 439-468.

Held I and Soden B, (2000), Water vapor feedback and global warming, *Ann. Rev. Energy and the Environ., 25*, 441-475

Herzberg G ,(1959), *Molecular spectra and molecular structure: II Infrared and Raman spectra of polyatomic molecules,* Van Nostrand, New York

IPCC (2001), *Climate Change 2001: The Scientific Basis*, Cambridge Univ. Press, UK

IPCC (2007), *Climate Change 2007: The Physical Science Basis*, Cambridge Univ. Press, UK

Jenkins F A and White H E, (1981), *Fundamentals of Optics (4th Edition),* McGraw Hill.

Kiehl JT, (1983), Satellite detection of effects due to increased atmospheric carbon dioxide, *Science, 222*, 504-506

Knuteson, R. O., F. A. Best, N. C. Ciganovich, R. G. Dedecker, T. P. Dirkx, S. Ellington, W. F. Feltz, R. K. Garcia, R. A. Herbsleb, H. B. Howell, H. E. Revercomb, W. L. Smith, and J. F. Short, 2004a: Atmospheric Emitted Radiance Interferometer (AERI): Part I: Instrument Design, *J. Atmos. Oceanic Technol., 21*, 1763-1776

Knuteson, R. O., F. A. Best, N. C. Ciganovich, R. G. Dedecker, T. P. Dirkx, S. Ellington, W. F. Feltz, R. K. Garcia, R. A. Herbsleb, H. B. Howell, H. E. Revercomb, W. L. Smith, and J. F. Short, 2004b: Atmospheric Emitted Radiance Interferometer (AERI): Part II: Instrument Performance, *J. Atmos. Oceanic Technol., 21,* 1777-1789

Li J, C.-Y Liu, A. Huang, T. J, Schmit, Wu Xuebao, W. P. Menzel, and J.J. Gurka, (2005), Optimal cloud-clearing for AIRS radiances using MODIS, *IEEE Trans. Geosci. Remote Sens., 43*, 1266-1278

Li J, Jinlong Li, E. Weisz, C-Y Liu, T. J. Schmit, A. Huang, M. D. Goldberg, and W. P. Menzel , (2007), Development and Demonstration of Hyperspectral Infrared Only Sounding Retrieval " in Fourier Transform Spectroscopy and Hyperspectral Imaging and Sounding of the Environment on CD-ROM (The Optical Society of America, Washington, DC, 2007), paper #HThB1.

Lindzen RS, (1990), Some coolness regarding global warming, *Bull. Am. Met. Soc., 71,* 288-299.

Liou KN, (1986), Influence of cirrus clouds on weather and climate processes – a global perspective, *Monthly Weather Rev., 114*, 1167-1199

Ma Q, and R.H. Tipping (2002), The frequency detuning correction and the asymmetry of line shapes: The far wing of H2O-H2O, *J. Chem. Phys., 116*, 4102-4115.

Maestri T., (2000), Il ruolo del vapor acqueo e delle nubi nel raffreddamento nel lontano infrarosso, Thesis, University of Study of Bologna, Italy,

Maestri T and Rizzi R, (2003), A study of infrared diabatic forcing of ice clouds in the tropical atmosphere, *J. Geophys. Res., 108*, Art. No. 4139

Mankin WG, (1975), Airborne Fourier transform spectroscopy of upper atmosphere, *Optical Eng., 17* , 39-43

Marten A and Y. Chauvel, (1975), Advantageous technique of stratospheric emission spectrometry in the far infrared, *Infrared Physics, 15,* 205-209

Martin DH and E. Puplett, (1969), "Polarised interferometric spectrometry for the millimetre and submillimetre spectrum", *Infr. Phys., 10*, 105-109,

Masiello G, M. Matricardi, R. Rizzi, and C. Serio, (2002), Homomorphism between Cloudy and Clear Spectral Radiance in the 800 -900- cm $^{-1}$ Atmospheric Window Region , *Appl. Opt., 41,* 965-973

Mencaraglia F, Bianchini G, Boscaleri A, Carli B, Ceccherini S, Raspollini P, Perrin A, and Flaud JM, , (2006), Validation of MIPAS satellite measurements of HNO3 using comparison

of rotational and vibrational spectroscopy, *J. Geophys. Res., 111 (D19)*: Art. No. D19305 OCT 5 2006

Mlawer EJ, S. A. Clough, and P. D. Brown, and D.C. Tobin, (1999), Recent Developments in the Water Vapor Continuum, in *Ninth ARM Science Team Meeting Proceedings, San Antonio, Texas, March 22-26,* pp. 1-6

Mlynczak MG; D. G. Johnson; G. E. Bingham; K. W. Jucks; W. A. Traub; L. Gordley; P. and Yang (2005), The far-infrared spectroscopy of the troposphere project, in Enabling Sensor and Platform Technologies for Spaceborne Remote Sensing, edited by G. Komar, J. Wang, and T. Kimura, *Proc. SPIE Int. Soc. Opt. Eng., 5569*, 81-87.

Mlynczak MG, Johnson DG, Latvakoski H, Jucks K, Watson M, Kratz DP, Bingham G, Traub WA, Wellard SJ, Hyde CR, and Liu, (2006), First light from the Far-Infrared Spectroscopy of the Troposphere (FIRST) instrument, *Geophys. Res. Lett.*, *33*, L07704, doi:10.1029/2005GL025114.

Murray J.E, Green PD, Canas A, Harries JE, and Last A, (2007), The Tropospheric Fourier Transform Spectrometer, TAFTS, *In preparation*.

National Research Council,(2007), *Earth Science and Applications from Space: National Imperatives for the Next Decade and Beyond,* ISBN: 0-309-66900-6, National Academy Press, 2007.

1   Nithianandam J, Guenther BW and Alison LJ, (1993), An anecdotal review of NASA Earth

2   observing satellite remote sensors and radiometric calibration methods, *Metrologia, 30*, 207-

3   212

4

5   Oldfield M, B.Moyna, E.Allouis, R.Brunt, U. Cortesi, B.Ellison, J.Eskell, T.Forward,

6   T.Jones, D.Lamarre, J.Langen, P. Maagt, D.Matheson, I.Morgan, J. Reburn, and R. Siddans,

7   (2001), MARSCHALS: Development of an Airborne Millimetre Wave Limb Sounder, *Proc.*

8   *SPIE Int. Soc. Opt. Eng.,* .4540, 221-228

    Palchetti L, G. Bianchini, F.Castagnoli, B. Carli, C. Serio, F.Esposito, V.Cuomo,

    Rizzi R, and T. Maestri, (2005), Breadboard of the Fourier transform spectrometer for the

    Radiation Explorer in the Far Infrared atmospheric mission, *Applied Optics, 44*, 2870-2878

9   Palchetti L., Belotti C., Bianchini G., Castagnoli F., Carli B., Cortesi U., Pellegrini M., Camy-

10   Peyret C., Jeseck P., and T´e Y., (2006), Technical Note: First spectral measurement of the

11   Earth's upwelling emission using an uncooled wideband Fourier transform spectrometer,

12   *Atmos. Chem. Phys., 6*, 5025–5030.

13

14   Penner S., (1959). *Quantitative Molecular Spectroscopy and Gas Emissivities,* Addison-
15
16   Wesley.
17

18   Poore KD, Wang JH, and Rossow WB., (1995): Cloud layer thickness from surface and

19   upper-air observation. *J. Clim., 8,* 550-568

20

1 Ptashnik I. V., K. M. Smith, K. P. Shine, and D. A. Newnham (2004), Laboratory

2 measurements 272 of water vapour continuum absorption in spectral region 5000-5600 cm-1:

3 Evidence for water 273 dimers, *Q. J. R. Meteorol. Soc. Soc., 130,* 2391-2408.

4

5 Rae A I M., (2002), *Quantum Mechanics* (4th Edition), Institute of Physics Publishing, UK.

6

7 Ramanathan, V.(1987): The role of Earth radiation budget studies in climate and general

8 circulation research, *J. Geophys. Res., 92*, 4075-4095

9

10 Randall, D.A., Harchvardhan, D. A. Dazlich, and T.G. Corsetti, (1989), Interactions among

11 radiation, convection and large-scale dynamics in a general circulation model*, J. Atmos. Sci.,*

12 *46*, 1943-1970

13

14 Raspollini,P., Belotti, C., Carli, B., Carlotti, M., Cecchrini, S., Dinelli, B.M., Dudhia, A.,

15 Flaud, J.M., Funke, B., Hoepfner, M., Lopez-Puertas, M., Payne,V., Piccolo, C., Remedios,

16 J.J., Ridolfi, M., Spang, R (2006): MIPAS Levl 2 operational analysis, *Atm. Chem. Phys., 6,*

17 5605-5630,.

18

19 Reburn, WJ, R. Siddans, B.J. Kerridge, S. Buhler, A. von Engeln, K. Kunzi, J. Urban, J.

20 Wohlgemuth, D. Feist, N. Kampfer, H. Czekala, (1998), "Study on Upper Troposphere/Lower

21 Stratosphere Sounding", Final Report of ESA Contract # 12053/97/NL/CN.

22

Rizzi R (1994), A comparison of simulated outgoing long-wave flux and estimates from raw

tovs radiances, *Nuovo Cimento della Societa Italiana di Fisica, C17*, 763-781

Rizzi R, C. Serio, G. Kelly,V. Tramutoli, A. McNally, and V. Cuomo, (1994), Cloud Clearing of Infrared Sounder Radiances, *J.ournal of Appl.ied Meteorol.ogy*, *33*, 179–194

1

2 Rizzi R. , B. Carli, J. E. Harries, J. Leotin, C. Serio, A. Sutera, R. Bonsignori and S. Peskett,

3 (2000), REFIR - Radiation Explorer in the Far InfraRed, *Final Report ENV4-CT6 0344, 2*

4 *Volumes, available from the EU DGXII Directorate and at*

5 *http://adgb.df.unibo.it/refir/report/index_final.html*

6

7 Rizzi R. and L. Mannozzi, (2000), Preliminary results on the planetary emission between 100

8 and 600 cm^{-1}, Final Report of the EU REFIR Project, Vol.1, pp 77-87, available at:

9 http://www.refir.org/report/index_final.html

10

11 Rizzi R., and T. Maestri, (2001), Quantitative role of far-infrared emission on diabatic forcing

12 of the middle and upper Troposphere in clear and cloudy conditions, SPIE Conference, San

13 Diego, USA

14

Rizzi R., B. Carli, J.E. Harries, J. Leotin, C. Serio A. Sutera, B. Bizzarri, R. Bonsignori, and S. Peskett, (2001), Mission objectives and instrument requirements for the REFIR (Radiation Explorer in the Far Infrared) Mission: An outline after the end of phase B0, *Proceedings of IRS 2000,* pp. 567-570, A. Deepak Publishing. Co, Hampton, Virginia.

15

16 Rizzi R., Serio C, and Amorati R. (2002), Sensitivity of broad-band and spectral

17 measurements of outgoing radiance to changes in water vapour content, *Proc. SPIE Int. Soc.*

18 *Opt. Eng., 4485*, 181-190.

19

Rizzi R and Maestri T,(2003), Some considerations on the infrared cloud forcing, *J. Geophys. Res., 108* (D14): Art. No. 4403

1   Rodgers, C.D., (1976). Retrieval of atmospheric temperature and composition from remote

2   measurements of thermal radiation. *Rev.iew of Geophysics and Space Physics, 14*, 609-624.

3

4   Rothman, L. S., Barbe, A., Benner, D. C., Brown, L. R., Camy-Peyret, C., Carleer, M. R.,

5   Chance, K., Clerbaux, C., Dana, V.,Devi, V. M., Fayt, A., Flaud, J.-M., Gamache, R. R.,

6   Goldman, A.,Jacquemart, D., Jucks, K. W., Lafferty, W. J., Mandin, J.-Y.,Massie, S. T.,

7   Nemtchinov, V., Newnham, D. A., Perrin, A., Rinsland,C. P., Schroeder, J., Smith, K. M.,

8   Smith, M. A. H., Tang, K.,Toth, R. A., Vander Auwera, J., Varanasi, P. and Yoshino, K.

9   (2003), The HITRAN molecular spectroscopic database: edition of 2000 including updates

10   through 2001 *J. Quant. Spectrosc. Radiat. Trans.fer, 82* 5-44

11

12   Rothman, L. S., Jacquemart, D., Barbe, A., Benner, D. C., Birk, M.,Brown, L. R., Carleer, M.

13   R., Chackerian, C., Chance, K., Coudert, L. H., Dana, V., Devi, V. M., Flaud, J. M.,

14   Gamache, R. R., Goldman, A., Hartmann, J. M., Jucks, K. W., Maki, A. G., Mandin, J. Y.,

15   Massie, S. T., Orphal, J., Perrin, A., Rinsland, C. P., Smith, M. A. H., Tennyson, J.,

16   Tolchenov, R. N., Toth, R. A., Vander Auwera, J., Varanasi, P. and Wagner, G. (2005), The

17   HITRAN 2004 molecular spectroscopic database *J. Quant. Spectrosc. Radiat. Trans.fer, 96*

18   139-204

19

20   Rothman, L. S., Rinsland, C. P., Goldman, A., Massie, S. T., Edwards, D. P., Flaud, J.-M.,

21   Perrin, A., Camy-Peyret, C., Dana, V., Mandin, J.-Y., Schroeder, J., McCann, A., Gamache,

22   R. R., Wattson, R. B., Yoshino, K., Chance, K., Jucks, K., Brown, L. R., Nemtchinov, V. and

23   Varanasi, P.(1998), The HITRAN Molecular Spectroscopic Database and HAWKS

(HITRAN Atmospheric Workstation): 1996 Edition *J. Quant. Spectrosc. Radiat. Trans.fer, 60*, 665-710

Serio C, A.M. Lubrano, F. Romano, and H. Shimoda (2000), Cloud Detection Over Sea Surface by use of Autocorrelation Functions of Upwelling Infrared Spectra in the 800 900-cm [-1] Window Region , *Appl. Opt*., 39, 3565-3572

Serio, C., F. Esposito, L. Palchetti, and R. Rizzi, (2002) R&D bread-board for a Fourier Transform Spectrometer to remotely sense the rotational water vapour band (10-1000 cm^{-1}), Italian Space Agency, Final Report, PROJECT ASI I/R/27/00.

Serio C, G. Grieco and G. Masiello, (2007), Capability of High Spectral Resolution Observations in the Infrared to Detect Water Vapor Structures ” in *Fourier Transform Spectroscopy and Hyperspectral Imaging and Sounding of the Environment on CD-ROM* (The Optical Society of America, Washington, DC, 2007), paper #HThB2.

Shaw JA, Bates JJ, Zorn HM, et al.(1999), Observations of downwelling infrared spectral radiance at Mauna Loa, Hawaii during the 1997-1998 ENSO event , *Geophys. Res. Letts*., 26, 1727-1730

Sinha A and Harries JE, (1995), Water-vapor and greenhouse trapping - the role of far-infrared absorption, *Geophys. Res Lett., 22*, 2147-2150

Sinha A and Harries JE, (1997), The earth's clear-sky radiation budget and water vapor absorption in the far infrared, *J. Climate, 10,* 1601-1614

Slingo J.M., and A. Slingo, (1988), The response of a general circulation model to cloud long-wave radiative forcing. I: Introduction and initial experiments. *Quart. J. Roy. Meteor. Soc., 114*, 1027-1062

Soden BJ, Wetherald RT, Stenchikov GL, and Robock A (2002), Global cooling after the eruption of Mount Pinatubo: A test of climate feedback by water vapour, *Science, 296*, 727-730

Spankuch, D. and W. Dohler, (1985), Radiative properties of cirrus clouds in the middle IR derived from Fourier spectrometer measurements from space, *Z. Meteorol., 35*, 314-324

Stackhouse, P. W., and G. L. Stephens, (1991), A Theoretical and Observational Study of the Radiative Properties of Cirrus: Results from FIRE 1986, *J. Atmos. Sci., 48,* 2044-2059

Stamnes, K., S. Tsay, W. Wiscombe and K. Jayaweera, (1988): Numerically stable algorithm for discrete-ordinate-method radiative transfer in multiple scattering and emitting layered media. *Appl. Opt.,* 27, 2502-2509.

Stephens, G.L., S-C. Tsay, P.W. Stackhouse, and P.J. Flatau, (1990), The relevance of the microphysical and radiative properties of cirrus clouds to climate and climatic feedback, *J. Atmos. Sci., 47*, 1742-1753

Straine G., (2005), Far infrared cooling rates in the upper troposphere: reconciling models and observations, PhD Thesis, University of London, UK.

1　Stuhlmann, R (1995), The impact of clouds on the radiaitve heating of the Earth surface-

2　atmosphere system determined from satellite data, *Adv. Space Res., 16,* 37-49

3

4　Tarantola, A., 1987. *Inverse Problem Theory*. Elsevier, New York.

5

6　Tian B and Ramanathan V, (2002), Role of tropical clouds in surface and atmospheric energy

7　budget, *J. Climate, 15*, 296-305

8

9　Taylor JP, W. L. Smith, V. Cuomo, A. M. Larar, D. K. Zhou, C. Serio, T. Maestri, R. Rizzi,

10　S. Newman, P. Antonelli, S. Mango, P. Di Girolamo, F. Esposito, G. Grieco, D. Summa ,R.

11　Restieri, G. Masiello, F. Romano, G. Pappalardo, G. Pavese, L. Mona, A. Amodeo and G.

12　Pisani, (2007), EAQUATE – An International Experiment For Hyper-spectral Atmospheric

13　Sounding Validation, Accepted for publication in, *Bull. Amer. Meteor. Soc.,* to be published

14

15　Tobin, D. C., Best, F. A., Brown, P. D., Clough, S. A., Dedecker, R. G., Ellingson, R. G.,

16　Garcia, R. K., Howell, H. B., Knuteson, R. O., Mlawer, E. J., Revercomb, H. E., Short, J. F.,

17　van Delst, P. F. W. and Walden, V. P., (1999), Downwelling spectral radiance observations

18　at the SHEBA ice station: Water vapor continuum measurements from 17 to 6μm , *J.*

19　*Geophys. Res.,, 104*, 2081-2092

20　Turner, D. D., S. A. Ackerman, B. A. Baum, H. E. Revercomb, and P. Yang, (2003), Cloud
21
22　phase determination using ground-based AERI observations at SHEBA, *J. Appl. Meteor.*, 42,
23
24　701-715.
25
26

1 Vaida V., J.S. Daniel, H.G Kjaergaard, L.M. Goss, and A.F. Tuck, (2001), Atmospheric 298

2 absorption of near infrared and visible solar radiation by the hydrogen bonded water dimer.,

3 *Q. J. R. Meteorol. Soc., 127*, 1627–164.

4

5 Waters JW, Froidevaux L, Harwood RS, Jarnot RF, Pickett HM, Read WG, Siegel PH,

6 Cofield RE, Filipiak MJ, Flower DA, Holden JR, Lau GK, Livesey NJ, Manney GL,

7 Pumphrey HC, Santee ML, Wu DL, Cuddy DT, Lay RR, Loo MS, Perun VS, Schwartz MJ,

8 Stek PC, Thurstans RP, Boyles MA, Chandra KM, Chavez MC, Chen GS, Chudasama BV,

9 Dodge R, Fuller RA, Girard MA, Jiang JH, Jiang YB, Knosp BW, LaBelle RC, Lam JC, Lee

10 KA, Miller D, Oswald JE, Patel NC, Pukala DM, Quintero O, Scaff DM, Van Snyder W,

11 Tope MC, Wagner PA, and Walch MJ (2006), The Earth Observing System Microwave Limb

12 Sounder (EOS MLS) on the Aura satellite, *IEEE Trans. Geosci. And Rem Sensing, 44*, 1075-

13 1092

14

15 Wielicki BA, Wong TM, Allan RP, Slingo A, Kiehl JT, Soden BJ, Gordon CT, Miller AJ,

16 Yang SK, Randall DA, Robertson F, Susskind J, and Jacobowitz H (2002), Evidence for large

17 decadal variability in the tropical mean radiative energy budget, *Science, 295*, 841-844

18

19 Wong T, Wielicki BA, Lee RB, Smith GL, Bush KA, and Willis JK, (2006), Re-examination

20 of the observed decadal variability of the earth radiation budget using altitude-corrected

21 ERBE/ERBS nonscanner WFOV data, *J. Climate, 19*, 4028-4040

22

23 Yang, P., M. G. Mlynczak, H.L. Wei, D. P. Kratz, B,A. Baum , Y. X. Hu, W. J. Wiscombe,

24 A. Heidinger, and M. I. Mishchenko, (2003), Spectral signature of cirrus clouds in the far-

25 infrared region: single-scattering calculations and radiative sensitivity study. *J. Geophys. Res.*

26 *108,* Art. 4560

1

2   Yang, P., H. Wei, H. L Huang, B. A. Baum, Y. X. Hu, M. I. Mishchenko, and Q. Fu, (2005):

3

4   Scattering and absorption property database of various nonspherical ice particles in the

5

6   infrared and far-infrared spectral region. *Appl. Opt.*, 44, 5512-5523.

7

1   Figure Captions

2

3   B1: Optical depth of lines due to water vapour and carbon dioxide throughout the IR. (T.

4   Maestri, PhD Thesis)

5

6   B2: Optical depth of lines due to remaining key absorbers throughout the IR. (T. Maestri,

7   PhD Thesis)

8

9   B3: Simulated upwelling emission spectrum at the TOA, for (a) Tropical, and (b) Sub-Arctic

10   Winter standard atmospheres. Dashed red lines show the equivalent black-body emission at

11   the given temperatures (H. Brindley, unpublished)

12

13   1: Transmittance in FIR: (a) Tropical standard, 12 km to TOA; (b) Tropical standard: surface

14   to TOA; (c) Sub-Arctic Winter standard, 8 km to TOA; (d) Sub-Arctic Winter standard:

15   surface to TOA (H. Brindley, unpublished)

16

17   2: Cooling rate across the infrared and from the surface to TOA, in units of K day^{-1} cm^{-1}. (a)

18   Tropical (TRP) and (b) Sub-Arctic Winter (SAW) standard atmospheres (Figure originally

19   published in Journal of Quantitative Spectroscopy and Radiative Transfer, Vol. 60., entitled:

20   'The impact of far ir absorption on clear sky greenhouse forcing: Sensitivity studies at high

21   spectral resolution', by Brindley and Harries, pp 151-180, Copyright Elsevier (1998))

22

23   3: Radiance difference at the TOA in W m^{-2} sr^{-1} (cm^{-1})$^{-1}$. Dashed line is the difference

24   between case A (Tropical standard atmosphere with water vapour concentration scaled by 0.9

25   and skin temperature decreased by 1K) and control case C (Tropical standard atmosphere).

1   Solid line is the difference between case B (Tropical standard atmosphere with only water

2   vapour concentration scaled by 0.9) and control case C (T. Maestri and R. Rizzi, unpublished)

3

4   4: (a) Energy balance in mW m^{-2} (cm^{-1})$^{-1}$ versus wave-number in cm^{-1} for a 1.8 km thick

5   tropical cirrus; ice water path (IWP) is expressed in g m^{-2}. Lower panels: vertical profiles of

6   net flux in W m^{-2} for the same clouds and for clear sky: (b) FIR band (10-600 cm^{-1}); (c)

7   Window (WIN) band (750-980 and 1100-1250 cm^{-1}) (Adapted from Maestri and Rizzi, 2003,

8   copyright 2003, American Geophysical Union)

9

10   5: Variation of surface emission, E_v, at surface temperature indicated, and greenhouse

11   parameter, G_v as function of wavenumber for (a) Tropical and (b) Sub-Arctic Winter

12   standard atmospheres (Figure originally published in Journal of Quantitative Spectroscopy

13   and Radiative Transfer, Vol. 60., entitled: 'The impact of far ir absorption on clear sky

14   greenhouse forcing: Sensitivity studies at high spectral resolution', by Brindley and Harries,

15   pp 151-180, Copyright Elsevier (1998))

16

17   6: Top panel: Spectral greenhouse parameter, G_v; Bottom panel: Normalized spectral

18   greenhouse parameter, g_v, for a set of tropical cirrus clouds comprised of aggregates and

19   placed between 9-12 km in altitude. The cloud optical depth, OD at 900 cm^{-1} is varied as

20   indicated. The legend in the top panel applies to both plots. (T. Maestri, adapted from PhD

21   thesis)

22

23   7: D as a function of the cloud transmittance. Three tropical cirri (top altitudes are 15.4 (h),

24   12.3 (m) and 9.7 (l) km) and a sub-arctic one (top altitude at 8.3 (a) km) are considered with a

25   filter cut-off at 350 cm^{-1} (From Rizzi and Maestri, 2003, Copyright, 2003, American

26   Geophysical Union)

8: Absolute value of the water vapour Jacobian (W/m^2-cm^{-1}-sr-(g/kg)) for a tropical atmosphere. The upper panel refers to the rotational band. For comparison the same computation, shown in the lower panel, has been performed for the vibrational band at 6.7 μm (C. Serio, unpublished)

9: Comparison of the accuracy of the H$_2$O retrieval of FIR rotational band 30 km aggregate resolution (solid line) with that of a MIR sounder (dash-dotted curve) for a standard tropical atmosphere (C. Serio, unpublished)

10: Extinction coefficient for spherical ice particles of different radii as a function of wavenumber for a constant IMC (Ice Mass Content) equal to1.E-8 g cm^{-3} (B. Carli, unpublished)

11: Changes in the wide-band TOA emission spectrum, including both the FIR and the MIR spectral regions, due to the different properties of clouds.

(a) simulated TOA spectra for a clear atmosphere and for two types of clouds with different phase (water and ice), but equal particle size (radius 10 microns) and equal ice water path (IWP=4.0 g m^{-2}) in the same atmospheric layer from 5 to 6 km.

(b) Differences between the clear and cloudy spectra shown in (a). The ice cloud produces a larger difference in the MIR and a smaller difference in the FIR.

(c) Differences between clear and cloudy spectra for ice clouds located at different altitudes (for equal particle size of 30 microns and equal IWP (=4.0 g m^{-2}).

(d) Differences between clear and cloudy spectra for ice clouds with different IWP (for equal particle size of 30 microns and the same altitude layer from 7 to 8 km).

(e) Differential effect of particle size for changes of ±10% in the particle radius for an ice cloud between 7 and 8 km with an IWP of 4.0 g m^{-2}.

(f) Difference in observed radiance for the case of different particle shapes when the other variables are kept constant (ice cloud between 7 and 8 km with an IWP of 4.0 g m^{-2} and equal mass of the single particle) .

(Private communication from S. Del Bianco, 2007)

12: Emission spectrum of the atmosphere observed in the far infrared from an altitude of 38 km with a zenith angle of 91.6°. The upper panel shows a synoptic view of a 20 cm^{-1} spectral interval and the lower panel shows an expanded view of a 2 cm^{-1} spectral interval. The observed features are due to the rotational spectra of the atmospheric constituents. (Carli, unpublished in this form)

13: (a) Comparison of MR-100 spectral observation against various computations. H-00, H-04 and H-06 stand for HITRAN 2000 [Rothman et al, 1998], 2004 [Rothman et al, 2003] and 2006 [Rothman et al, 2005], respectively. Computations have been obtained with LBLRTM v9.4 [Clough et al. 1992, Clough and Iacono 1995], with the water vapour continuum model MT_CKD [Tobin et al. 1999]. The version 1.0 of this model is used in conjunction with H-00, while for H-04 and H-06 the version 1.2 has been used. (b) Observed-calculated differences and ± 1 σ error bars (Serio and Masiello, unpublished).

14: Schematic of the TAFTS optical system. The instrument is, optically, divided into three sections; the pointing optics box (POB), main interferometer unit (MI) and cryostat (CRYO). The MI and CYRO sections are evacuated. The passage of the radiation is described in the main text. The labeled elements are three polarizers, P1 (the beamcombiner, BC), P2 (the beamsplitter, BS) and P3, the power optics, L1, L2 and L3, and the four detectors, either in

1   the longwave (LW) and shortwave(SW) for channels 0-3 (CHi). Two long pass filters exist,

2   one on each of the liquid nitrogen (LN2) and Helium (He) jackets (P.Green and J.Murray,

3   unpublished)

4

5   15: Noise equivalent temperature for single output (a) longwave and (b) shortwave TAFTS

6   channels. The integration time is 60 s at 0.12 cm^{-1} resolution. Blackbody target temperatures

7   were at 337 K and 304 K in the up-welling and down-welling arms respectively (J. Murray,

8   unpublished)

9

10   16: Net radiance spectra measured by TAFTS during EMERALD II at altitudes between 7.50

11   and 13.55 km (marked on figure). Data taken on 19/11/02. The spectral resolution is 1 cm^{-1}.

12   The growth of the transparent windows between individual water vapour absorption lines is

13   shown.   It is in these transparent regions that heating rates can be calculated from the vertical

14   divergence of the net flux measured at each altitude. (G. Straine, unpublished)

15

16   17: Atmospheric cooling rate derived from the spectra in Figure 15, in units of

17   K (day cm^{-1})$^{-1}$ x 10^3. The band structure is due to the positions of the water vapour lines

18   (G. Straine, PhD thesis)

19

20   18: Conceptual optical scheme of the REFIR interferometer. Scanning of the optical path

21   difference is achieved in an efficient double sided Roof-top mirror unit (RTMU); Pol.

22   Indicates polarisers, with polarisation angle in brackets (From L. Palchetti, C Serio and B.

23   Carli, unpublished)

24

25   19: Noise Equivalent Spectral Radiance (NESR) as a function of wavenumber measured

26   under vacuum on the two REFIR prototypes (L. Palchetti, C Serio and B. Carli, unpublished)

20: Outgoing Longwave Radiation (OLR) measurements in clear sky conditions from Toppo di Castelgrande, Italy, on June 10-11th, 2004. The comparison between REFIR-BB (blue line) and BOMEM MR100 (red line) is shown in the top panel, and the difference in the bottom panel. (L. Palchetti, C Serio and B. Carli, unpublished)

21: Brightness temperature (BT) measured in clear sky conditions from Toppo di Castelgrande, Italy, on June 10-11th, 2004. The comparison between REFIR-BB (blue line), BOMEM MR100 (red line), and LBLRTM (green line) is shown in the top panel. Differences between REFIR-BB and BOMEM (labelled Diff R.-B. on y-axis), and between REFIR-BB and LBLRTM (labelled Diff R.-L. on y-axis) are shown in the central and bottom panels, respectively. (L. Palchetti, C Serio and B. Carli, unpublished)

22: Measurement of OLR from 34 km altitude in clear sky conditions in tropical atmosphere (Brazil, June 30th, 2005). The comparison between REFIR-PAD (blue line) and IASI-balloon (red line) is shown in the top panel, and difference in the bottom panel (L. Palchetti, C Serio and B. Carli, unpublished)

23: A single spectrum recorded by the FIRST instrument on June 7 2005, from an altitude of 28 km. The entire energetically significant portion of the Earth's thermal emission spectrum is recorded by a single detector. (After *Mlynczak et al*., 2006. Copyright 2006 American Geophysical Union. Reproduced by permission of the American Geophysical Union.)

24: FIRST spectrum (black line) and two spectra (red, green lines) from the AIRS instrument recorded June 7, 2005. The spectral range covers the entire span measured by the AIRS

instrument in the mid-infrared. This figure illustrates the agreement between FIRST and AIRS and confirms the calibration of the FIRST instrument. (M. Mlynczak, unpublished)

25:   FIRST measurements of the far-IR portion of the Earth's emission spectrum from June 7, 2005 (blue) and September 18, 2006 (red). The black line shows the difference between the June and September cases. The higher values in 2005 are due primarily to a much warmer lower troposphere (M. Mlynczak, unpublished)

1   Annex 1: Examples of atmospheric constituents for which a vertical profile has been

2   measured using FIR spectroscopy

Species	Reference
H_2O	B.M. Dinelli, B. Carli, M. Carlotti, 1991, "Measurement of stratospheric distribution of $H_2^{16}O$, $H_2^{17}O$, $H_2^{18}O$, and HDO from far-infrared spectra", J. Geophys. Res. 96, 7509-7514.
O_3	M.M. Abbas, J. Guo, B. Carli, F. Mencaraglia, M. Carlotti, I.G. Nolt, 1987, "Heavy ozone distribution in the stratosphere from far infrared observations", J. Geophys. Res. 92 D11, 13231. M. Carlotti, A. Barbis, B. Carli, 1989, "Statospheric ozone vertical distribution from far-infrared balloon spectra and statistical analysis of the errors", J. Geophys. Res. 94, 16,365 - 16,372.
HCl, HF	Traub W.A., and Chance K.V., "Stratospheric HCl and HF observations" Geophys. Res. Lett. 8, 1075-1077 (1981).
OH	B. Carli, M. Carlotti. B.M. Dinelli, F. Mencaraglia, J.H. Park, 1989, "The mixing ratio of stratospheric hydroxyl radical from far-infrared emission measurements" J. Geophys. Res. 94, 11049 - 11058.
CO	M.M. Abbas, M.J. Glenn, I.G. Nolt, B. Carli, F. Mencaraglia, M. Carlotti, 1988, "Far infrared measurements of stratospheric carbon monoxide", J. Geophys. Res. Lett. 15, 140.
HNO_3	F. Mencaraglia, G. Bianchini, A. Boscaleri, B.Carli, S. Ceccherini, P.Raspollini, A. Perrin, J-M Flaud, "Validation of MIPAS satellite measurements of HNO3 using comparison of rotational and vibrational spectroscopy" J.G.R. 111, D19305, doi: 1029/2005JD006099, 2006.
HCN	M.M. Abbas, J. Guo, B. Carli, F. Mencaraglia, M. Carlotti, I.G. Nolt, 1987, "Stratospheric distribution of HCN from far infrared observations", Geophys. Res. Lett. 14, 531.
ClO	B. Carli, F. Mencaraglia, M. Carlotti, B.M. Dinelli, I. Nolt, 1988,

	"Submillimeter measurement of stratospheric chlorine monoxide", J. Geophys. Res. 93 D6, 7063 - 7068.
HBr	J.H.Park, B. Carli, A.Barbis, 1989, "Stratospheric HBr mixing ratio obtained from far infrared emission spectra", Geophys. Res. Lett. 16, 787 - 790.
HOCl	Chance K.V., Johnson D.G., and Traub W.A., (1989), Measurements of stratospheric HOCl: concentration profiles including diurnal variation, J. Geophys. Res. 94, 11,059-11069
H_2O_2	Chance K.V., Johnson D.G., Traub W.A., and Jucks K.W., (1991), Measurement of stratospheric hydrogen peroxide concentration profile using far IR thermal emission spectroscopy, Geophys. Res. Lett. 18, 1003-1006
HO_2	Chance KV, Park K, Evenson KM, Zink LR, and Stroh F, (1995), Far-Infrared Spectrum of HO2, J. Mol Spec., 172, 407-420.

1

2

1   **Tables**

Table 1. Variation in Greenhouse Parameters between the TRP and SAW Atmospheres

	TRP	SAW
Greenhouse effect, G (Wm^{-2})	170	50
Proportion of G in the far infra-red	27 %	35 %
Normalised greenhouse effect, g	0.372	0.202
Change in OLR upon doubling CO_2 (Wm^{-2})	-3.76	-1.86
Water vapour change giving same forcing as CO_2 doubling	+17 %	+43 %
Fraction of forcing from water vapour change in far infra-red	19 %	53 %
s_{fir} (m^2 kg^{-1}) ($0 < v < 500$ cm^{-1})	1.00×10^{-3}	7.26×10^{-3}
s_{win} (m^2 kg^{-1}) ($800 < v < 1250$ cm^{-1})	2.15×10^{-3}	0.59×10^{-3}
s_{rest} (m^2 kg^{-1}) ($500 \leq v \leq 800$; $v \geq 1250$ cm^{-1})	1.00×10^{-3}	4.67×10^{-3}

2

3

1   Table 2. TAFTS instrument specifications and performance

2

Interferometer	Martin-Puplett
Spectral range	80 - 600 cm^{-1}
Spectral resolution	0.1 cm^{-1} unapodised
Radiometric sensitivity	1 mW m^{-2} sr^{-1} (cm^{-1})$^{-1}$
Integrated sensitivity	0.10 W m^{-2} (80 - 600) cm^{-1}
Field of view	$\pm 0.8^0$
Aperture diameter	25 mm nominal
Optical input ports	2: polarisation coded
Output signals	4: two true differential pairs
Detectors	Ge:Ga and Si:Sb photo-conductors
Detector cooling	Liquid helium, 4.2 K
Cryostat hold time	12 hours measured
Scan sampling	HeNe laser (2.5312 μm spatial interval)
Signal sampling rate	4 channels, 20 kHz per channel
Digital Converters	2 stereo Σ-Δ ADCs, 20 bit resolution
Data volume	560 kBytes per scan, 806 Mbytes per hour
Data storage	Twin 18 Gbyte SCSI-2 hard disks
Control PC	AMPRO P5V, 266 MHz Pentium
Software/operating system	GNU C/ real time Linux
Power Consumption	< 1 kW from 220V ac, 400 Hz
Dimensions	900 x 415 x 550 mm
Mass (main instrument/control box)	90 kg/30 Kg

3

1   Table 3. Main characteristics of REFIR FTS prototypes

Interferometer	Mach-Zehnder scheme
BS type	Amplitude multilayer, Ge-coated PET film
Spectra coverage	100-1400 cm^{-1}
Spectral resolution (max)	0.25 cm^{-1}
Optical throughput	0.01 cm^2 sr
Field of view	133 mrad
Detectors	2 room-temperature pyroelectrics (DLATGS)
Reference laser	monomode laser diode at 780 nm
Control PC	PC-104, 486DX100 CPU, Linux operating system
Acquisition time	30-120 s
Acquisition frequency	5-20 kHz
NESR	0.3-10 mW/(m^2 sr cm^{-1}), see Figure 18
Absolute calibration error	< 0.5 K at 280 K
Size	62 cm diam., 26 cm height
Weight/power consumption	55 kg / 50 W

2

(a) Tropical Atmosphere, Surface temperature = 299.7 K

(b) Sub-Arctic Winter Atmosphere, Surface temperature = 257.2 K
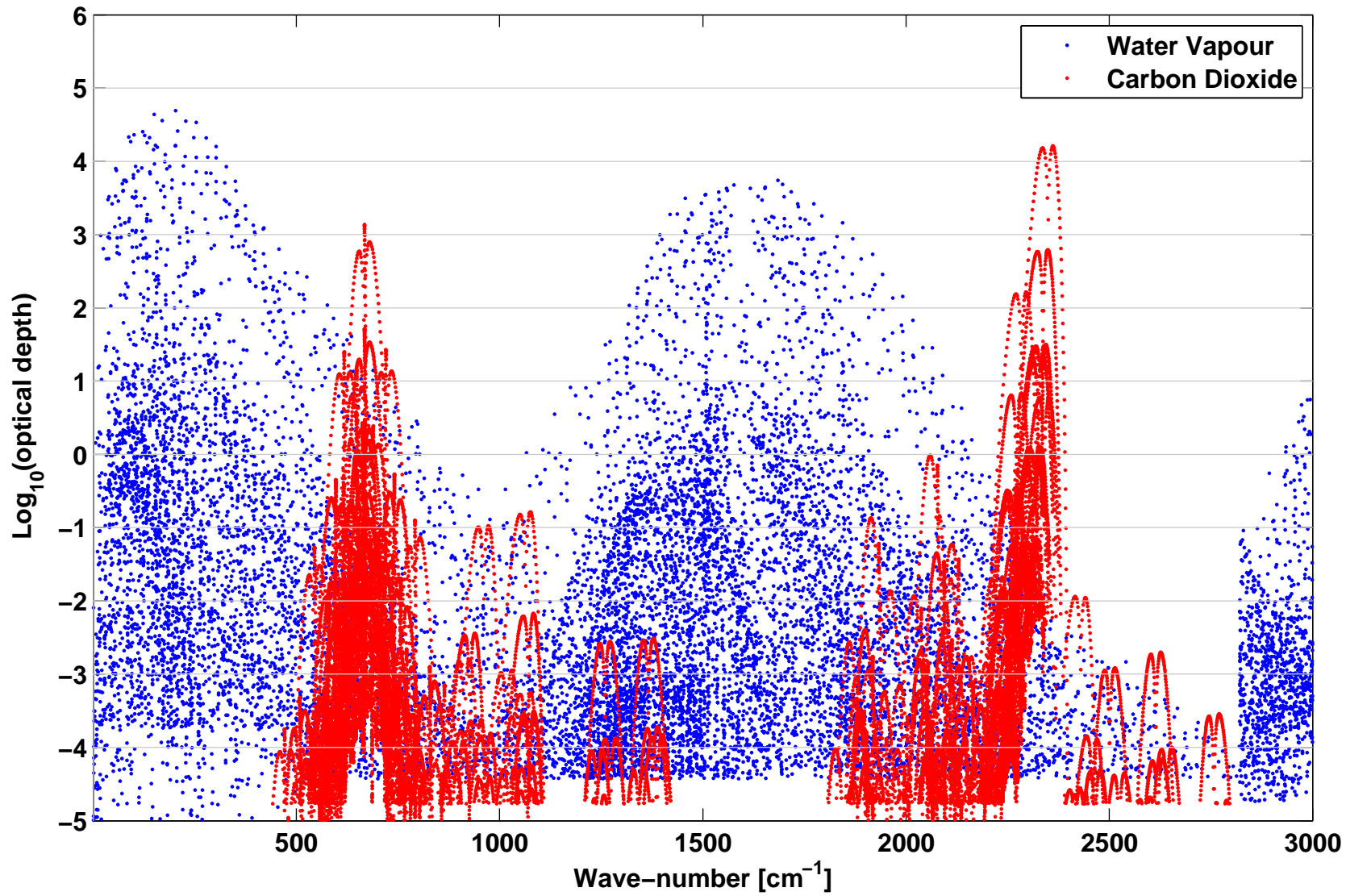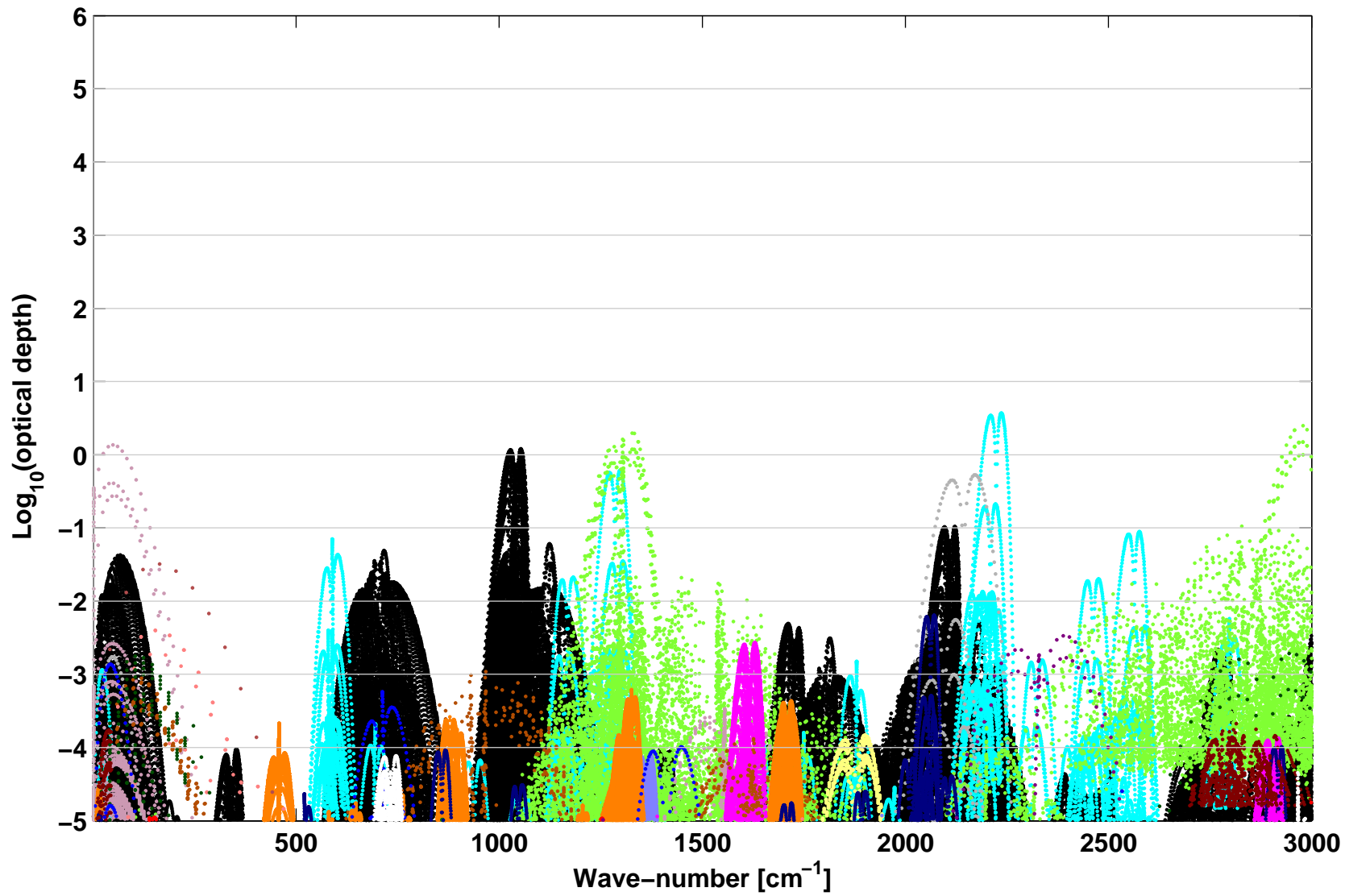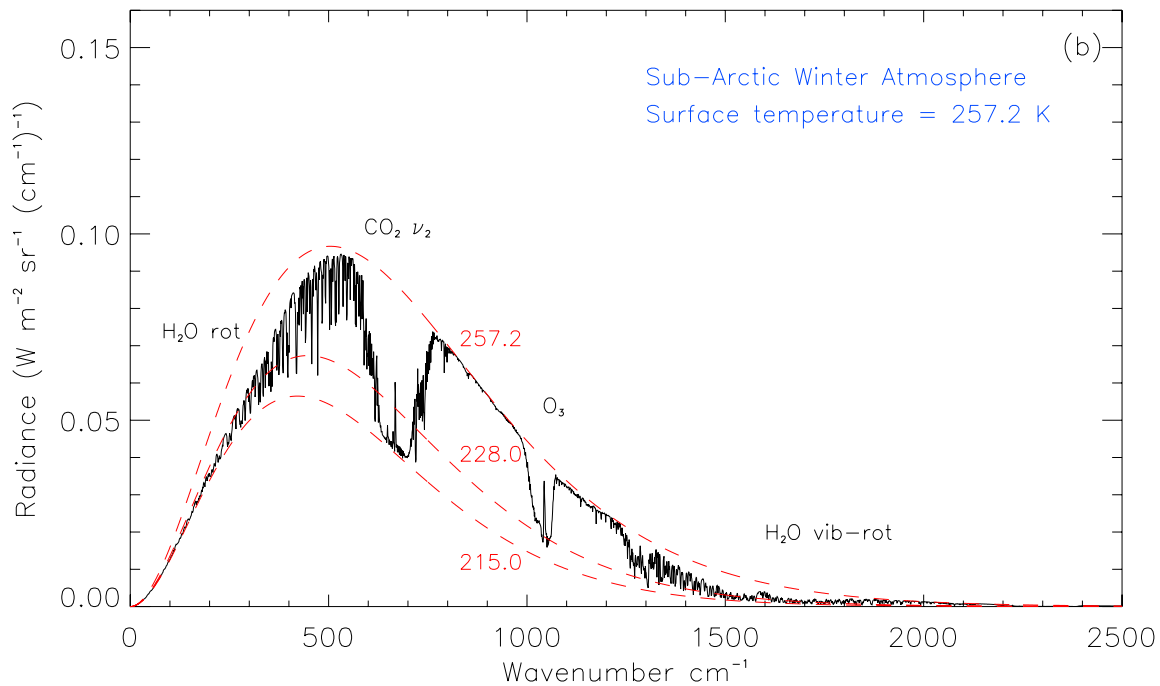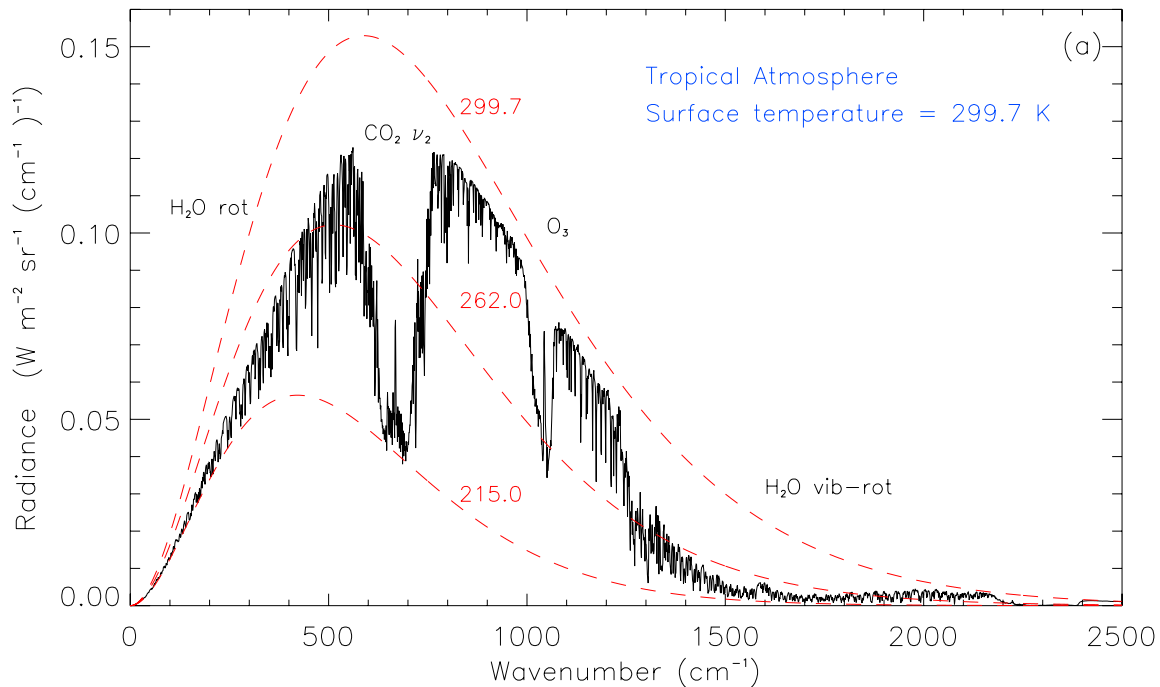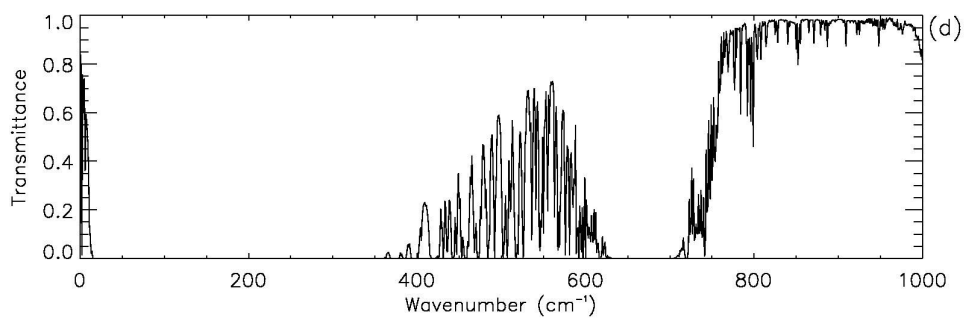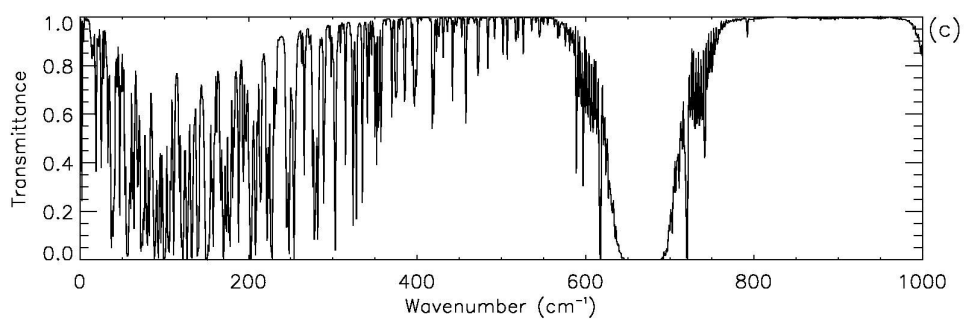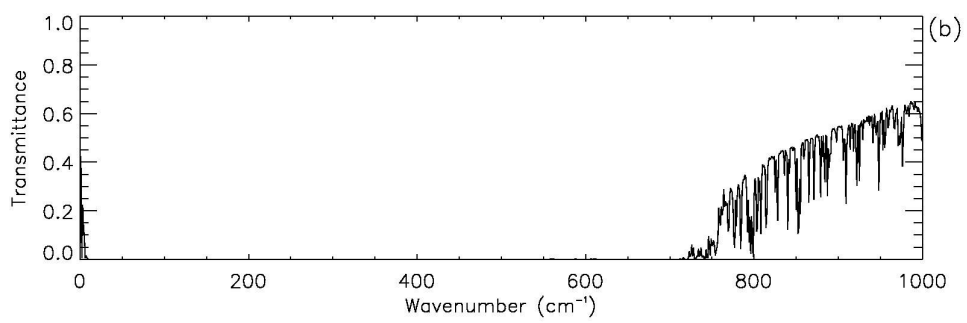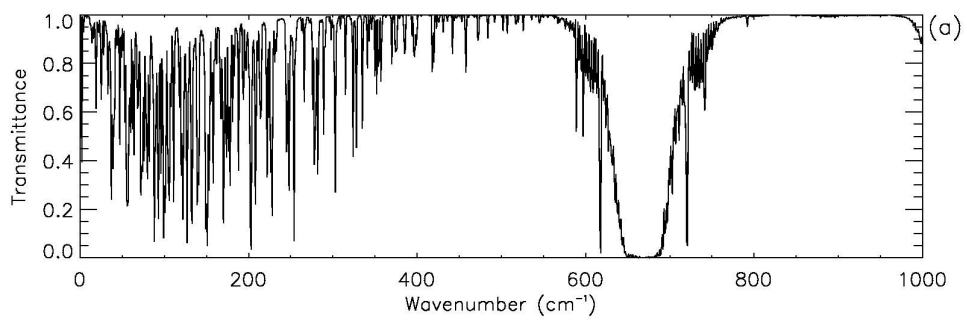
Variation of longwave cooling rates with pressure and wavenumber: (a) TRP cntrl, (b) SAW cntrl
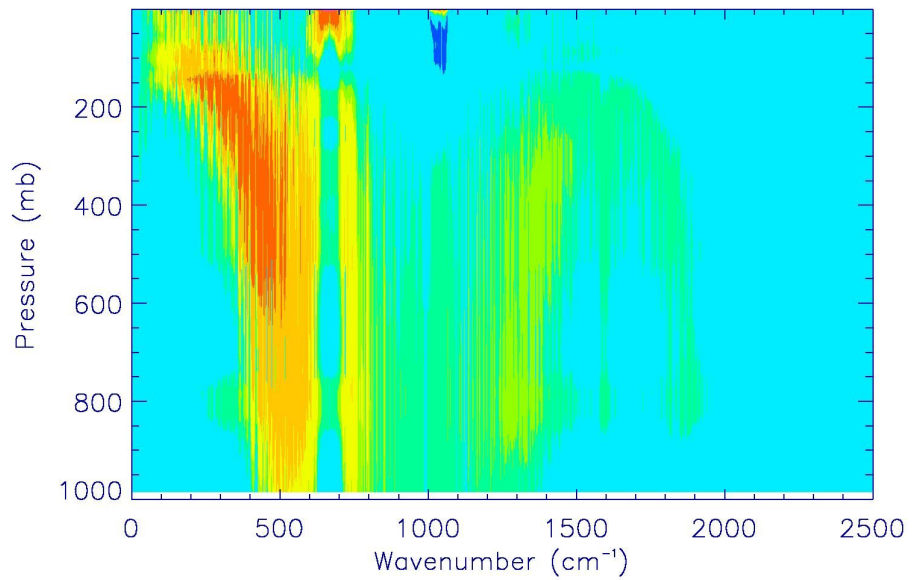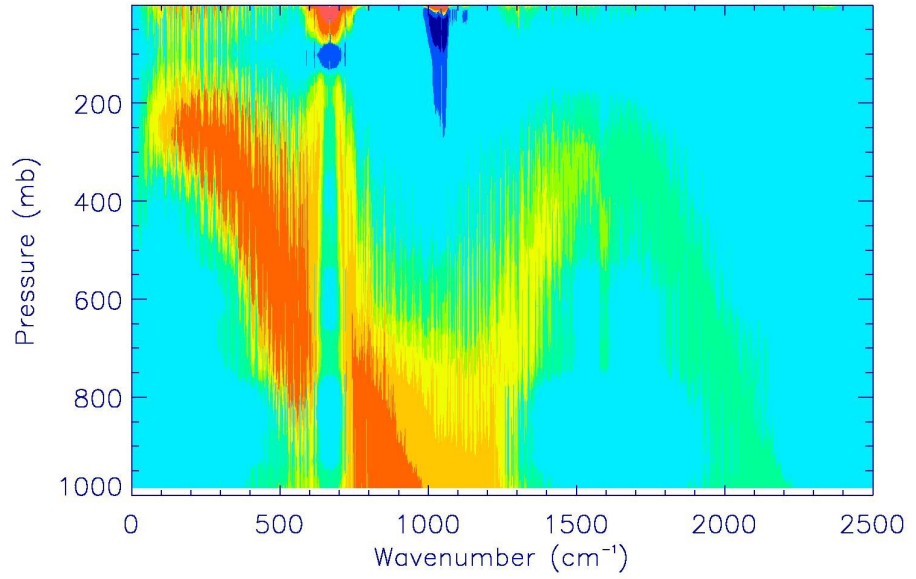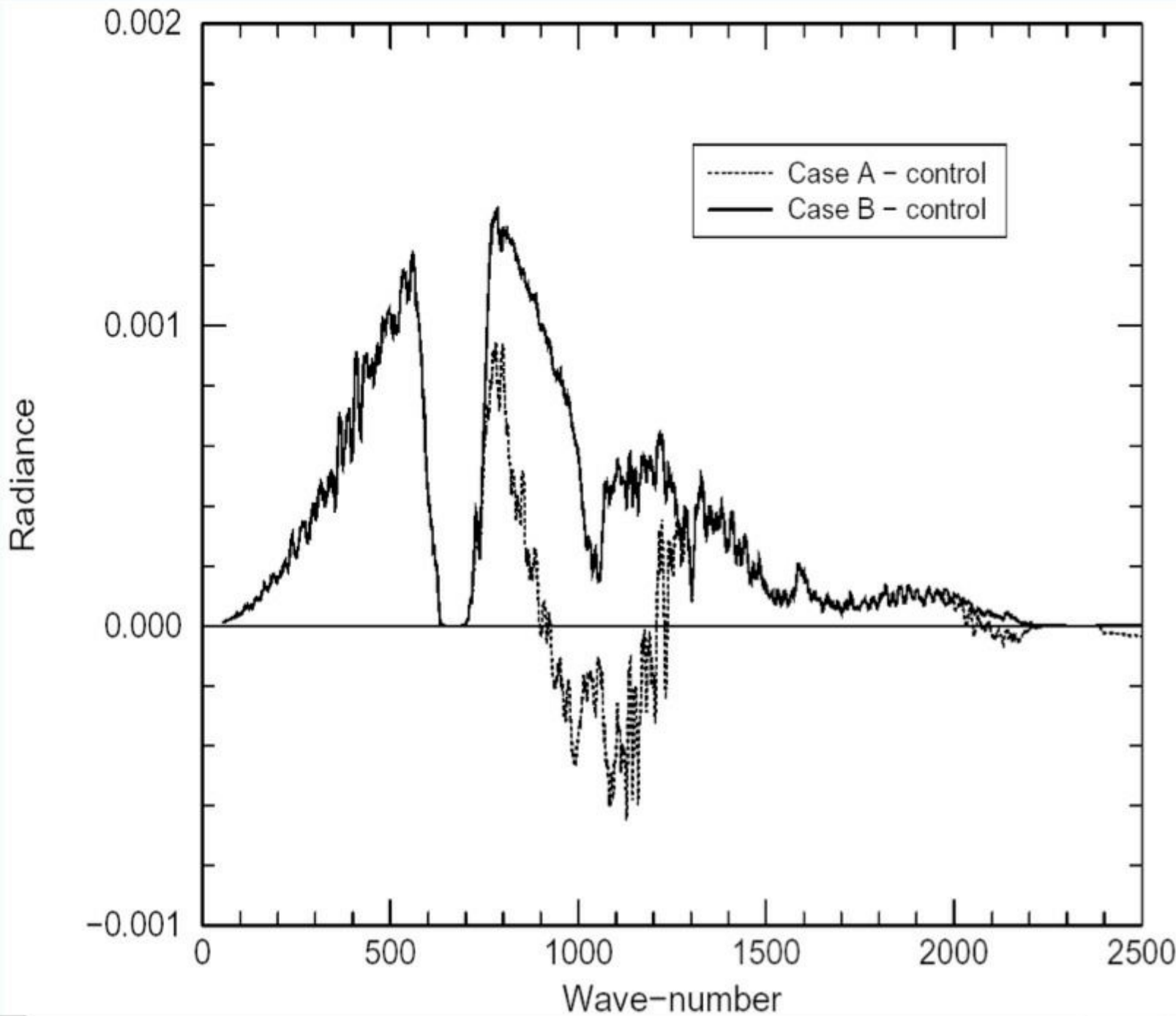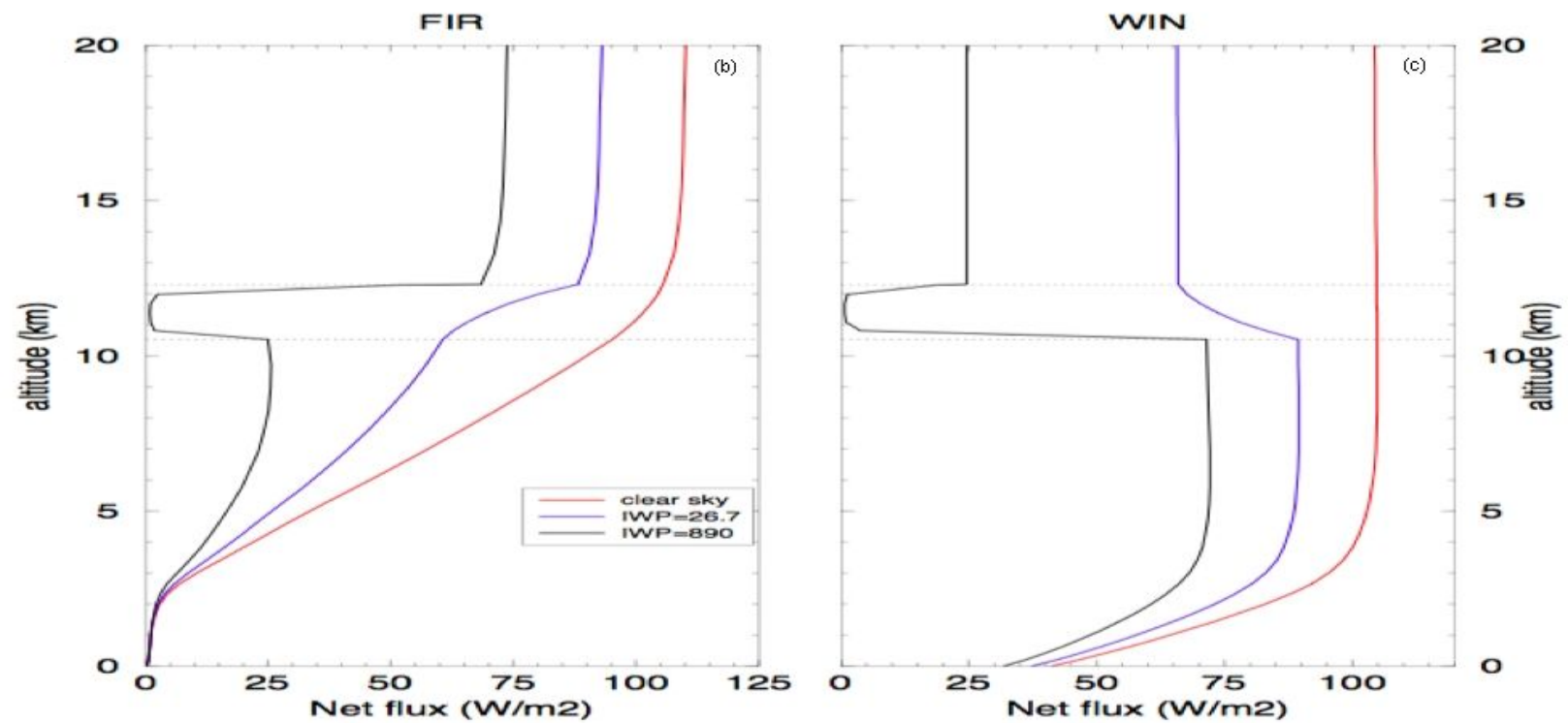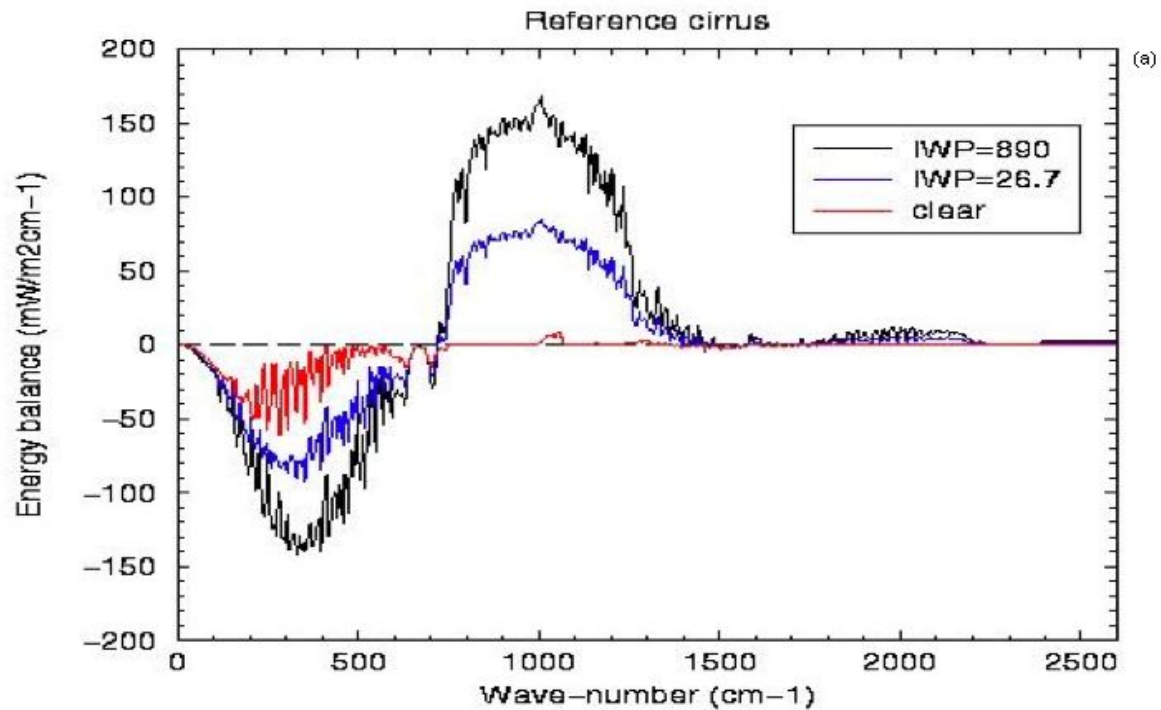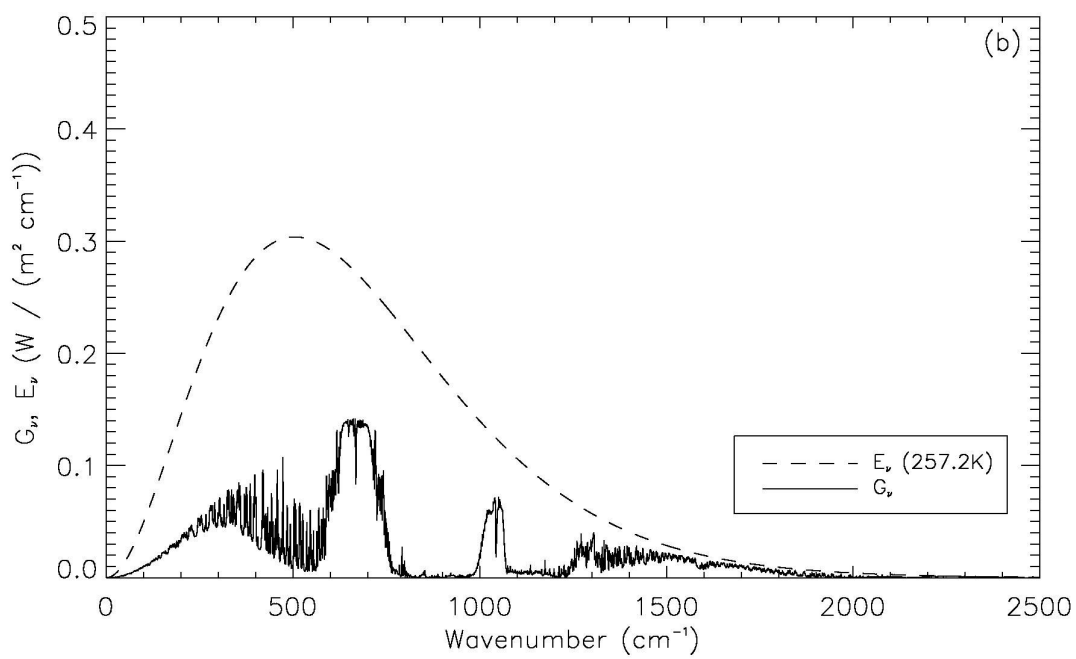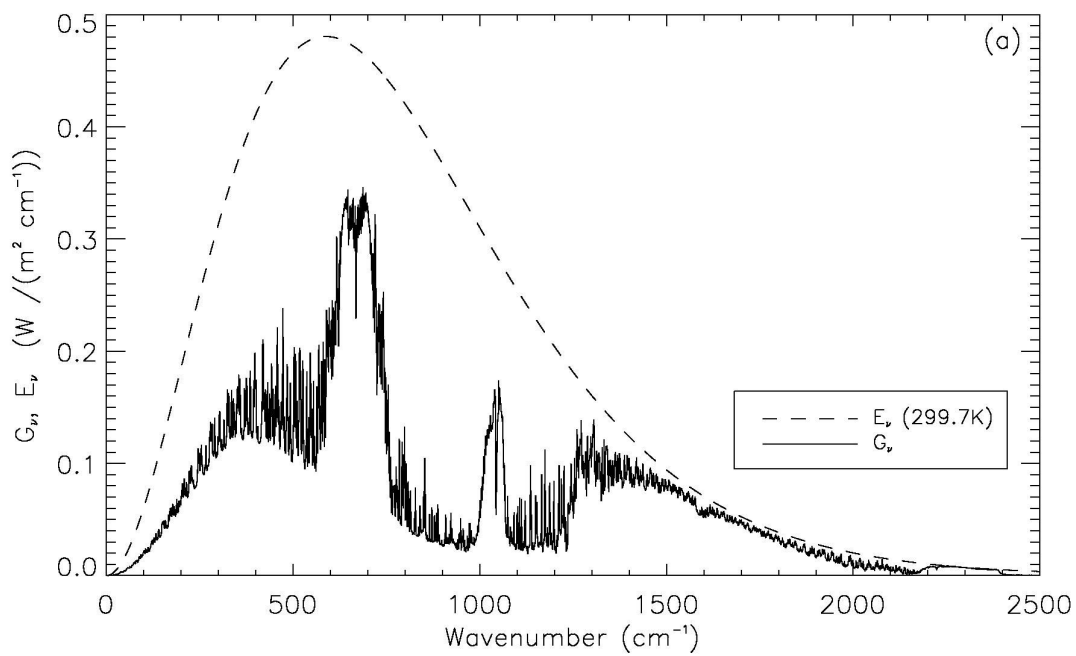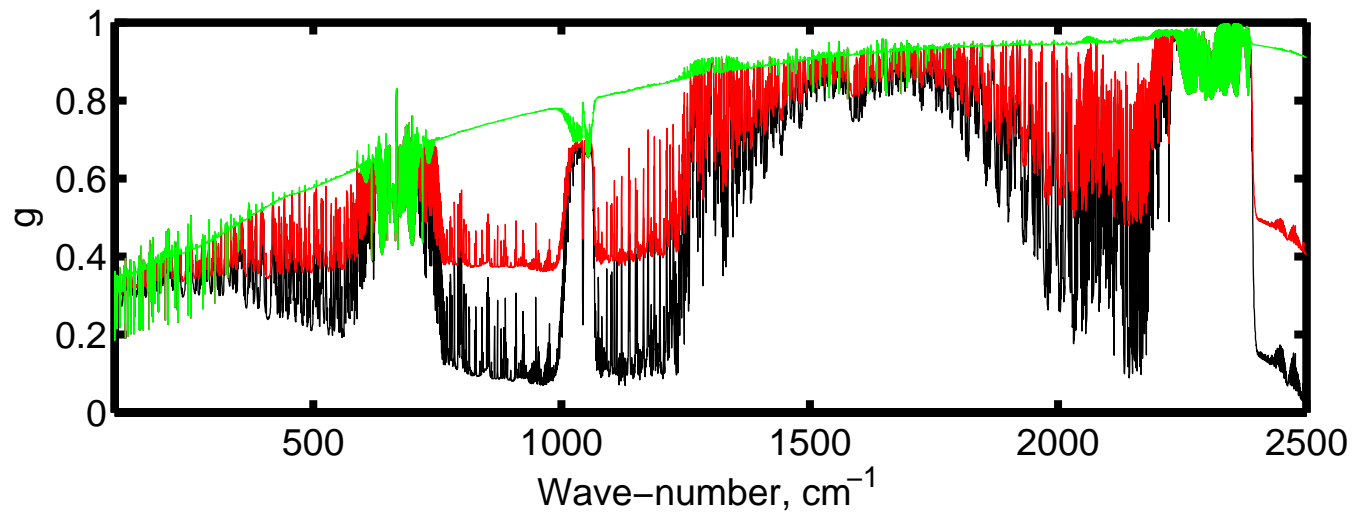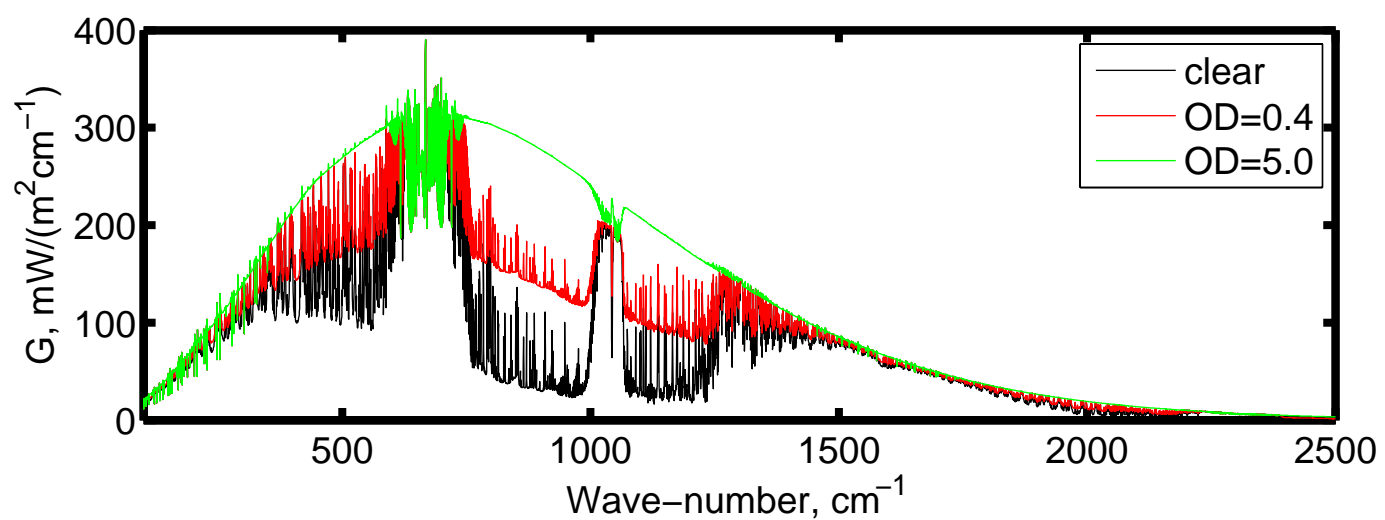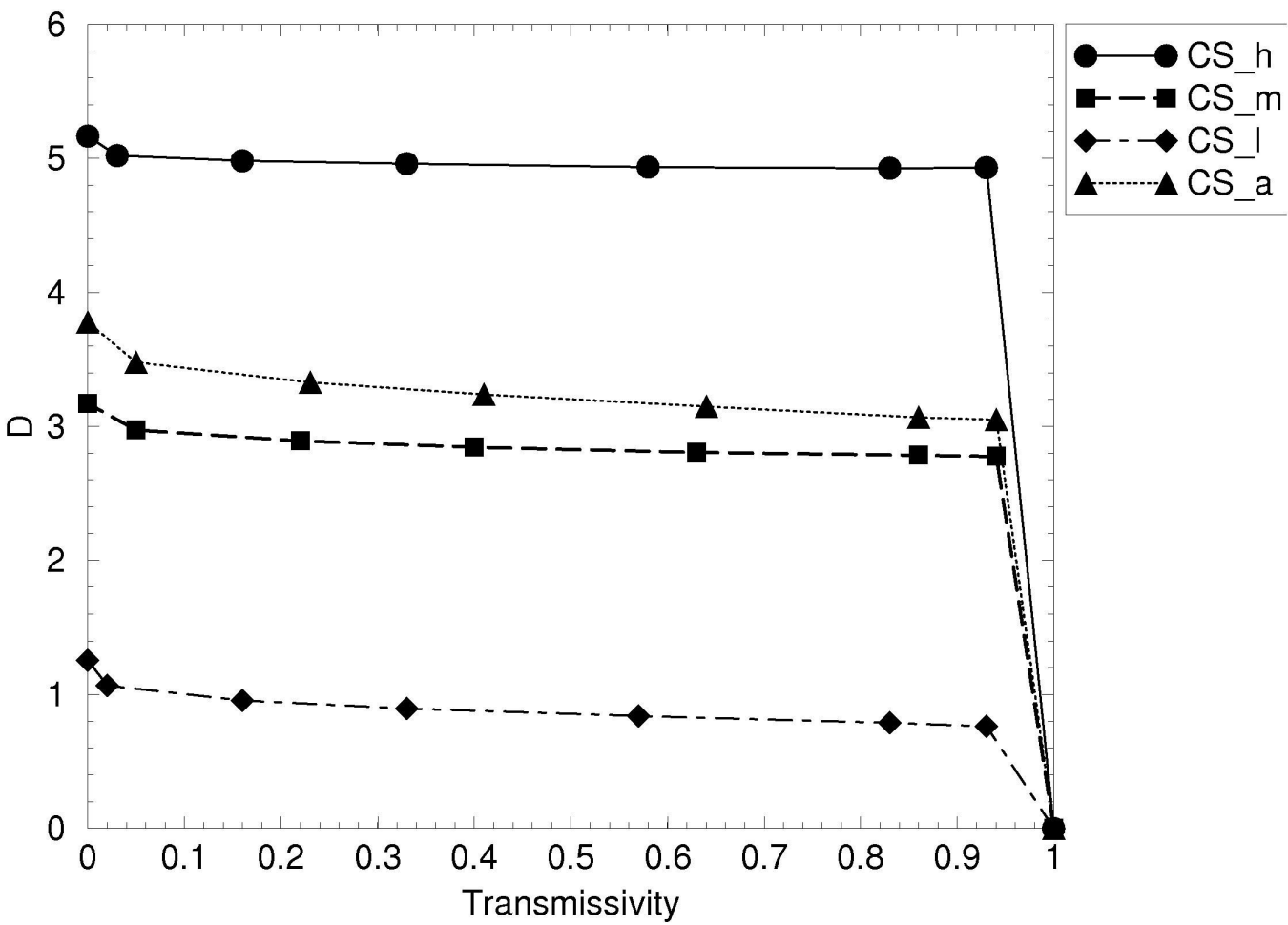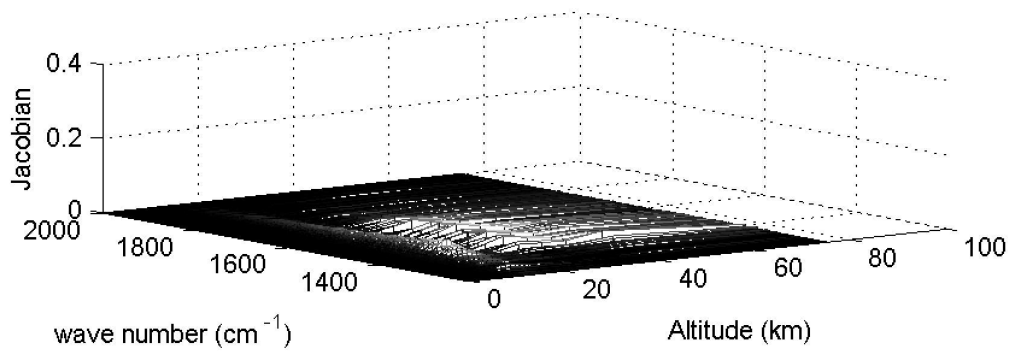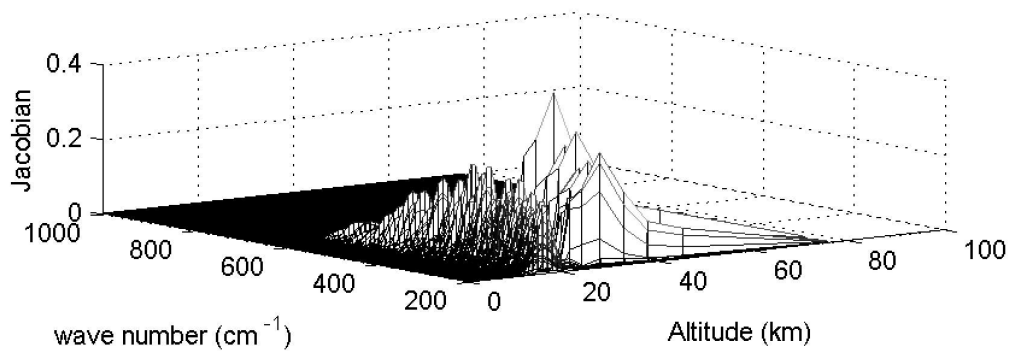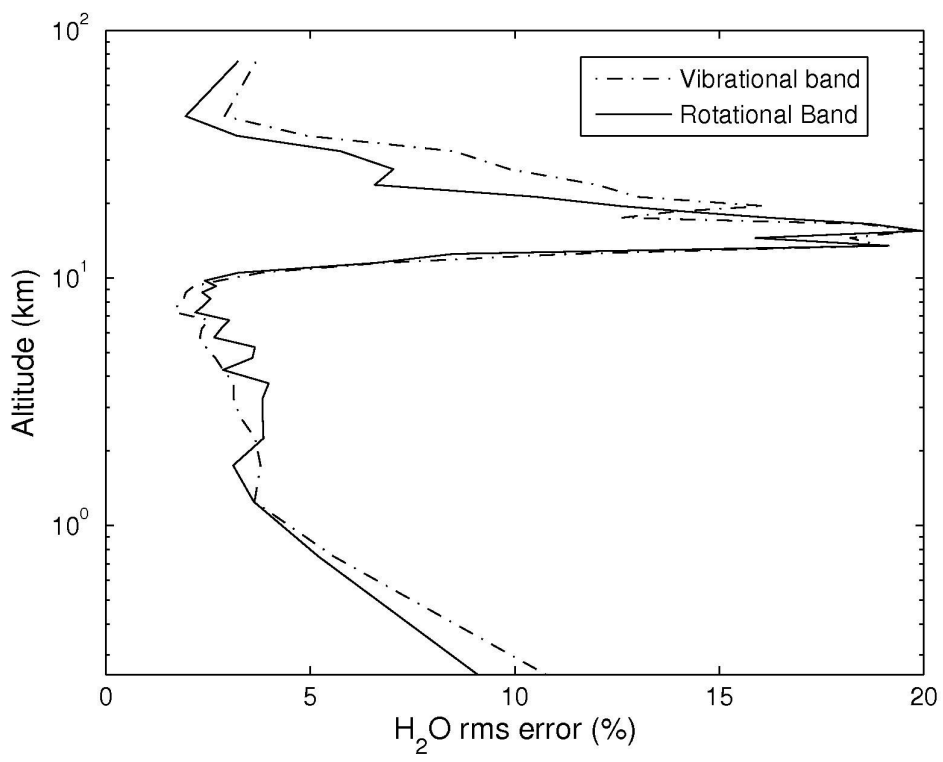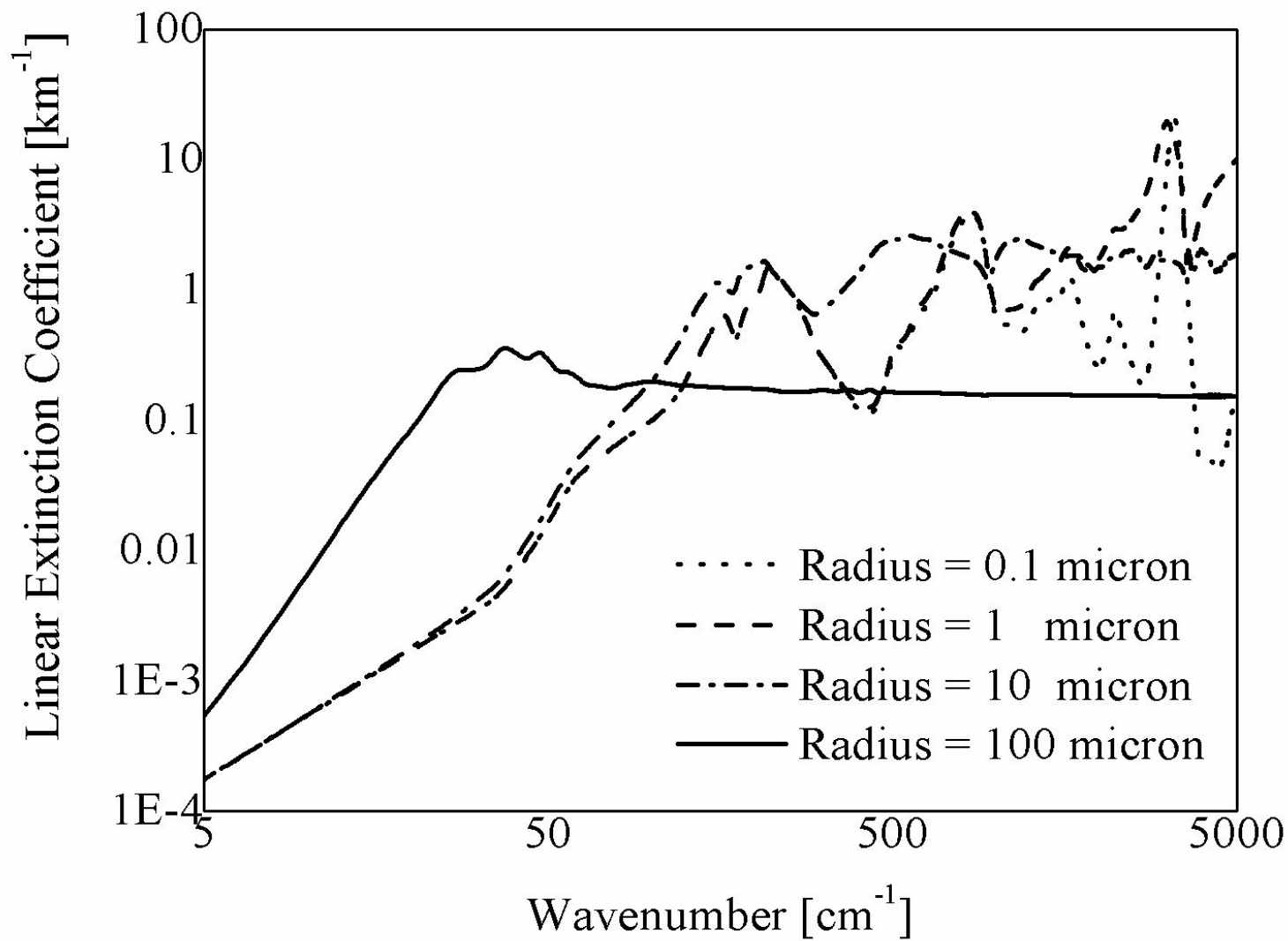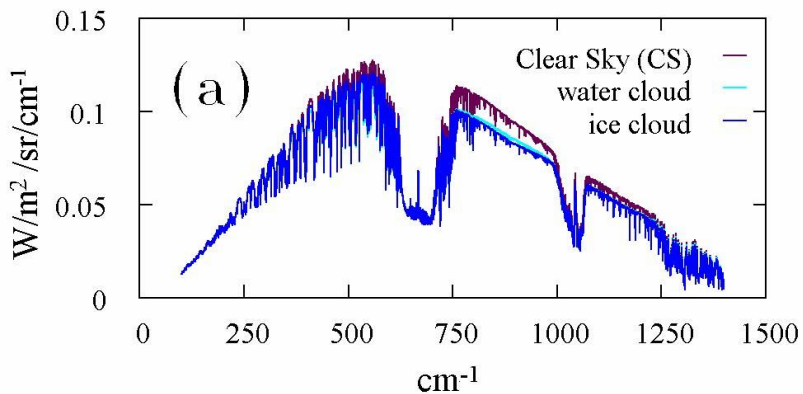
Reference cirrus (a)

- IWP=890
- IWP=26.7
- clear

FIR (b)

- clear sky
- IWP=26.7
- IWP=890

WIN (c)

TOA spectrum

(a) Clear Sky (CS), water cloud, ice cloud

Different phase

(b) CS - water cloud, CS - ice cloud

Different altitude

(c) CS - cloud from 7 to 8 km, CS - cloud from 5 to 6 km

Different IWP

(d) CS - 4.0 g/m2 cloud, CS - 2.8 g/m2 cloud

Different radius

(e) 30 - 27 micron, 33 - 30 micron

Different shape

(f) Hexagonal prism - Spherical
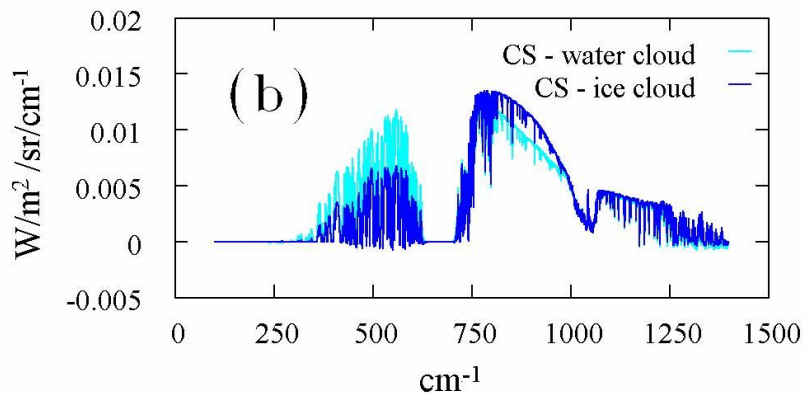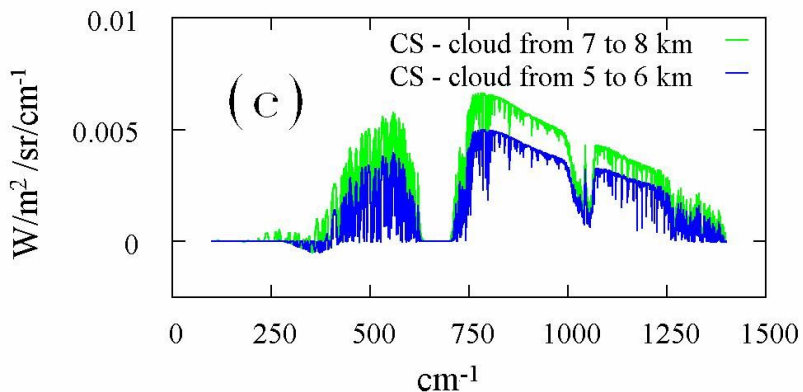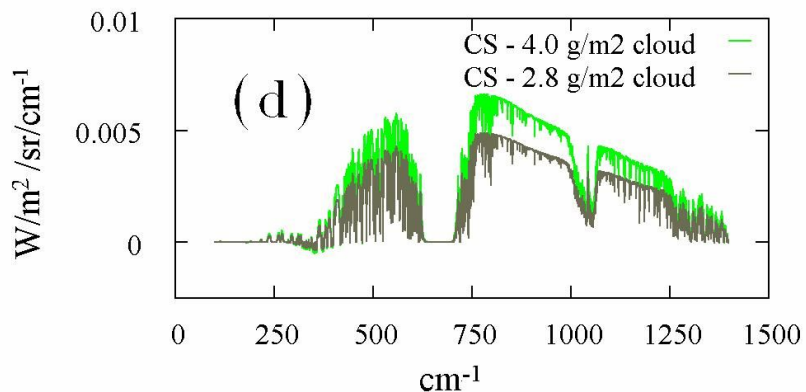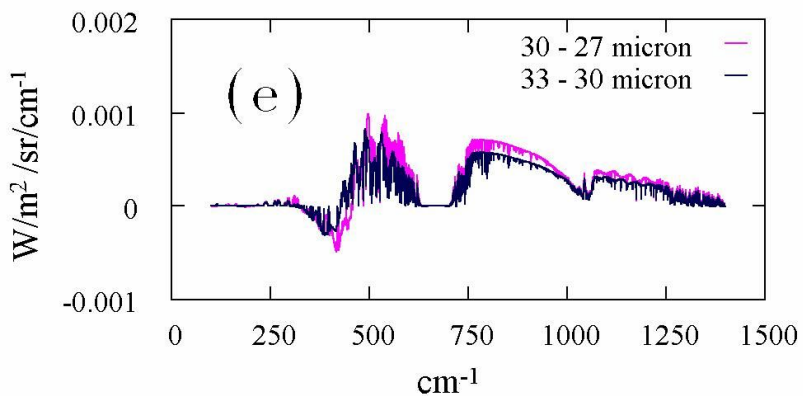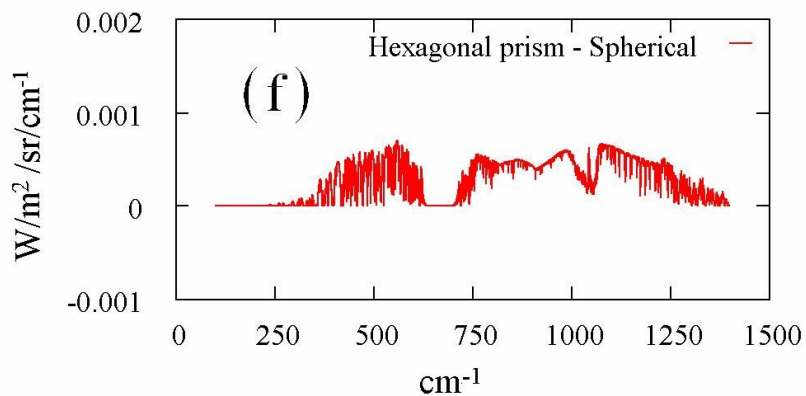
06-Sep-2004, 20:31:00-20:42:12 GMT (pw=17.32 mm)

DW sky view

UW sky view

POB

MI

RT mirror

P1 (BC)

P2 (BS)

L1

CRYO

LW CH1

SW CH3

LW CH0

L3

P3

LN2   He

L2

SW CH2

vacuum window

Steering mirror

Flat mirror

Polarizer

Power optic

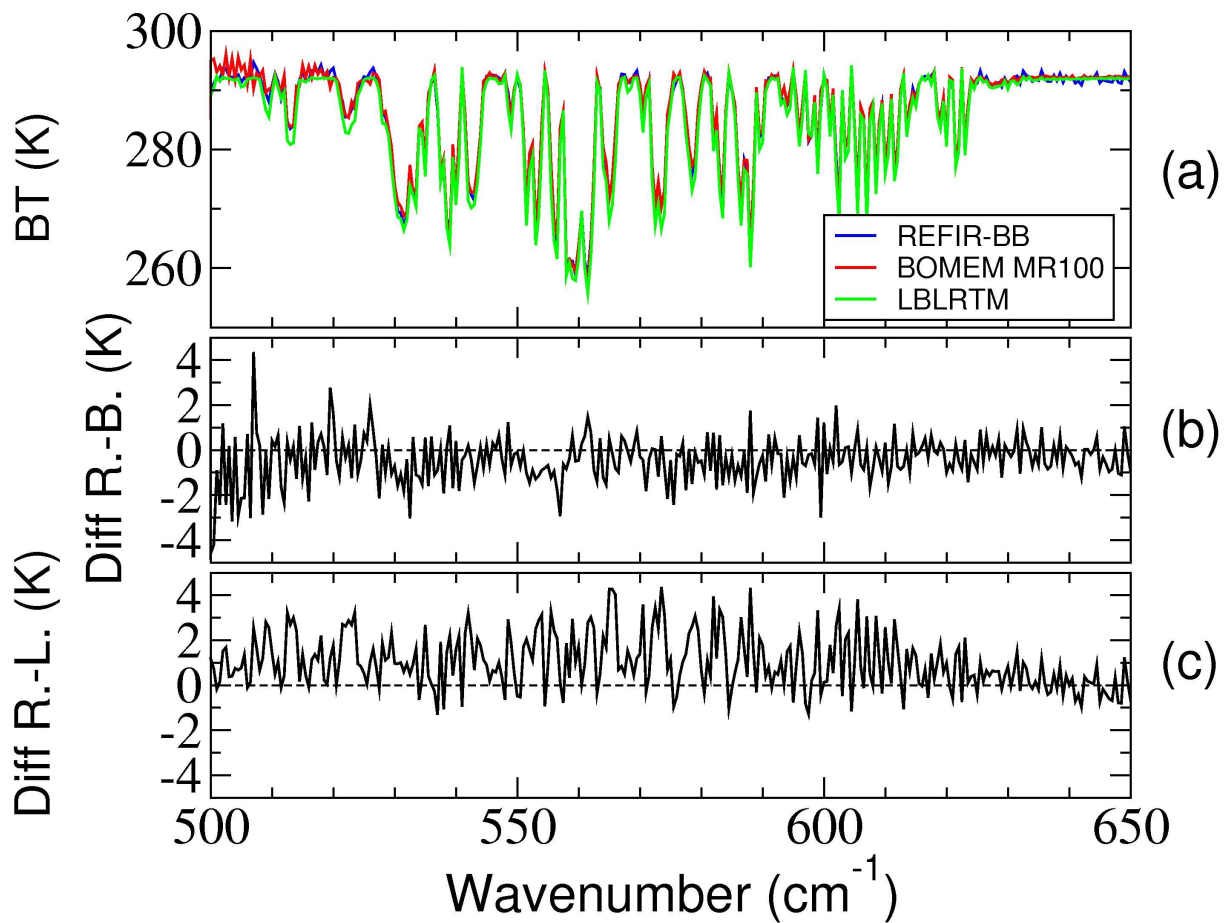Blackbody
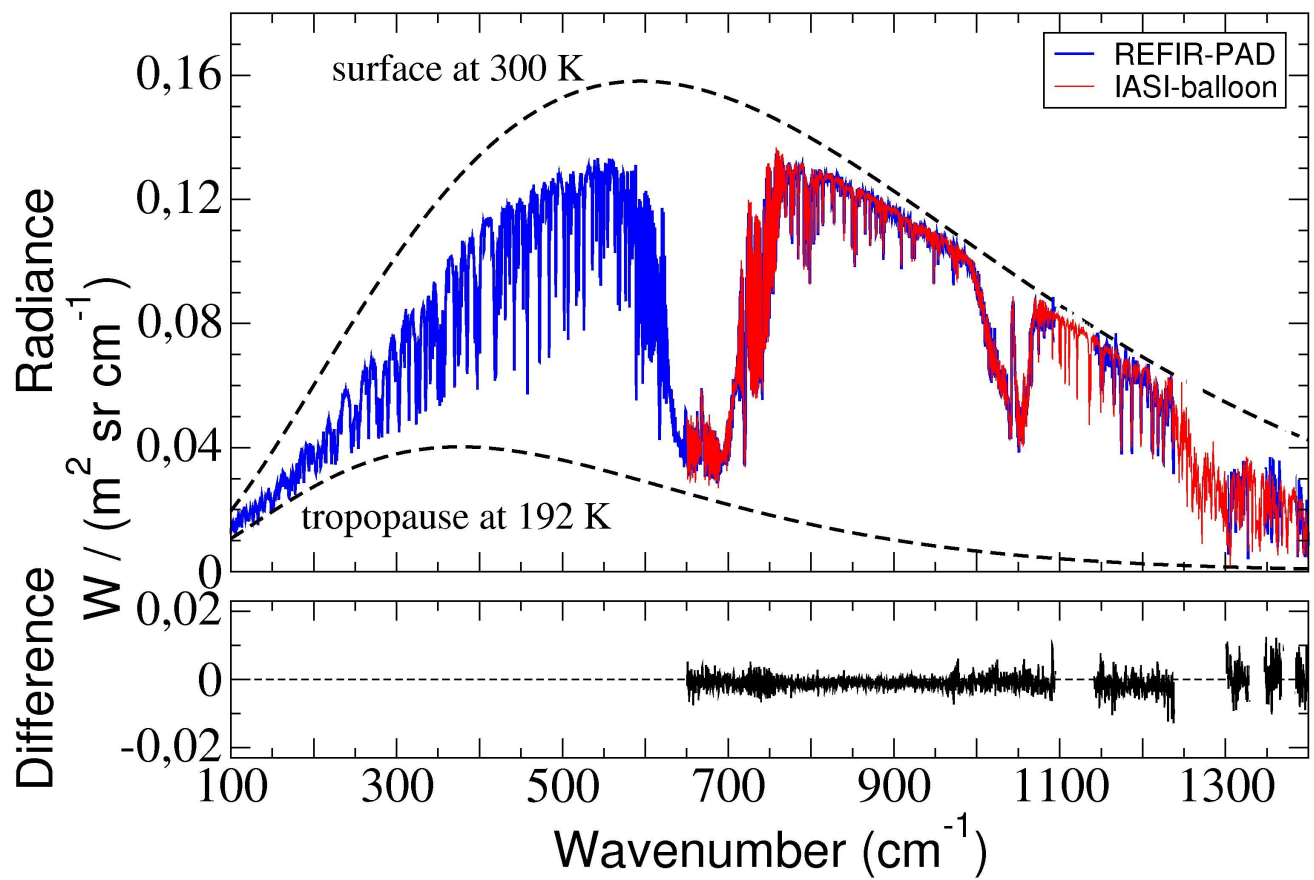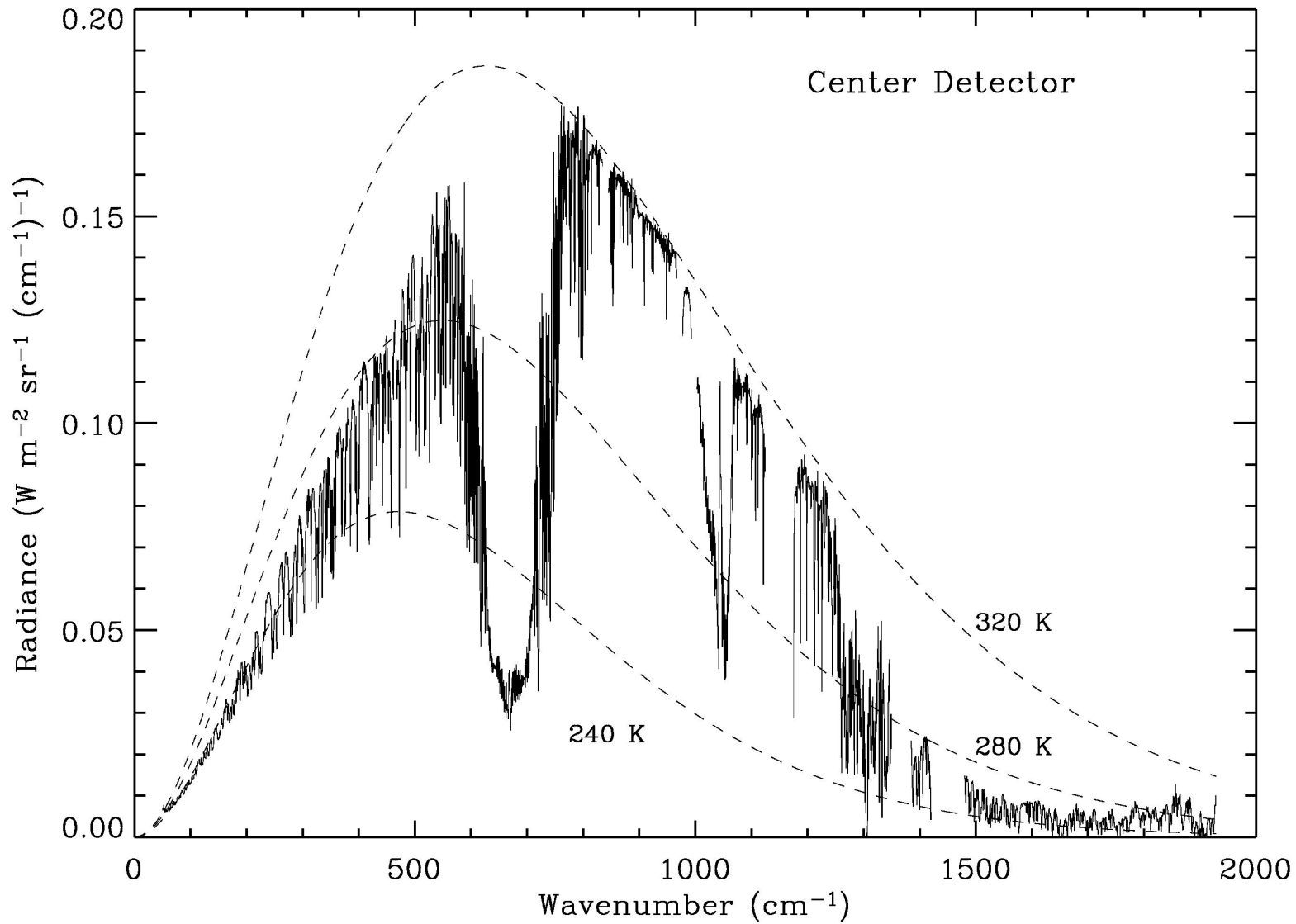
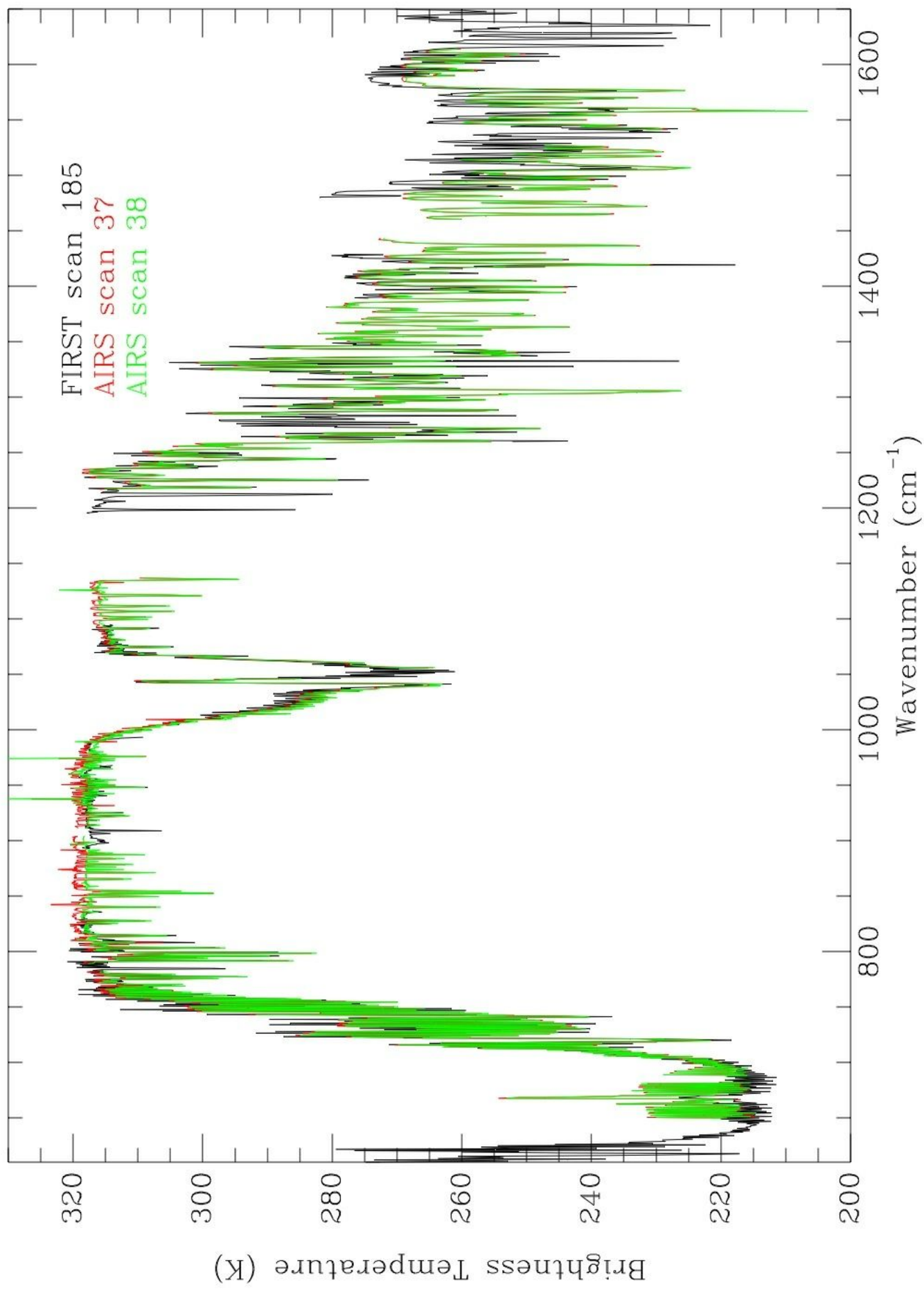Low pass filter

Dichroic filter

Detector

RTMU

Pol. (90°)

Pol.(45°)
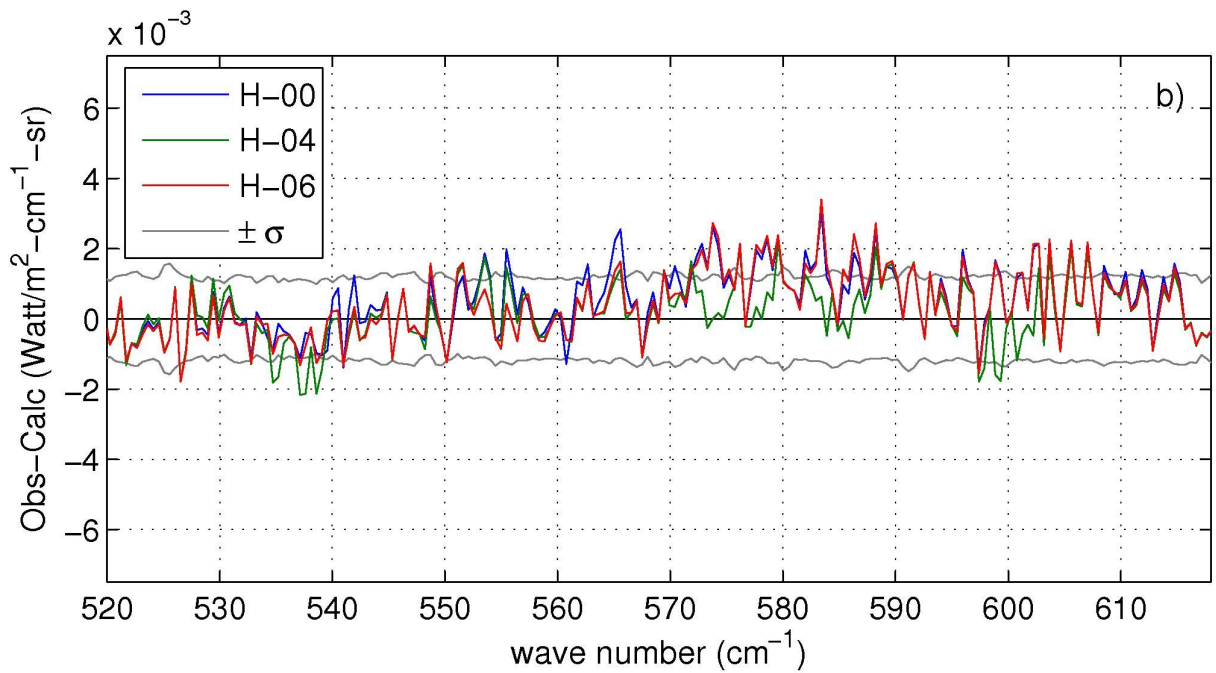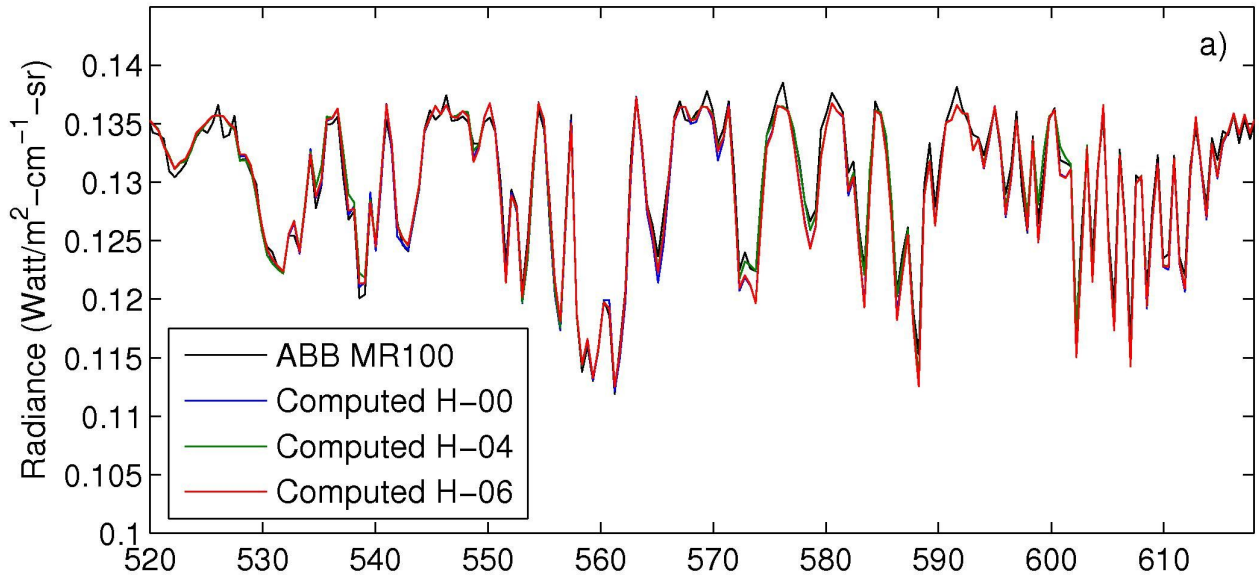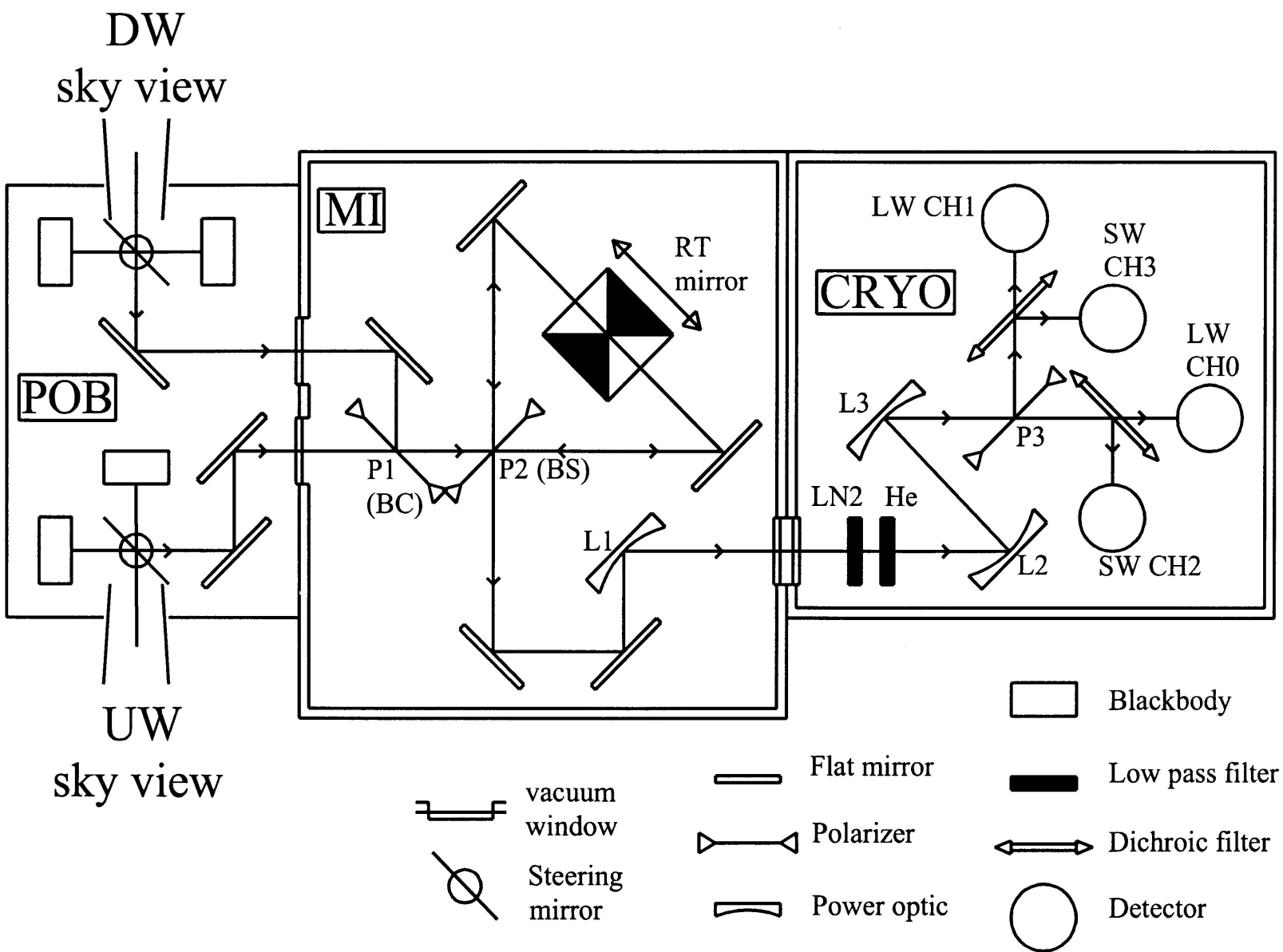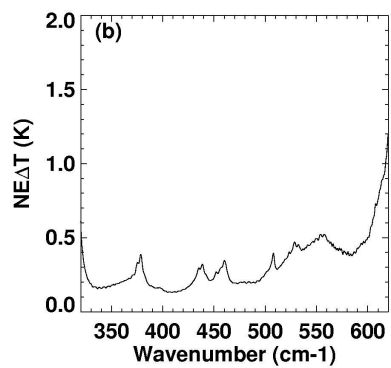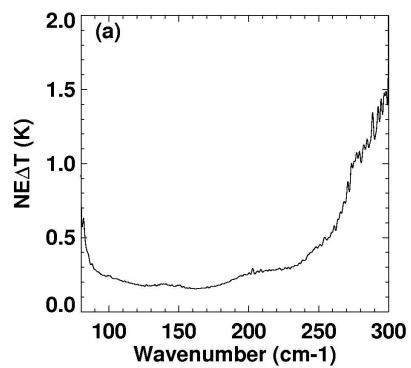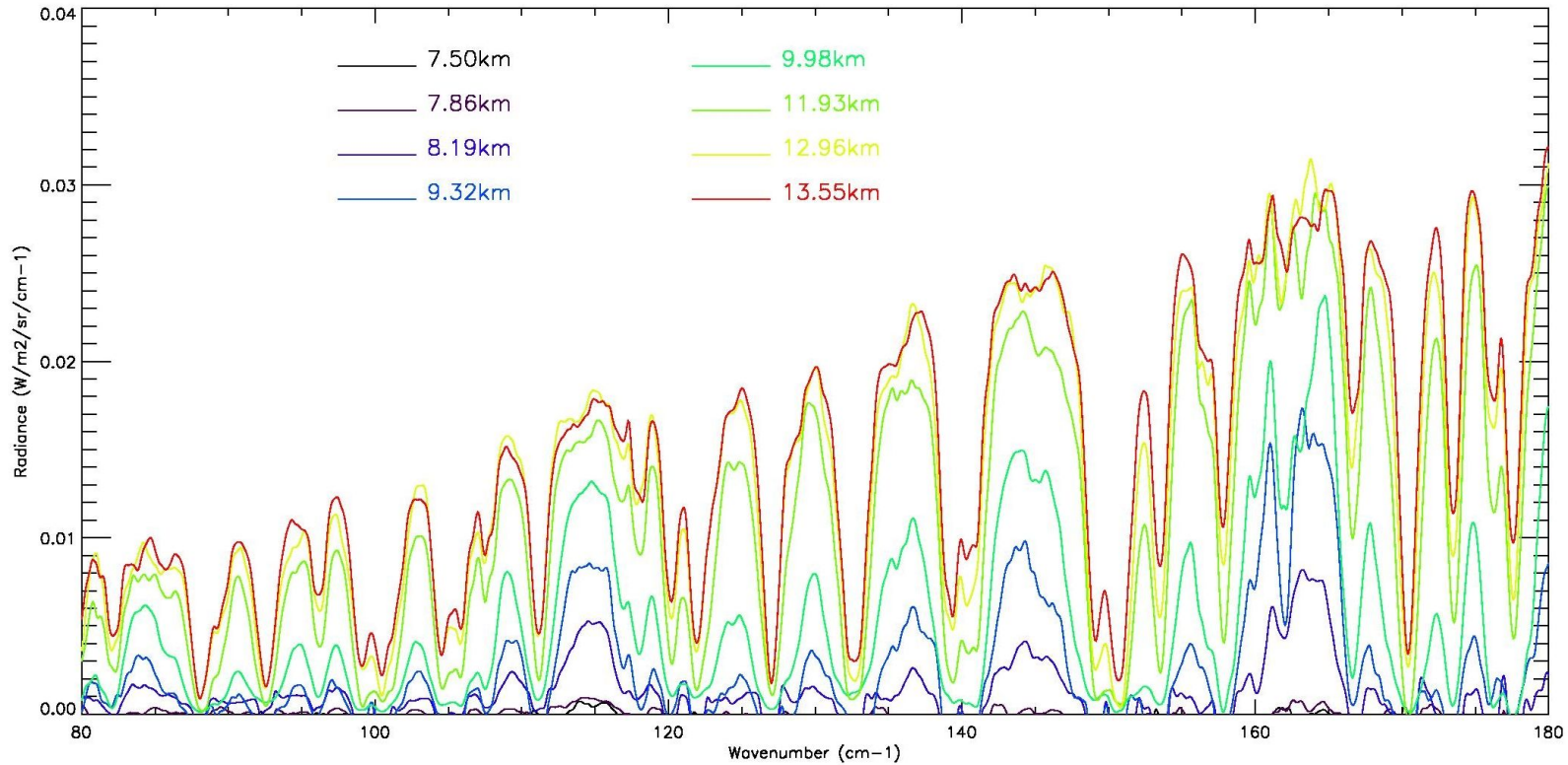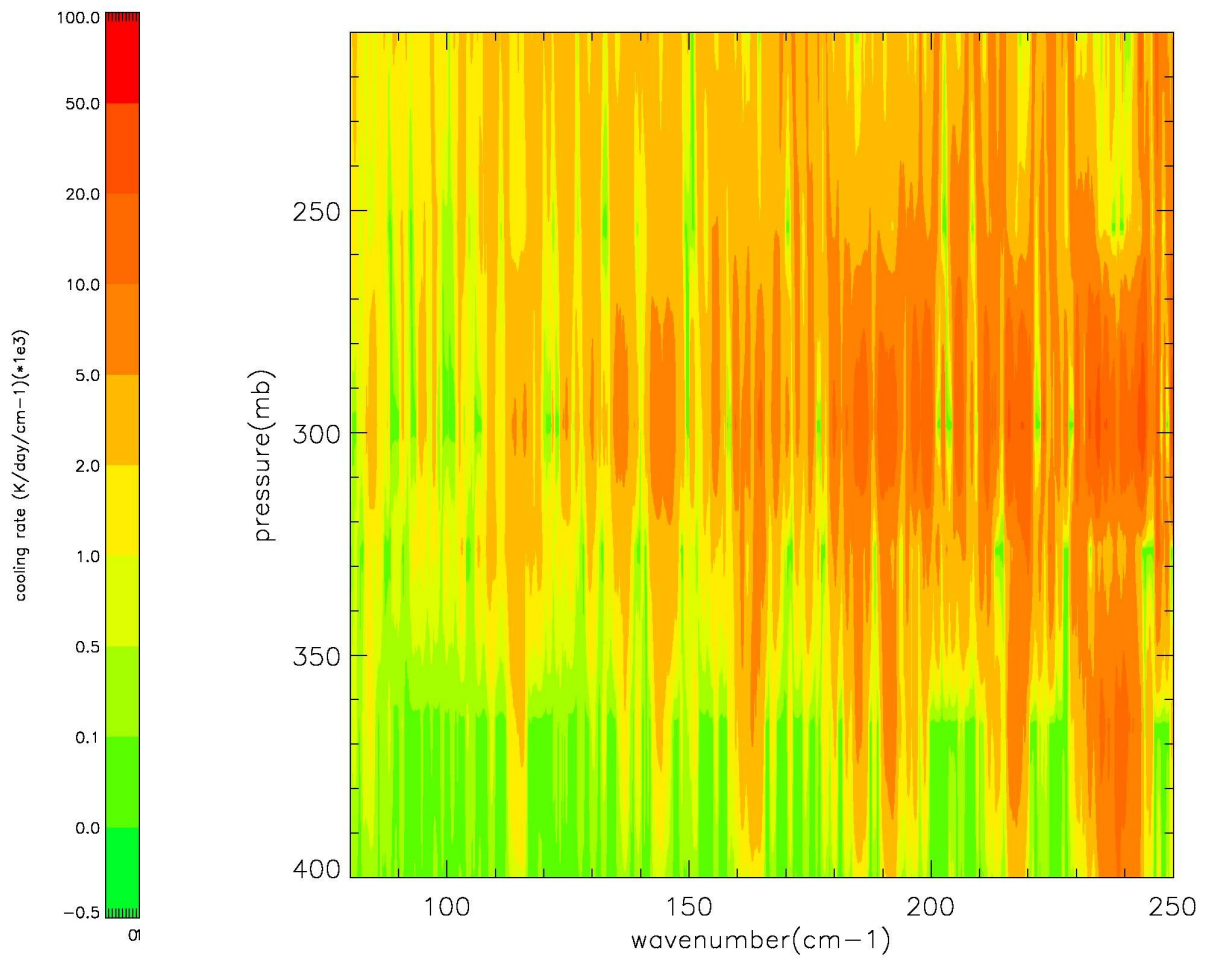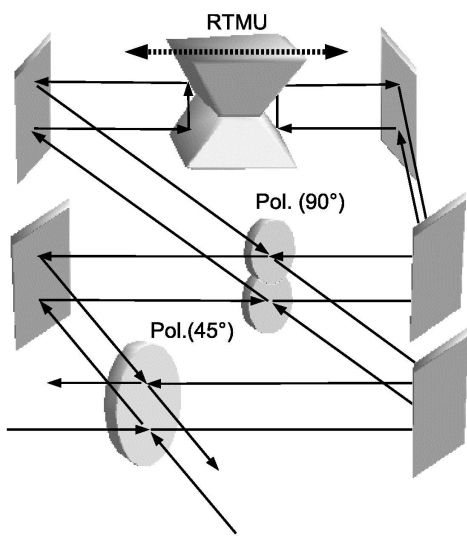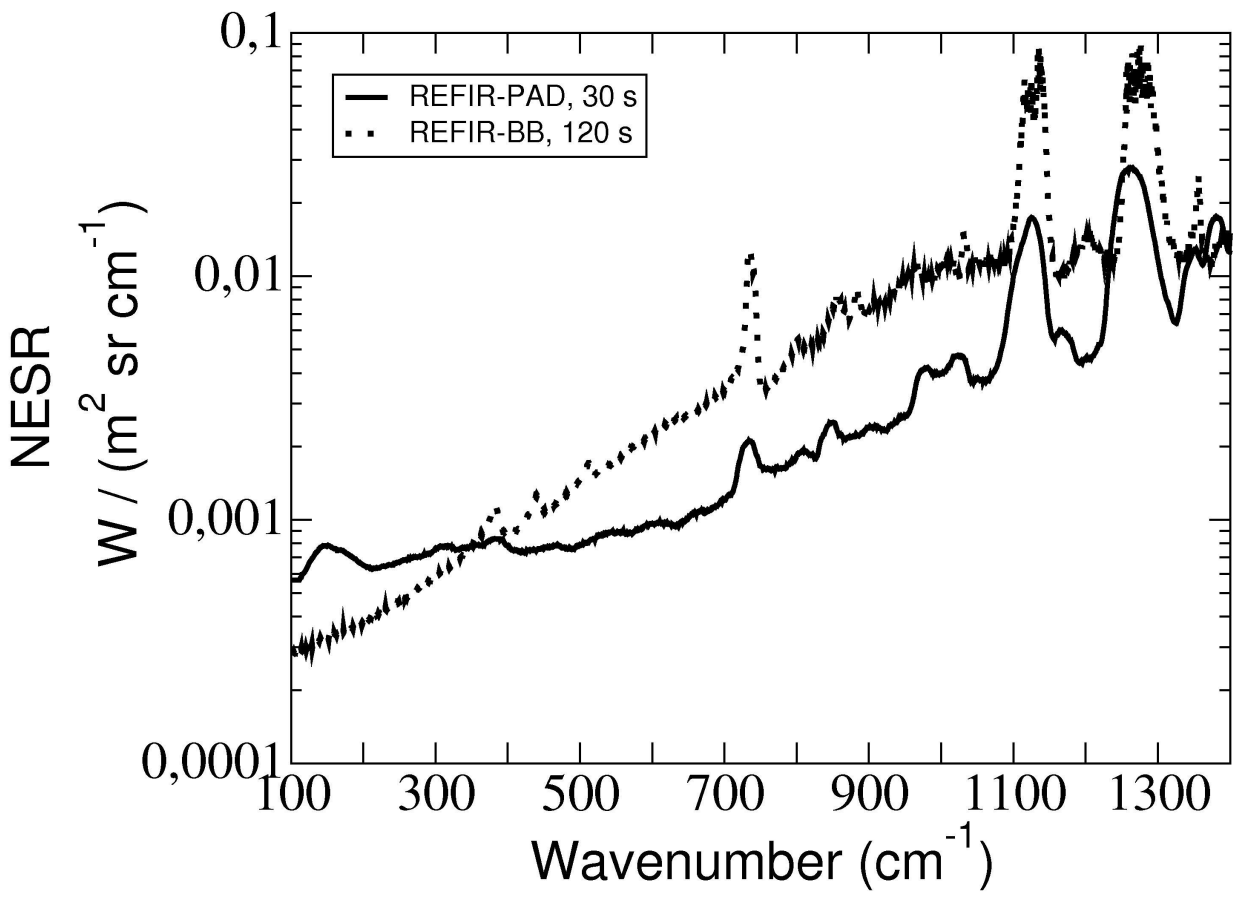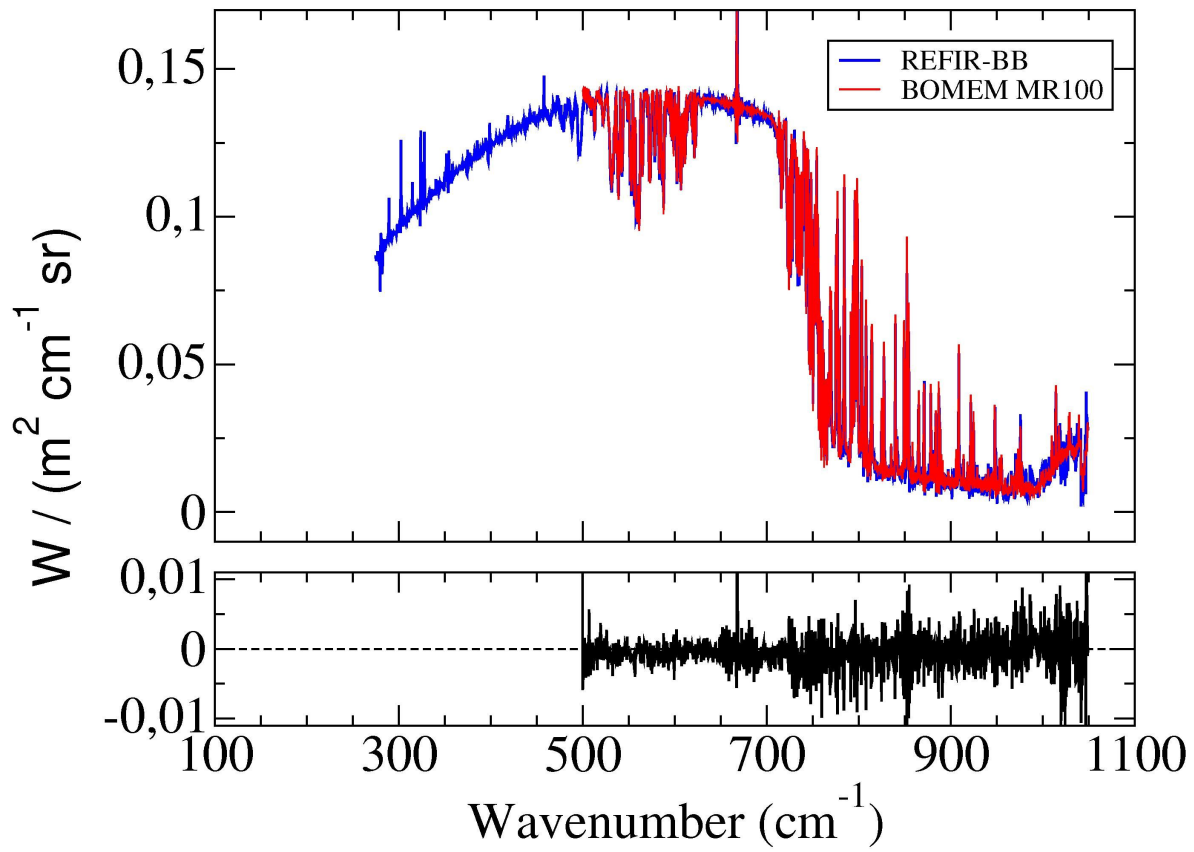
FIRST Radiance June 7 2005 14:25 LT

FIRST Measured Radiances

June 7 2005 14:25 LT
September 18 2006 14:03 LT
June − September